U.S. DEPARTMENT OF COMMERCE
National Technical Information Service

PB-249 912

The Formation of Nitric Oxide in Diffusion Flames

Wisconsin Univ, Madison Dept of Mechanical Engineering

Prepared for

Environmental Protection Agency, Washington, D C Office of Air Programs

7 Oct 72

PB 269 912

Motor Vehicle Emission Lab
LIBRARY

THE FORMATION OF NITRIC OXIDE IN DIFFUSION FLAMES

By

Arjun Dev Tuteja

Prepared For
Office of Air Programs
Environmental Protection Agency
Grant No. R-801339

Motor Vehicle Emission Lab
LIBRARY

October 7, 1972

University of Wisconsin
Department of Mechanical Engineering
Madison, Wisconsin

REPRODUCED BY
NATIONAL TECHNICAL
INFORMATION SERVICE
U.S. DEPARTMENT OF COMMERCE
SPRINGFIELD, VA. 22161

845

BIBLIOGRAPHIC DATA SHEET

1. Report No.

2.

3. Recipient's Accession No.

4. Title and Subtitle
The Formation of Nitric Oxide in Diffusion Flames

5. Report Date
October 1972

6.

7. Author(s)
Arjun Dev Tuteja

8. Performing Organization Rept. No.

9. Performing Organization Name and Address
University of Wisconsin
Department of Mechanical Engineering
Madison, Wisconsin

10. Project/Task/Work Unit No.

11. Contract/Grant No.
R-801339

12. Sponsoring Organization Name and Address
Office of Air Porgrams
Environmental Protection Agency
Ann Arbor, Michigan 48105

13. Type of Report & Period Covered
Final Report

14.

15. Supplementary Notes

16. Abstracts The purpose of this work has been to investigate the processes leading to the formation of nitric oxide in a vertical, co-axial, atmospheric pressure, methane-air diffusion flame burner; which models many of the physio-chemical processes occuring in combustion systems using fuel sprays, for example diesel engines, and gas turbines. Experimentally, radial concentration profiles of nitric oxide have been determined in this burner at prescribed axial locations. Major conclusions: Nitric oxide is formed in diffusion flames in the high temperature zone and diffuses towards both the fuel-rich and oxidant-rich regions; the nitric oxide concentration profiles can be adequately predicted by using the Zeldovich mechanism in conjunction with equilibrium relations between the atomic and molecular species for oxygen and nitrogen. This presupposes that the flame structure can be properly established.

17. Key Words and Document Analysis. 17a. Descriptors
Diffusion flames
Nitric oxide
Computation
Combustion

17b. Identifiers/Open-Ended Terms
Zeldovich mechanism
Saltzman technique

17c. COSATI Field/Group

18. Availability Statement
Release Unlimited

19. Security Class (This Report)
UNCLASSIFIED

20. Security Class (This Page)
UNCLASSIFIED

21. No. of Pages
243

22. Price
PC A11 / MF A01

TECHNICAL REPORT

THE FORMATION OF NITRIC OXIDE
IN DIFFUSION FLAMES

BY

ARJUN DEV TUTEJA

Prepared For

Office of Air Programs
Environmental Protection Agency
Grant No. R-801339

October 7, 1972

The University of Wisconsin
Department of Mechanical Engineering
Madison, Wisconsin

THE FORMATION OF NITRIC OXIDE IN DIFFUSION FLAMES

Arjun Dev Tuteja

Under the supervision of
Associate Professor Henry K. Newhall

ABSTRACT

The oxides of nitrogen are among the major pollutants associated with combustion processes. The principal oxide of nitrogen formed in such processes is nitric oxide, and as a consequence its formation in combustion processes is of interest.

The purpose of this work has been the experimental and theoretical investigation of the formation of nitric oxide in a steady laminar diffusion flame.

The experimental work has involved determination of nitric oxide concentration profiles within the flame. In addition, concomitant temperature profiles and concentration profiles for CO, CO_2, O_2, N_2 and methane, the fuel used in the study, have been determined.

A co-axial diffusion flame burner was designed to produce the desired flame. The flame is enclosed in a vertical quartz tube interposed with steel flanges to provide for sample probe insertions at a number of axial locations.

Radial concentration profiles at prescribed axial locations were determined for nitric oxide and other species, through analysis of the samples extracted from the flame by means of quartz microprobes.

Nitric oxide concentrations were determined using a modified Saltzman technique. Combustion product and reactant concentrations were determined through use of a thermal conductivity gas-chromatograph.

Radial temperature profiles were determined with a Pt-10% Rh/Pt thermocouple of 0.001" diameter.

The radial position of sampling probe and thermocouple were varied and determined by a micromanipulator.

Experimental results indicate that nitric oxide is formed primarily in a narrow region corresponding to the high temperature zone and diffuses into both fuel-rich and oxidant-rich regions.

A literature survey indicated that the following two elementary chemical reactions are sufficient to predict accurately the rate of formation of nitric oxide in premixed flames

$$N_2 + O \rightleftharpoons NO + N \qquad (1)$$

$$O_2 + N \rightleftharpoons NO + O \qquad (2)$$

Using this reaction scheme, the rate of formation of NO in an elementary control volume is obtained as

$$\frac{d[NO]}{dt} = k_{1f}(T)[N_2][O] + k_{2f}(T)[N][O_2] - k_{1b}[NO][N] - k_{2b}(T)[NO][O] \quad (3)$$

However, to calculate NO concentration profiles in the system under consideration NO conservation equation

$$\nabla \cdot (\rho \underline{V} Y_{NO} - \rho D_{NO} \nabla Y_{NO}) = R_{NO} = M_{NO} \frac{d[NO]}{dt} \quad (4)$$

has to be solved. This solution requires a complete knowledge of the structure of the flame. It was estimated that the formation of NO did not affect the structure of the flame, so that the structure could be computed without coupling it with the NO conservation equation, and that the computed structure could then be used for calculation of NO concentration profiles. It was deduced that atomic oxygen and nitrogen could be taken in equilibrium with their molecular species for calculating the rate of formation of nitric oxide.

The computation of the flame structure was attempted by solving the conservation equations of mass, momentum, energy and species together with combustion kinetics of the fuel. It was shown that present knowledge of methane combustion kinetics in diffusion flames is insufficient to compute a flame structure in adequate detail for NO predictions. Experimental values of temperature and species concentrations were therefore used in conjunction with the simultaneous solution of the momentum equation and the NO conservation equation to establish the structure of the flame and calculate local concentrations of nitric oxide. The calculated NO concentration profiles compare fairly well with the experimentally measured values.

The following major conclusions are derived from the present work:

1. Nitric oxide is formed in diffusion flames in the high temperature zone and diffuses towards both the fuel-rich and oxidant-rich regions.
2. The nitric oxide concentration profiles can be adequately predicted by using the Zeldovich mechanism in conjunction with equilibrium relations between the atomic and molecular species for oxygen and nitrogen. This presupposes that the flame structure can be properly established.

TABLE OF CONTENTS

Page

ABSTRACT iii

TABLE OF CONTENTS vii

LIST OF ILLUSTRATIONS x

LIST OF TABLES xiii

NOMENCLATURE xvi

SUMMARY xviii

CHAPTER

1 INTRODUCTION . . . . .

- 1.1 Literature Survey 1
- 1.2 Purpose of this Work 7

2 EXPERIMENTAL APPARATUS AND MEASUREMENT TECHNIQUES 10

- 2.1 Choice of Burner System 10
- 2.2 Burner System 12
- 2.3 Sampling System 13
- 2.4 Measurement Techniques 14
  - 2.4.1 Measurement of Nitric Oxide Concentration 15
  - 2.4.2 Measurement of Temperature 17

3 EXPERIMENTAL PROCEDURE, RESULTS AND INTERPRETATION 26

- 3.1 Experimental Procedure 26
- 3.2 Experimental Results and Interpretation 27
- 3.3 Summary of Interpretation of Experimental Results . 37

4 THEORETICAL CONSIDERATIONS 63

- 4.1 Formation Kinetics of Nitric Oxide 63
- 4.2 The System under Consideration 66
- 4.3 Calculation of Nitric Oxide Concentration Profiles . 66
- 4.4 Flame Structure 69
  - 4.4.1 Generalised Equations 70
  - 4.4.2 Equations for the Particular System under Consideration 72
  - 4.4.3 Reaction Rate Term R_i in the Species Conservation Equation for Methane Combustion 75

CHAPTER Page

4 THEORETICAL CONSIDERATIONS (Cont.)

4.4.4 Thermodynamic and Transport Properties . . 80
4.4.5 Incorporation of term R_i in the Species Conservation Equation-Flame Sheet Assumption 84
4.4.6 Simplification of Energy Equation 89
4.5 Final form of Differential Equations 90

5 COMPUTATIONAL PROCEDURES 94

5.1 Introduction 94
5.2 Computations by Solution of Elliptic Form of Equations 95
5.2.1 Computational Details 98
5.2.2 Attempted Solution with Finite Global Reaction Rate 100
5.3 Computations by Solution of Parabolic Form of Equations 101
5.3.1 Computational Details 105
5.3.2 Reaction Rate 107
5.3.3 Final Comments about this Method 111
5.4 Computations Using Experimental Results 111
5.4.1 General Outline of Approach 112
5.4.2 Introduction of the Experimental Data in the Computer Program 114
5.4.3 Final Remarks 116

6 RESULTS AND DISCUSSION 117

6.1 Presentation of Results 117
6.2 Inadequacy of Kinetic Models for Combustion in Diffusion Flames 119
6.2.1 Temperature 119
6.2.2 Oxygen Concentration Profile 121
6.2.3 Flow Field 121
6.3 Discussion of Assumptions 122
6.3.1 Emissivity of the Thermocouple 122
6.3.2 Equilibrium Atomic Oxygen Concentration . 126
6.4 Discussion of Nitric Oxide Formation in Diffusion Flames . . . .
6.4.1 Effect of Residence Time 131
6.4.2 Comparison with NO formed in Premixed Flames 133

CHAPTER Page

6 RESULTS AND DISCUSSION (Cont.)

6.4.3 Effect of Air-Fuel Velocity Ratio and Overall Eq. Ratio 135
6.5 Conclusions 136

REFERENCES 154

APPENDICES

Appendix

A EXPERIMENTAL DATA 162
B IGNITION SYSTEM 211
C OUTLINE FOR MISCELLANEOUS CALCULATIONS 214
D OUTLINE OF ADIABATIC FLAME TEMPERATURE PROGRAM 218

LIST OF ILLUSTRATIONS

Figure	Title	Page
2.1	Schematic of Counter-flow Diffusion Flame Burner showing Probed Region	19
2.2	Laboratory diffusion burner	20
2.3	Combustion gas sampling system	21
2.4	Calibration for modified Saltzman analysis technique (Reagent Volume 10.0 cc)	22
2.5	Calibration for modified Saltzman analysis technique (Reagent Volume 5.0 cc)	23
2.6	Photograph of Overall Burner System	24
2.7	Photograph of the system, showing flame, micromanipulator and probe	25
3.1	Temperature Profile, Flame Condition A-0.5	41
3.2	Temperature Profile, Flame Condition A-1.0	42
3.3	Temperature and Species Concentration Profiles, Flame Condition A-2.0	43
3.4	Temperature and Species Concentration Profiles, Flame Condition A-17.0	44
3.5	Temperature and Species Concentration Profiles, Flame Condition A-47.5	45
3.6	Temperature and Species Concentration Profiles, Flame Condition A-117.5	46
3.7	Temperature and Species Concentration Profiles, Flame Condition A-324.0	47
3.8	Temperature Profile, Flame Condition B-0.5	48
3.9	Temperature Profile, Flame Condition B-2.0	49
3.10	Temperature and Species Concentration Profiles, Flame Condition B-17.0	50
3.11	Temperature and Species Concentration Profiles, Flame Condition B-47.5	51
3.12	Temperature and Species Concentration Profiles, Flame Condition B-117.5	52

Figure	Title	Page
3.13	Temperature and Species Concentration Profiles, Flame Condition B-324.0	53
3.14	Temperature Profile, Flame Condition C-0.5	54
3.15	Temperature Profile, Flame Condition C-2.0	55
3.16	Temperature Profile, Flame Condition C-17.0	56
3.17	Temperature and Species Concentration Profiles, Flame Condition C-47.5	57
3.18	Temperature and Species Concentration Profiles, Flame Condition C-117.5	58
3.19	Temperature and Species Concentration Profiles, Flame Condition C-324.0	59
3.20	Oxygen Concentration Profile, Flame Condition A-17.0	60
3.21	Comparison of NO Concentration Profiles at different axial locations, Flame Condition A	61
3.22	Comparison of Temperature Profiles at different axial locations, Flame Condition A	62
4.1	Schematic of Theoretical System Considered	65
5.1	Grid and Boundary Conditions for solution of elliptic form of equations	99
6.1	Calculated and Experimental NO Concentration Profiles, Flame Condition A-47.5	140
6.2	Calculated and Experimental NO Concentration Profiles, Flame Condition A-117.5	141
6.3	Calculated and Experimental NO Concentration Profiles, Flame Condition B-117.5	142
6.4	Calculated and Experimental NO Concentration Profiles, Flame Condition C-117.5	143
6.5	Calculated rate of formation of NO at two axial locations, Flame Condition A	144
6.6	Calculated Temperature and Species Concentration Profiles 1" (25.4 mm) above burner entrance; using Flame Sheet assumption, Flame Condition A	145

Figure	Title	Page
6.7	Calculated Temperature and Species Concentration Profiles 2" (50.8 mm) above burner entrance; using Flame Sheet assumption, Flame Condition A	146
6.8	Calculated Temperature and Species Concentration Profiles 5" (127.0 mm) above burner entrance; using Flame Sheet assumption, Flame Condition A	147
6.9	Calculated Temperature and Species Concentration Profiles 13" (330.2 mm) above burner entrance; using Flame Sheet assumption, Flame Condition A	148
6.10	Calculated Temperature and Species Concentration Profiles; using Finite Global Reaction Rate, Flame Condition A-47.5	149
6.11	Calculated Temperature and Species Concentration Profiles; using Finite Global Reaction Rate, Flame Condition A-117.5	150
6.12	Extrapolation of maximum temperature at 10.0 mm axial location; Flame Condition A	151
6.13	Calculated NO Concentration Profiles using different emissivity values for temperature correction; Flame Condition A-47.5	152
6.14	NO Mass Flow Rate - Residence Time History, Flame Condition A	153

Appendices

B.1	Circuit diagram of modified automotive ignition system	212
B.2	Modified spark plug.	213

LIST OF TABLES

Table	Title	Page
3.1	Burner Operating Conditions	39
3.2	Type of determinations made at each axial location corresponding to each flame condition	40
5.1	Values of Coefficients in Equation 5.1	97
5.2	Values of d and f in Equation 5.2	104
6.1	Integrated Values of Calculated and experimental NO profiles in terms of mass and number of moles of NO flowing through a particular axial plane of burner per sec.	138
6.2	Integrated Values of experimental NO profiles for Flame Condition A in terms of mass of NO flowing per second through an axial plane	139

Appendices

Table	Title	Page
A-A-1	Temperature Profile, Flame Condition A-0.5	164
A-A-2	Temperature Profile, Flame Condition A-1.0	165
A-A-3-1	Temperature Profile, Flame Condition A-2.0	166
A-A-3-2	Species Concentration (Dry) Profiles, Flame Condition A-20	167
A-A-4-1	Temperature Profile, Flame Condition A-17.0	168
A-A-4-2	Species Concentration (Dry) Profiles, Flame Condition A-17.0	170
A-A-4-3	NO Concentration (Dry) Profile, Flame Condition A-17.0	172
A-A-5-1	Temperature Profile, Flame Condition A-47.5	173
A-A-5-2	Species Concentration (Dry) Profiles, Flame Condition A-47.5	174
A-A-5-3	NO Concentration (Dry) Profiles, Flame Condition A-47.5	175
A-A-6-1	Temperature Profiles, Flame Condition A-117.5 . . .	176
A-A-6-2	Species Concentration (Dry) Profiles, Flame Condition A-117.5	177

Table	Title	Page
A-A-6-3	NO Concentration (Dry) Profile, Flame Condition A-117.5	178
A-A-7-1	Temperature Profile, Flame Condition A-324.0	179
A-A-7-2	Species Concentration (Dry) Profiles, Flame Condition A-324.0	180
A-A-7-3	NO Concentration (Dry) Profile, Flame Condition A-324.0	181
A-B-1-1	Temperature Profile, Flame Condition B-0.5	183
A-B-2-1	Temperature Profile, Flame Condition B-2.0	184
A-B-3-1	Temperature Profile, Flame Condition B-17.0	185
A-B-3-2	Species Concentration (Dry) Profiles, Flame Condition B-17.0	186
A-B-4-1	Temperature Profile, Flame Condition B-47.5	188
A-B-4-2	Species Concentration (Dry) Profiles, Flame Condition B-47.5	189
A-B-4-3	NO Concentration (Dry) Profile, Flame Condition B-47.5	191
A-B-5-1	Temperature Profile, Flame Condition B-117.5	192
A-B-5-2	Species Concentration (Dry) Profiles, Flame Condition B-117.5	193
A-B-5-3	NO Concentration (Dry) Profile, Flame Condition B-117.5	194
A-B-6-1	Temperature Profile, Flame Condition B-324.0	195
A-B-6-2	Species Concentration (Dry) Profiles, Flame Condition B-324.0	196
A-B-6-3	NO Concentration (Dry) Profile, Flame Condition B-324.0	197
A-C-1-1	Temperature Profile, Flame Condition C-0.5	199
A-C-2-1	Temperature Profile, Flame Condition C-2.0	200
A-C-3-1	Temperature Profile, Flame Condition C-17.0	201
A-C-4-1	Temperature Profile, Flame Condition C-47.5	202
A-C-4-2	Species Concentration (Dry) Profiles, Flame Condition C-47.5	203

Table	Title	Page
A-C-4-3	NO Concentration (Dry) Profiles, Flame Condition C-47.5	204
A-C-5-1	Temperature Profile, Flame Condition C-117.5	205
A-C-5-2	Species Concentration (Dry) Profile, Flame Condition C-117.5	206
A-C-5-3	NO Concentration (Dry) Profile, Flame Condition C-117.5	207
A-C-6-1	Temperature Profile, Flame Condition C-324.0	208
A-C-6-2	Species Concentration (Dry) Profiles, Flame Condition C-324.0	209
A-C-6-3	NO Concentration (Dry) Profile, Flame Condition C-324.0	210

NOMENCLATURE

$\underline{V}$	the velocity vector
u	the velocity along the stream
v	the velocity in the cross stream direction
p	the fluid pressure
T	the fluid temperature
ρ	the density of the mixture
h'	the stagnation enthalpy of the mixture
h	the enthalpy of the mixture
h_j	the enthalpy of component j
^0h_j	the negative heat of formation of component j
c_{pj}	the specific heat per unit mass of component j at constant pressure
c_p	the specific heat of the mixture per unit mass
Y_j	the mass fraction of species j
X_j	the mole fraction of species j
C_j	the concentration (moles/c.c.) of species j
R_j	the rate of production of species j in terms of mass per unit volume
μ_j	the viscosity of species j
μ	the viscosity of the mixture
D_j	the binary diffusion coefficient of species j with all other species
λ	the thermal conductivity of the mixture
R	the universal gas constant

M_j	the molecular weight of species j
M	the mean molecular weight of the mixture
τ	the stress tensor
Γ_j	exchange coefficient of species j $(= \rho D_j)$
Γ_h	exchange coefficient of thermal energy $(= \frac{\lambda}{c_p})$
J_j	diffusional flux of species j $(= -\Gamma_j \text{ grad } Y_j)$ according to Fick's law of diffusion
J_h	heat flux $(= -\Gamma_h c_p \text{ grad } T)$ according to Fourier's Law of conduction

Subscripts 1, 2, 3, 4, 5 and 6 stand for CH_4, O_2, N_2, CO_2, H_2O and NO respectively

SUMMARY

The purpose of this work has been to investigate the processes leading to the formation of nitric oxide in a vertical, co-axial, atmospheric pressure, methane-air diffusion flame burner; which models many of the physico-chemical processes occurring in combustion systems using fuel sprays, for example diesel engines, and gas turbines. Experimentally, radial concentration profiles of nitric oxide have been determined in this burner at prescribed axial locations. In addition, in order to produce an overall picture of the flame structure, concomitant temperature and concentration profiles for CO, CO_2, O_2, N_2 and CH_4 have been determined. In order to analytically predict NO concentration profiles, the NO conservation equation was solved using known models of its formation kinetics, in conjunction with the experimental values of temperature and species concentrations and the solution of the momentum equation.

A literature survey on the formation kinetics of nitric oxide in combustion systems and diffusion flames is presented in Chapter 1. This survey indicates that in premixed flames the rate of formation of NO can be accurately predicted by using the Zeldovich mechanism i.e.:

$$N_2 + O \rightleftharpoons NO + N \qquad (1)$$

$$O_2 + N \rightleftharpoons NO + O \qquad (2)$$

In most of these studies, the NO formation is approximated by assuming that the combustion reactions have been equilibrated prior to the onset of NO formation. However from measurements in premixed hydrocarbon-air flames, it is reported that immediately within the flame front NO formation rates exceed those predicted by the above mechanism along with the equilibrium assumption. This extra NO is termed "prompt NO" and is especially prominent in rich mixtures. In a shock tube study, it has been shown that above reaction mechanism is sufficient for all cases if the hyper-equilibrium concentration of atomic oxygen in the initial stages is taken into account. This is achieved by considering the combustion kinetics and the NO formation kinetics together, thereby eliminating the equilibrium assumption. With regard to diffusion flames, the literature survey indicates that the fuel is initially decomposed primarily by pyrolysis reactions, and that in the hottest part of the flame, (i) chemical reaction is not the rate determining process, and (ii) the average temperature of the reaction zone is near the theoretical maximum.

The experimental apparatus and the measurement techniques used in this study are presented in Chapter 2. A co-axial diffusion flame burner has been designed to produce the desired flame. The flame is enclosed in a vertical quartz tube interposed with steel flanges to provide for sample probe insertions at a number of axial locations. Radial concentration profiles at prescribed axial locations were determined for nitric oxide and other species through analysis of samples extracted from the flame by means of a quartz microprobe having a diameter of the order of 0.002". Nitric oxide concentrations were determined using a modified Saltzman technique. Combustion product and reactant concentrations were determined through use of a thermal conductivity gas chromatograph. Radial temperature profiles were determined with a Pt/Pt-10% Rh thermocouple of 0.001" diameter wire.

The experimental results and their interpretation are presented in Chapter 3. These results show that this diffusion flame can be roughly divided in four regions, namely:

- A non-reactive space near the base of the flame
- A premixed-like annular region downstream of non-reactive space
- A true diffusion flame zone in which energy release reactions are mainly confined to a narrow but finite annular zone
- A carbon zone, beginning at the level where all of the fuel on the flame axis has been either consumed or transformed to soot, and extending to the luminous tip of the flame

These results further show that nitric oxide is formed mainly in the narrow intense temperature region and diffuses both to the fuel-rich and oxidant-rich regions. The slopes of concentration profiles show that the formation of NO in the fuel-rich region is not significant, indicating absence of "prompt NO" or the effects of hyper-equilibrium 'O' concentration. This last point is discussed further in Chapter 6.

The temperature profiles show the existance of an endothermic zone in the fuel-rich region, most probably due to pyrolysis reactions. The oxygen concentration profiles show a finite concentration of oxygen in the fuel-rich region.

Theoretical considerations involved in predicting the NO concentration profiles from first principles are presented in Chapter 4. Using the Zeldovich mechanism, the rate of formation of NO in an elementary control volume is obtained as

$$\frac{d[NO]}{dt} = k_{1f}(T)[N_2][O] + k_{2f}(T)[O_2][N] - k_{1b}[NO][N]$$
$$-k_{2b}(T)[NO][O]$$

However, the prediction of the NO concentration profiles in the burner also requires the solution of the NO conservation equation,

$$\nabla \cdot (\rho \underline{V} Y_{NO} - \rho D_{NO} \nabla Y_{NO}) = R_{NO} = M_{NO} \frac{d[NO]}{dt}$$

which requires a complete knowledge of the flame structure. It was argued that, because of low concentration levels, the formation of NO did not affect the flame structure. Thus the analysis of the latter could be decoupled from the NO conservation equation, and the computed structure could then be used for the calculation of NO concentration profiles, using equilibrium relations between the atomic and molecular species for oxygen and nitrogen. Hyper-equilibrium concentrations of atomic oxygen were not considered to be important in the present case, based on the experimental data and the time scales involved. A detailed discussion of this is given in Chapter 6.

The conservation equations required for the computation of the flame structure are developed and known models of combustion kinetics of methane in diffusion flames are discussed. The final form of these equations based on global finite reaction rate for methane combustion, is presented at the end of Chapter 4.

The computational methods used to solve the equations developed in Chapter 4 are detailed in articles 5.2 and 5.3. The results of these computations, presented and discussed in Chapter 6, show that the widely used models of combustion kinetics in diffusion flames are insufficient to compute a flame structure in adequate detail for NO predictions. Consequently, experimental values of temperature and species concentration were used in conjunction with a simultaneous solution of momentum and NO conservation equations to compute the flame structure and the local concentrations of nitric oxide. The thermocouple emissivity value for radiation correction of experimental temperatures is discussed in Chapter 6. Computational aspects of combining experimental values of temperature and species concentrations with the solution of momentum and NO conservation equations are detailed in article 5.4.

Finally, the calculated NO concentration profiles based on the Zeldovich mechanism and O and N equilibria are presented and discussed in Chapter 6. They compare very well with the experimental results in oxidant-rich regions and only moderately well in fuel-rich regions.

The following major conclusions are derived from the present work:

1. Nitric oxide is formed in diffusion flames in the high temperature zone and diffuses towards both the fuel-rich and oxidant-rich regions.
2. The nitric oxide concentration profiles can be adequately predicted by using the Zeldovich mechanism in conjunction with equilibrium relations between the atomic and molecular species for oxygen and nitrogen. This pre-supposes that the flame structure can be properly established.

CHAPTER 1
INTRODUCTION

1.1 Literature Survey

Combustion generated oxides of nitrogen are presently recognised as major pollutants, which react in the atmosphere to form photochemical smog and also are toxic (48)*. It has been demonstrated that nitric oxide (NO) is the principle oxide of nitrogen associated with combustion products (4,11,45), and is later oxidised to nitrogen dioxide (NO_2) in the atmosphere contributing to formation of smog and toxity.

For this reason, emission of NO from combustion systems has been studied extensively over the past years. For the most part these studies have been related to spark ignition engines in which premixed flames occur, as these engines have been the major contributors to the total man made oxides of nitrogen (48). Early investigations in this area studied the effects of engine operating parameters like fuel air ratio, ignition timing, engine load etc., on exhaust concentration of nitric oxide. With the refinement of techniques, studies relating to the behaviour of NO after its formation in the spark ignition engines have demonstrated that once formed in combustion process, nitric oxide remains fixed throughout the expansion and exhaust processes (52,79). Recent studies investigating the formation mechanism of nitric oxide in a combustion vessel (51,63) and in the cylinder of an engine (42) have shown that nitric oxide is formed primarily in post flame combustion gases and that the time required for formation is significant. Similar results have been arrived at in a theoretical study in flow reactors (46). Further, the combustion vessel studies (51,63) have demonstrated that nitric oxide formation rates can be predicted with reasonable accuracy through consideration of two elementary reactions

---

*Number in parenthesis designate References at the end.

$$N_2 + O \rightleftharpoons NO + N$$

$$O_2 + N \rightleftharpoons NO + O$$

normally known as the Zeldovich mechanism for NO formation, with oxygen and nitrogen atom concentrations set equal to their chemical equilibrium value. Most other studies agree with above mechanism.

From steady flow burner measurements for a hydrocarbon premixed flame (18), this author suggested that the above mechanism is not sufficient to predict the formation of nitric oxide immediately within the flame front. The formation of this "prompt NO" through some fuel derived specie reaction in that region was then postulated. In recent shock tube studies (6,8), it has been shown that initial rate of formation of nitric oxide can be explained by taking into account the non-equilibrium concentration of atomic oxygen during the initial time period. However these findings have not been observed by other workers (42,51,63).

Combustion systems based on burning of fuel sprays, as example diesel engines and gas turbines involve diffusion flames in which mixing of the fuel with oxidizer occurs simultaneously with combustion. It is generally recognized that these systems can be designed to emit smaller quantities of hydrocarbons and carbon monoxide as compared with conventional spark-ignition engines. However, they emit significant quantities of nitric oxide. Studies of nitric oxide from gas turbines and from diesel engines have for the most part been related to determination of measured exhaust concentration as influenced by engine operating parameters (4,45, 61,65...).

Some commonly studied diesel engine variables are air-fuel ratio, injection timing, engine load, combustion chamber design, speed, air swirl etc. Such studies, while quite valuable in themselves, do not provide basic knowledge of the formation mechanism of nitric oxide in systems with simultaneous mixing and chemical reaction. As in the case of spark ignition engine, it is found that the time available, temperature and oxygen concentration are important variables and that any engine parameters affecting the above variables will affect the formation of nitric oxide. Khan et al (38) have attempted to predict NO formation in diesel engines, however, due to the complexity of the hetrogeneous combustion model their results are not conclusive.

Similarly, in the case of gas turbines, effects of parameters like air fuel ratio, pressure, nozzle configuration etc. on nitric oxide formation has been studied. Detailed studies of gas turbine combustion have demonstrated that the concentrations of nitric oxide in exhaust gases are always below the chemical equilibrium level (12,13). In one case, experimental results obtained with a laboratory combustor have been interpreted as indicative of significant NO decomposition late in the combustion process (12). However, this cannot be accounted for by known kinetic mechanisms. Using a simplified thermodynamic model for the primary zone - a plug flow or a well stirred reaction - and the Zeldovich mechanism for nitric oxide kinetics, nitric oxide concentrations have been predicted (32), however, simplifying assumptions in the thermodynamic model render the results inconclusive.

It is thus apparent from above that due to the complexity of the thermodynamic model the study of NO formation in complex industrial combustion systems is very difficult. However, as these combustion systems essentially involve diffusion flames, it would seem reasonable that a study of simple diffusion flame, more amenable to experimental and theoretical investigation, will be able to provide significant information.

Formation of nitric oxide in simple diffusion flames has received little attention so far. Recently nitric oxide formation in droplet diffusion flames has been studied theoretically (9). However, in absence of experimental data the conclusions are only qualitative.

Diffusion flames, as such have been studied for many years, though not as intensely as premixed flames, because of their obvious complexity. These early studies related to determination of flame height and shape only. Burke & Schumann in 1928 (10) were first to present a comprehensive study of diffusion flame and introduced the assumption of an infinitely fast reaction rate. As a consequence, they took the actual zones of combustion to be infinitely thin with the mixing process alone being responsible for the rate of burning and for flame location and size. Burke & Schumann (10) successfully used their assumption for the calculation of shape and length of the laminar diffusion flame formed when a fuel jet discharges within a confined air stream moving at the same velocity as the fuel jet. The same assumption has been used by Hottel & Hawthorne (36), Wohl, Gazley & Kapp (80), Yagi & Saji (86) and Barr (3) for prediction of the length of open flames, both laminar and turbulent. A flame height expression containing an unknown function is approximated, which is then determined empirically from the results of their experiments. Fay (16) has determined theoretically the shape and characteristics of a laminar diffusion flame based on the same assumption. In addition this assumption has been used quite frequently in fuel droplet combustion studies.

The Burke-Schumann assumption eliminates chemical kinetics from the process, simplifying the governing equations and their solution. However, this solution does not establish complete structure of the flame, nor does it provide a criterion for the extinction of the flame or for the validity of assumption and solution.

Zeldovich (66) was the first to take into account the finite reaction rate and thus the finite thickness of the reaction zone to explain the blowing-off phenomenon. Similar studies have been performed by Spalding (67-69) with the purpose of relating the fuel consumption rate for unit area at extinction and the fuel consumption rate per unit area in a premixed flame.

The first detailed experimental study of the structure of the reaction zone of a flat diffusion flame using a rectangular burner was made by Wolfhard & Parker (61,62) by measurements on emission and absorption spectra of the zone. They found that the reaction zone is of finite thickness and can be upto a few millimeters thick for flames with air as oxidant. They also concluded that the usual assumption made for diffusion flames, i.e. the chemical reaction rate is not the rate determining process, is true, but only for the hottest part of the reaction zone; the preheating zones on both sides of reaction zone show an interesting sequence of chemical reaction. Further, it was noted that in the diffusion flame the average temperature of the reaction zone is near the theoretical maximum. In hydrocarbon - oxygen flames, they noted that fuel is destroyed primarily by pyrolysis before coming into contact with oxygen.

Smith & Gordon (1956) (64) and Gordon, Smith & McNesby (26) conducted sampling studies of methane - air diffusion flames, using quartz microprobes and mass-spectrometer for analysis. They support and further emphasize that pyrolysis is the most important route for disappearance of methane, though it is not possible to determine the percentage of methane disappearing through this path.

This aspect has been further confirmed by Pandya & Weinberg (56,57) using a counter flow diffusion flame and by Tsuji & Yamaoka (71-73) using a porous cylinder for supplying fuel and establishing a counter flow diffusion flame in the forward stagnation region. Both investigators have calculated heat release profiles and found negative heat release in the carbon zone of the fuel core and attributed it to pyrolysis of fuel.

1.2 Purpose of this Work

From the foregoing survey, it is apparent that the formation mechanism of NO in premixed flames is well understood, however there is no definite indication that this mechanism applies to the diffusion flames, particularly in view of simultaneous mixing and chemical reaction which results in fuel pyrolysis. The study of nitric oxide formation directly in industrial combustion systems, though useful, does not provide any new information or confirmation to widely believed concepts about NO. A basic reason for this is the fact that nitric oxide formation is extremely sensitive to temperature, and it is difficult to arrive at exact local temperatures with existing thermodynamic models. Study of nitric oxide formation in a laboratory diffusion flame, on the other hand, can yield this type of information. A literature survey of laboratory diffusion flames indicates that the structure of the flame can be established reasonably well experimentally and that it may be possible to arrive at it theoretically as well.

This program of study has thus been undertaken with the object of investigating the formation of nitric oxide in a diffusion flame, which has physical conditions similar to those occuring in combustion systems of interest.

The study has involved experimental and theoretical investigation of nitric oxide formation and its concentration profiles in laminar diffusion flames.

Local combustion gas samples were extracted from flames, at various downstream positions, using quartz microprobes and analysed for NO by a modified Saltzman technique, thus establishing NO concentration profiles. In addition to NO concentration profiles, concomitant temperature and concentration profiles for CO, CO_2, O_2, N_2 and the fuel, CH_4 have been obtained.

A theoretical study has been carried out to predict the formation of nitric oxide and its concentration profiles. This has involved the development and simultaneous solution of conservation equations involving mass, momentum and energy transfer together with the combustion kinetics of methane and formation kinetics of nitric oxide to establish the local temperature and species concentration values. It is subsequently shown that only partial knowledge of combustion kinetics of methane in diffusion flames, renders existing models inadequate to establish detailed structure even in this simple flame. Experimental values of temperature and species concentrations are then used in conjunction with the simultaneous solution of the momentum equation and NO conservation equation to establish the structure of the flame and calculate local concentrations of nitric oxide.

CHAPTER 2

EXPERIMENTAL APPARATUS AND MEASUREMENT TECHNIQUES

2.1 Choice of Burner System

Three main types of laboratory diffusion flame burners have been used in past by various investigators. Burke & Schumann (10) and some others used a co-axial burner in which fuel is supplied through the central tube and the oxidant through the surrounding tube. Wolfhard and Parker (81, 82) used two parallel rectangular tubes having one side in common to supply fuel and air. The flame front is kept stabilised, in this case, by surrounding it with a stream of nitrogen which flows in the outer jacket. A counterflow diffusion flame was established by Pandya & Weinberg (56, 57) in the counterflow region of two directly opposed jets of individual reactant streams.

The flat flame burner and counterflow diffusion flame burner were primarily designed to study the flames optically or spectroscopically.

In a preliminary survey for determining the most suitable method for NO concentration, it was realised that spectroscopic technique could not be used for this purpose, particularly in the fuel-rich region, due to the presence of carbon. Further, Weinberg (76) indicates that in flat flame burner, the uncertainities associated with the flame's vertical edges, where mixing with atmosphere occurs, may be particularly damaging to quantitative optical methods. The counterflow diffusion flame burner has a complicated aerodynamic structure and though extremely useful for determining overall reaction rates, will be disturbed significantly if sample probes were introduced. Thus it was decided to use a simple co-axial diffusion flame burner, which is axially symmetric but has uncertainities concerning the flame base.

Towards the end of this investigation, this author came across a counterflow diffusion flame burner used by Tsuji & Yamaoka (71,72,73) in which the flame is stabilized in the forward stagnation region of a porous cylinder. Tsuji & Yamaoka (73) made a structural study of the flame by probing it along a plane normal to the luminous flame zone, as shown in Figure 2.1, so that for most part of the flame a one dimensional approximation could be used. This is a true diffusion flame and does not have any unreactive space or premixed-like region as in the case of the co-axial type of burner, discussed in Chapter 3. It would be advantageous to consider this burner for any future studies of this type.

In a review of literature of flame studies, Fristrom and Westenberg (23), Surugu (70) indicated that quartz microprobes could be used for extracting reliable gas samples. This survey also indicated that local temperature measurement by proper thermocouples was probably one of the best and definitely the simpliest of all available methods. The obvious drawback is of course to reliably account for radiation and conduction losses.

2.2 Burner System

A vertical co-axial diffusion flame burner shown schematically in Figure 2.2 has been designed to produce an enclosed steady laminar diffusion flame burner. The fuel, methane in the present case is fed from a compressed methane cylinder and metered through a sonic nozzle. The fuel is fed to the burner, downstream of the nozzle through a 30" long straight vertical fuel tube of nominal 5/8" (15.9 mm) size, in order to have a fully developed flow. Air, obtained from a laboratory supply is metered in a similar manner and is fed through a 30" long straight vertical outer tube of 43 mm inside diameter, surrounding and concentric with the fuel tube. Fuel and air flow rates can be regulated by adjusting pressures upstream of the sonic nozzles. Upstream pressures are read on precision pressure gauges.

Air and fuel flow rates for the desired experimental conditions were determined by using wet test meters, which in turn were calibrated against a positive water displacement apparatus. The velocity profiles for both fuel and air were checked for the experimental conditions used, by making a traverse with an Alnor portable hot wire anemometer. The profiles were found to be parabolic, as expected under laminar flow conditions. An automotive type ignition system has been modified (Appendix B) to produce a continuous spark discharge as an ignition source. The flame is enclosed in vertical quartz tubing elements interposed with steel flanges providing for sample probe insertion at a number of prescribed axial locations.

Sealing between the quartz tubes and metal flanges is achieved with O rings. Each flange has four radially drilled holes tapped for 1/8" pipe fittings. These holes are ordinarily closed by suitable pipe plugs.

2.3 Sampling System

Combustion gas samples are withdrawn from various radial positions across the flange by means of a horizontal quartz microprobe introduced through the flame. The quartz microprobes were prepared according to the suggestion of Fristrom and Westenberg (23). The microprobe has an inside diameter of the order of 0.002" and maximum outside diameter of the order of 0.020" at the probe tip. The probe assembly is attached to the flange by mounting the central part of the probe in a 1/4" stainless steel tube which is then introduced into the radial flange hole and held by a drilled 1/4" Swagelok tube fitting. Sealing of the stainless steel tube is achieved by means of an 'O' ring kept in place by a ferroule and Swagelok fitting nut. The outer end of the stainless steel tube is rigidly held with a micromanipulator mounted on the frame of the burner housing. The radial position of the sampling probe is adjusted and measured by means of this micromanipulator having a least count of 0.1 mm. The radial position of probe was read as distance from the flange wall. The axial position of the probe was estimated by taking the thickness of the flange, and height of the quartz tubing element into account.

The sampling system is shown schematically in Figure 2.3. Gas samples are collected in a previously purged and evacuated variable volume sampling vessel. Operation of a valve diverts the continuous sample flow from the vacuum system to the sampling vessel. Water is removed from the sample by means of an ice bath located in the sampling line upstream of the sampling vessel. Sonic flow conditions are maintained at the probe tip by maintaining a prescribed vacuum in the sampling line. Thus rapid freezing of reactions involving chemical species of interest is ensured. From the observed sampling rates the residence time of sampling gases in the high temperature portion of the probe is found to be on the order of 0.1 m sec. Finally the sample is brought to atmospheric pressure by permitting the volume to adjust itself to atmospheric pressure and is withdrawn for analysis, by means of a 100 ml syringe through a rubber septum.

In some fuel-rich regions of flame, blockage of the passage through the probe was experienced due to soot accumulation and the probe had to be cleaned. The best method of cleaning appeared to be the oxidation of the soot by heating on a Bunsen burner.

2.4 Measurement Techniques

Combustion gas samples are analysed for nitric oxide using a modified Saltzman technique to be described later, and for CO, CO_2, N_2, O_2 and CH_4 through use of a Barber-Colman, Model 5340, thermal conductivity gas chromatograph. This chromatograph employs two columns, silica gel (50/60 mesh) and molecular sieve (type 5A) packed in 1/4" stainless steel tubing of one foot and six feet length respectively, in series, to separate CO_2 and CO, N_2, and CH_4. The columns were maintained at room temperature. The carrier gas used was high purity helium supplied by Matheson Company. The flow rate of helium was 60 c.c./min and was measured with the help of a soap bubble flow meter. The sample, 2.0 c.c., was introduced into the carrier gas stream using a standard sampling valve. The chromatograph was calibrated using standard analysed mixtures of appropriate gases in nitrogen, supplied by Matheson Company.

Chromatograms were recorded by a Barber-Colman chromtography recorder model PR 25. The millivolt span used was 1 mv. Peak heights of species in chromatogram were used in quantitative calibrations as well as subsequent determination of species in samples.

2.4.1 Measurement of Nitric Oxide Concentration

During the initial phase of study, nitric oxide concentrations were determined by an ultraviolet spectroscopic technique developed by Nicksic & Harkins (53). This technique involves oxidation of NO to NO_2 and measurement of ultraviolet absorption by NO_2. It was found that the sensitivity of the ultraviolet technique was not sufficient to accomodate the entire concentration range of interest, and consequently these determinations could not be considered reliable. However, the initial work did establish the order of magnitude of concentration of NO in the flame as ranging from 10 to 100 p.p.m.

The Saltzman analytical technique (21,27,59,60) often used for measurement of atmospheric concentrations of NO_2 up to concentration of not more than 5 p.p.m. and similar concentration of NO by first oxidising to NO_2, appeared amenable to modification for measurement of higher concentrations in the range of interest in this work. While developing a modified technique, it was considered desirable that in the interest of minimising sampling time the total amount of sample required for analysis should be limited.

After lengthy trials, the following procedure was finally adopted for nitric oxide analysis.

- A measured quantity (usually 10 c.c.) of Saltzman reagent is pipetted into a 250 c.c. Erlenmeyer flask.
- The flask is evacuated.
- A measured quantity of gas sample (usually 50 c.c.) is introduced into the flask through a septum using a syringe. The flask is then filled with pure oxygen bringing it to atmospheric pressure.
- The resulting mixture of sample, oxygen and reagent is stirred with a teflon coated motor-driven magnetic stirrer for 15 minutes.

- The optical density or absorbance of the reagent from the flask is measured against that of unreacted reagent using a Beckman Model B spectrophotometer set at 550 mμ wave length.
- The NO concentration is determined from calibration curves prepared earlier using standard analysed NO - N_2 mixture.

Standard analysed NO - N_2 mixture supplied by the Matheson Company containing 20, 53, 105, and 310 p.p.m. of NO were used initially for establishing the method and later for calibration purposes.

The above procedure yielded generally satisfactory results. Repeatability of measurements was better than ± 3% in optical density for samples in the range of 20 - 105 p.p.m.

The quantity of Saltzman reagent has to be varied depending upon the NO concentration in order to maintain the optical density within reasonable limits.

Figures 2.4 and 2.5 show two typical calibration curves using 10 c.c. and 5c.c. of Saltzman reagent respectively.

2.4.2 Measurement of Temperature

Radial temperature profiles at fixed axial locations were measured with a silica coated Pt/Pt - 10% Rh thermocouple of 0.001" diameter wire having a junction of 0.005" diameter.

Thermocouples were constructed by flame welding fine wires of about 0.5 cm length to support leads of the same material 0.012" in. diameter. The assembly of wires was essentially Y-shaped with heavy wires forming the Y and in turn being supported by a length of insulated tubing with the fine wires strung across the top of the Y. The heavy wires were bent, so as to put the fine wires in tension; thus the fine wires could be held taut and normal to the flow. The junction itself was made by carefully manipulating the fine wires and then welding with a microtorch. Silica coating of the thermocouples was done according to the method of Fristrom & Westenberg (23).

As in the case of the sample probe, the thermocouple was mounted in a stainless steel tube and introduced radially through the flange. Its radial position was adjusted and measured by means of the micromanipulator. The E.M.F. generated was measured by using a precision potentiometer and temperature read from standard thermocouple tables for Pt/Pt - 10% Rh.

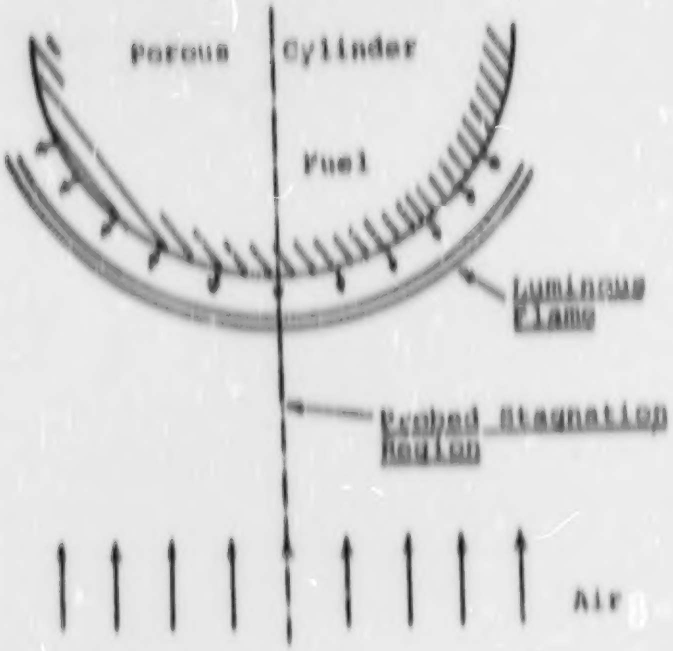
Porous Cylinder
Fuel
Luminous Flame
Probed Stagnation Region
Air

Figure 2.1: Schematic of counter-flow diffusion flame burner showing probed region

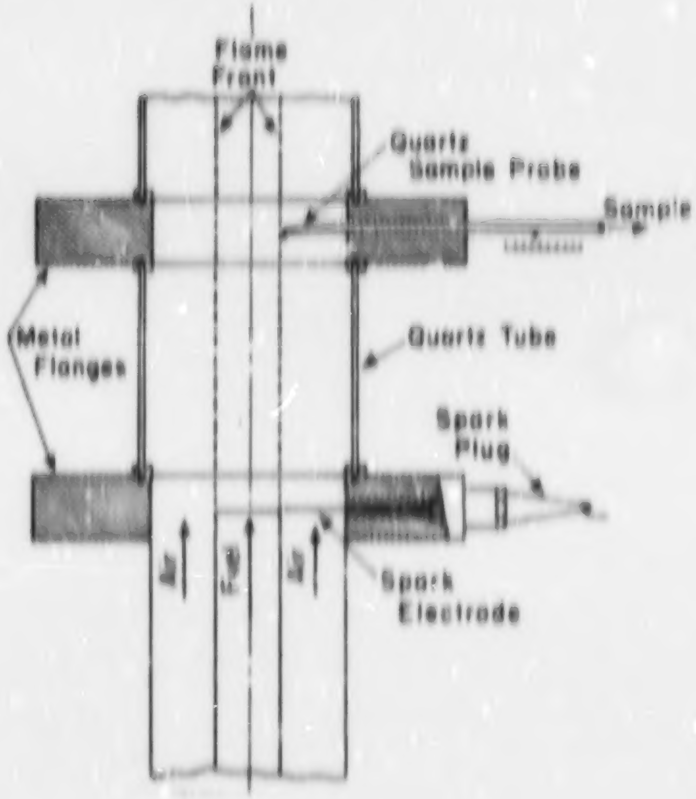
Flame Front
Quartz Sample Probe
Sample
Metal Flanges
Quartz Tube
Spark Plug
Air
Fuel
Air
Spark Electrode

Figure 2.2: Laboratory diffusion burner

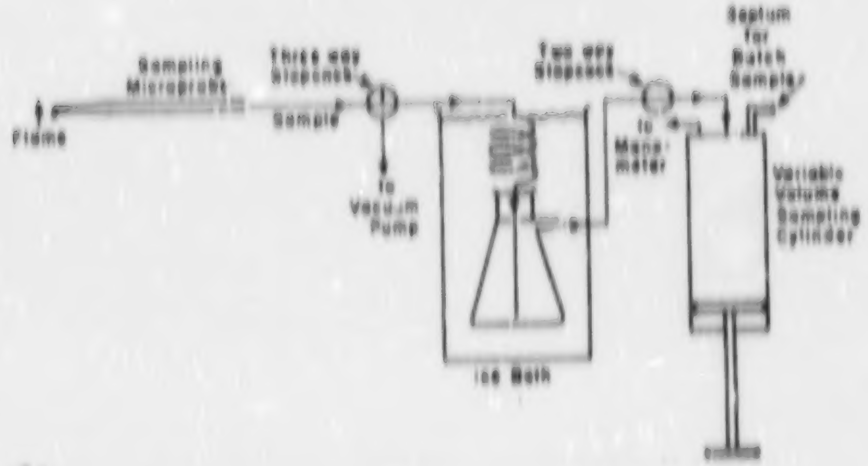
Sampling Microprobe
Flame
Three way Stopcock
Sample
To Vacuum Pump
Ice Bath
Two way Stopcock
To Manometer
Septum for Batch Samples
Variable Volume Sampling Cylinder

Figure 2.3: Combustion gas sampling system

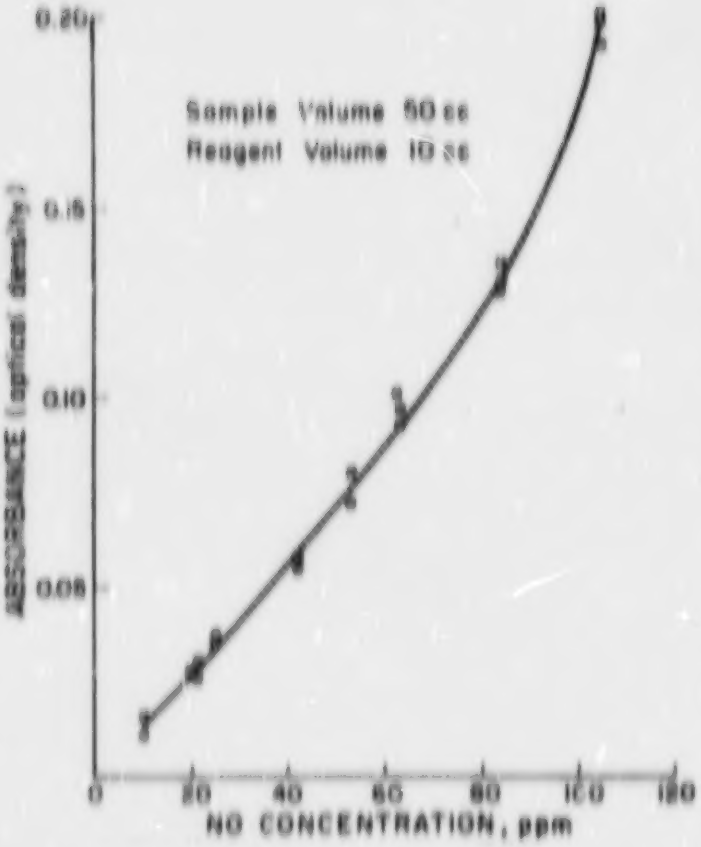

Figure 2.4: Calibration for modified Saltzman analysis technique

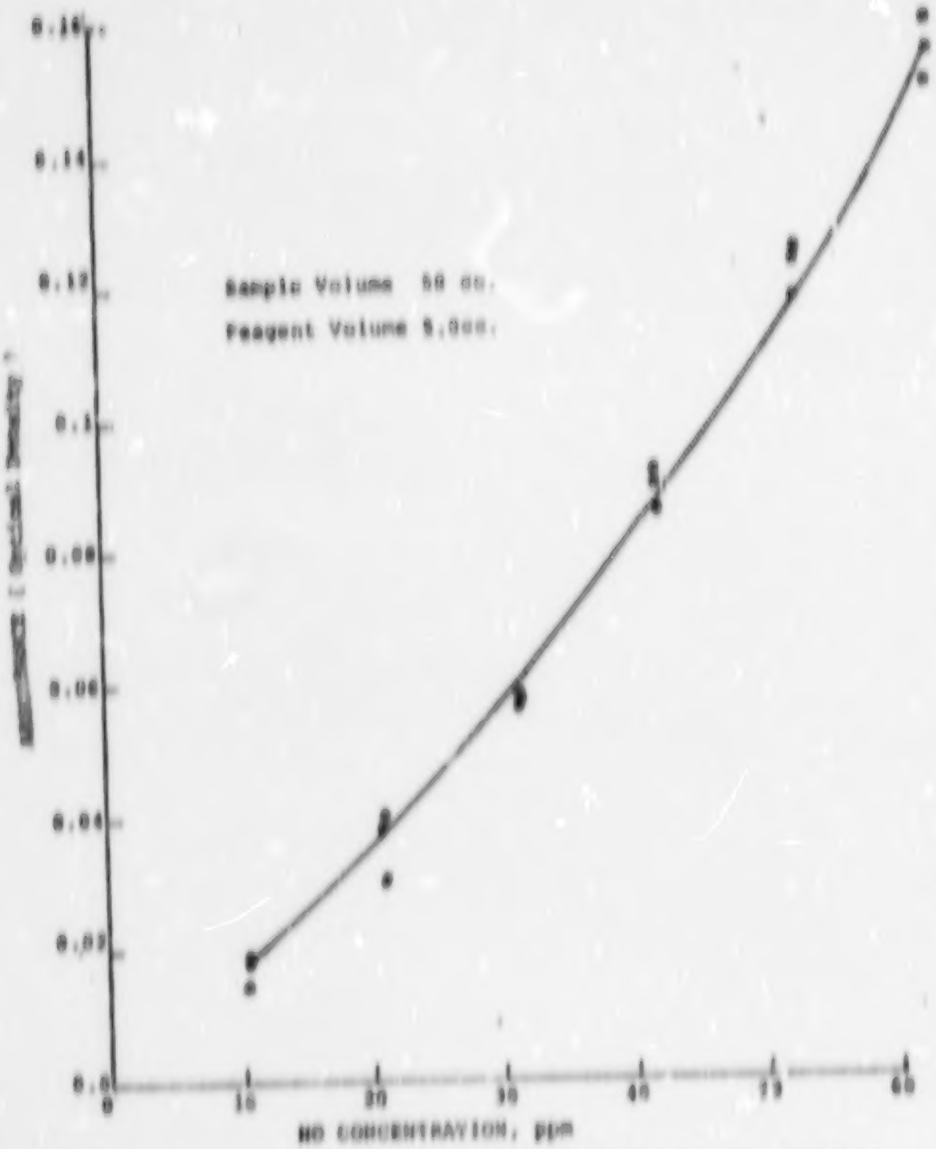

Figure 2.5: Calibration for modified Saltzman analysis technique

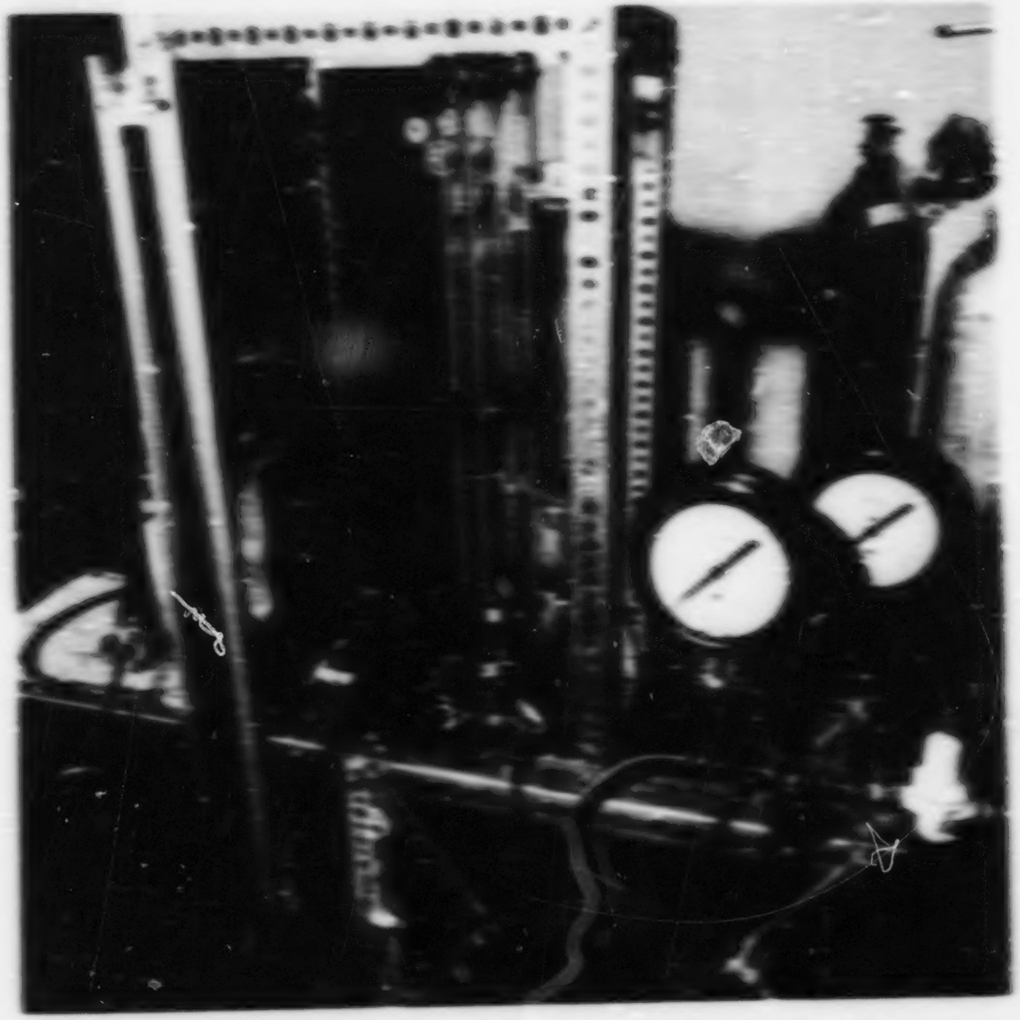

Figure 2.6 Photograph of Overall Burner System

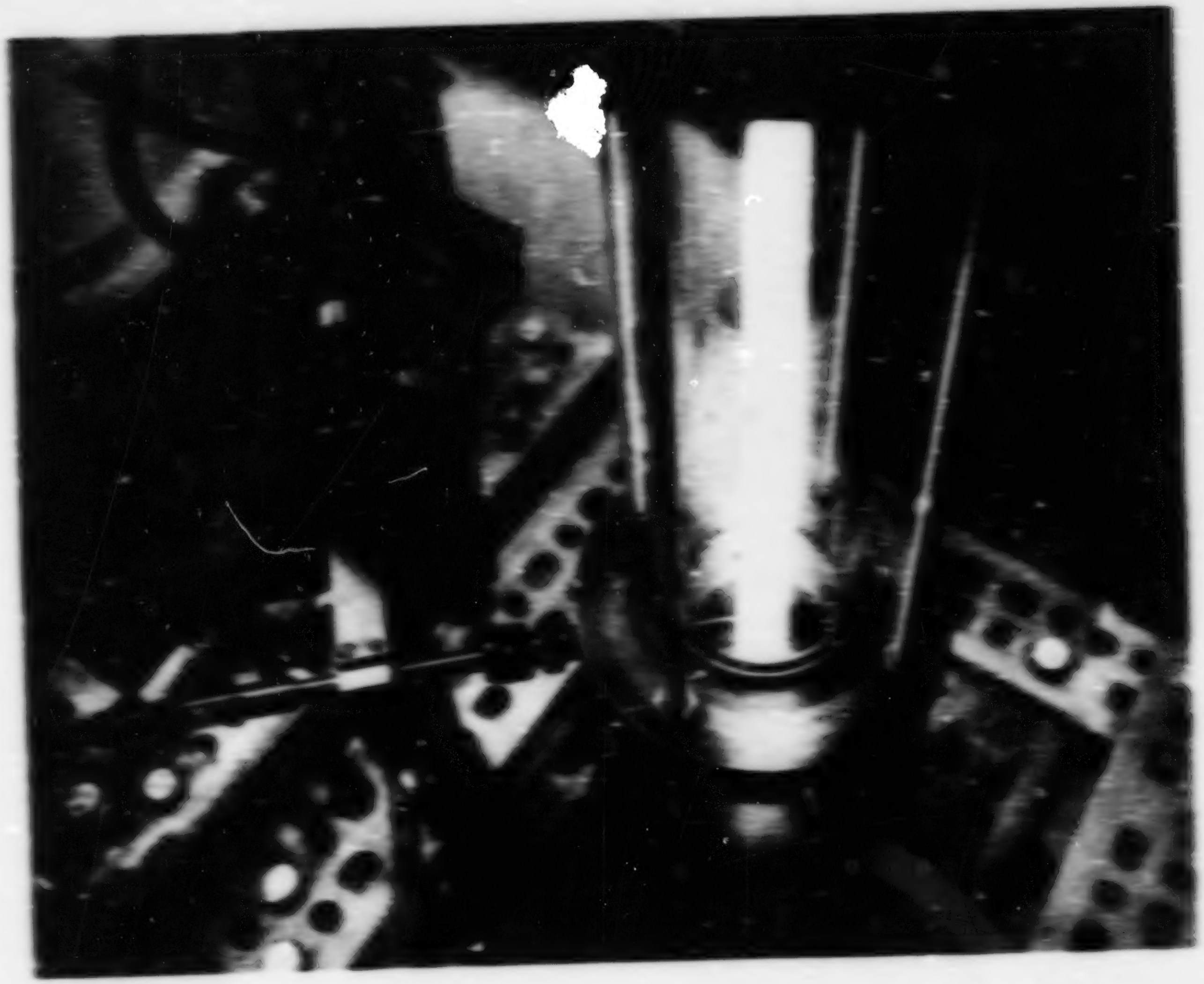

Figure 2.7 Photograph of the system, showing flame, micromanipulator and probe

CHAPTER 3

EXPERIMENTAL PROCEDURE, RESULTS AND INTERPRETATION

3.1 Experimental Procedure

Nitric oxide concentration profiles and concommitant temperature and concentration profiles of O_2, CO, CO_2, N_2 and fuel, CH_4 were determined, using the methods detailed in Chapter II. These profiles were determined at various axial locations for three flame conditions corresponding to overall fuel/air equivalence ratios of 0.5755, 0.433 and 0.351, here after denoted flame conditions A, B and C, respectively. Table 3.1 gives the details of these conditions. Flame condition A was analysed more completely than flame conditions B and C. Table 3.2 indicates the axial positions, for each flame condition, at which measurements were made and also indicates the details of measurements made.

For determination of concentration profiles at each axial position, samples were withdrawn from the flame using microprobe, from about 40 radial positions extending from the outer wall of the burner to the center line or axis of the burner. Samples were withdrawn at close intervals (0.2 mm radial increments) in the region of steep gradients and inversion points, while nearer the wall, where gradients were not severe, samples were taken at larger intervals (1 mm increment). At some axial positions, there existed a narrow annular zone in the fuel-rich region, from which samples could not be withdrawn, a result of excessive sooting of the sample probe.

Temperature profiles for the conditions and axial locations indicated in Table 3.2 were established from thermocouple readings taken at each of the points from which samples were withdrawn.

Reproducibility of results was checked by repeated sampling and analysis on different days. The reproducibility for CO, CO_2, N_2 and CH_4, the species determined by chromatographic analysis, was high, generally better than 5%. The reproducibility for O_2, an other species determined by chromatographic analysis, was high, generally better than 5%, in the oxygen rich region, however, in fuel rich region it was relatively low i.e. 20%. Nitric oxide concentrations were reproducible generally within 5% for concentrations above 20 p.p.m. and within 20% of concentrations below 20 p.p.m. Measured temperatures were reproducible within ± 10°F.

In general, reproducibility in the fuel-rich region was poorer than that in the oxygen rich region.

3.2 Experimental Results and Interpretation

Figures 3.1 through 3.19 show the radial concentration profiles of NO, CO, CO_2, O_2, N_2 and CH_4 along with concomitant temperature profiles, all together or separately for condition A, B and C, at axial positions indicated in Table 3.2. This data is presented in tabular form in Appendix A. The concentration profiles are presented on a dry basis. The temperature profiles are direct thermocouple readings without corrections for losses due to radiation or thermal conduction. Thus absolute accuracy of reported temperature is not claimed. However, the structure of temperature profiles and the locations of temperature maxima as indicated by these results should be of acceptable precision. The burner was operated at atmospheric pressure for these measurements. In the soot formation region, where samples could not be taken, the data have been graphically interpolated. This region is represented by dashed lines.

Examination of the above results leads to suggestive and definite observations regarding the structure of the flame and nitric oxide formation. In the following, it is intended to examine the results for flame condition A, in detail, as it has been studied most thoroughly, and refer to other conditions to illustrate some particular aspects.

Figures 3.1 and 3.2 show the radial temperature profiles for flame condition A, at two axial locations, 0.5 and 1.0 mm downstream of the fuel tube mouth, hereafter referred to as A - 0.5 and A - 1.0 etc. Figure 3.1 shows a maximum of about 979°F and Figure 3.2 a maximum of 1103°F. However, Figure 3.2 shows a valley at about the radial location of fuel tube wall indicating the quenching effect of fuel tube. It appears that at the 1.0 mm axial portion the reaction is just starting while at the 0.5 mm axial position there is no reaction. The temperature rise at 0.5 mm could then be attributed to heat transfer from the flame. Species concentrations were not determined at these locations.

These quenching effects are further demonstrated in Figure 3.3 giving temperature and concentration profiles for conditions A = 2.0. Nitric oxide concentrations were determined at this location, however, as the reproducibility was extremely poor, perhaps due to quenching, these results have not been reported. As an indication, the NO profile showed peaks and valleys similar to that of CO_2. The maximum value was around 12 p.p.m. The irregularity of the temperature profile at the location of the fuel tube wall and of the CO and CO_2 profiles around the same region further indicates a quenching effect. The space upstream of 2.0 mm, thus seems to be an unreactive region in which very little or no energy release occurs. As a result, high concentrations of oxygen appear in the fuel-rich region due to diffusion or possibly recirculation, as shown by Figure 3.3. Visually, very little blue radiation, generally attributed to the reaction of CO with oxygen was observed. Further, an examination of the oxygen profile in Figure 3.3 indicates that downstream of this location i.e. 2.00 mm, where quenching effects are no longer important, a small cylindrical premixed flame region exists. Here the excess oxygen is heavily diffused into the fuel-rich zone and consumed. This assertion is confirmed by the oxygen profile at the next downstream position, 17.0 mm, presented in Figure 3.4, which shows a typical oxygen profile for a diffusion flame and shows little oxygen concentration in the fuel-rich region. This upstream premixed like flame should then exhibit very high temperatures (close to adiabatic flame temperature for stochiometeric combustion) and this could be an important source of nitric oxide formation. Visually this premixed zone was estimated to be in the vicinity of 6-10 mm downstream of the fuel tube mouth. Unfortunately, this location could not be probed to confirm the above hypothesis directly due to the finite axial thickness of the quartz tube and metal flange combinations used to establish probe locations.

Measurements made at a distance 17 mm downstream of the mouth as shown in Figure 3.4, confirm above view point. The maximum concentration of NO is found to be 84 p.p.m. indicating that a significant amount of NO was formed upstream. Some of the profiles presented in Figure 3.4 will now be discussed in detail.

At the 17 mm location nitric oxide exhibits a fairly sharp peak in concentration in the intense temperature zone just external to the fuel-rich region. This peak coincides with that of temperature and approximately with that of carbon dioxide.

It is well known that the rate of formation of nitric oxide becomes insignificant for temperatures below 2800°F. Examination of the recorded temperature profile suggests that nitric oxide formation should be confined to a very narrow region of maximum temperature and that the nitric oxide formed there diffuses to both the fuel-rich and fuel-lean regions.

Furthermore, the sharpness of the nitric oxide peak suggests highly localized nitric oxide formation. Also, the slopes of the nitric oxide profile on both fuel-rich and fuel-lean side exhibit a characteristic similarity to concentration profiles of a specie generated by an axial line source in a cylindrical flow system.

In premixed rich hydrocarbon flames, formation of "prompt NO" has been suggested by Fenimore (18). The nitric oxide profile in Figure 3.4 does not suggest any evidence of "prompt NO" being formed in the fuel-rich region of this diffusion flame. This aspect is discussed more completely in article 6.3.2

A further point suggested by Figure 3.4 regards the structure of the flame. In the fuel-rich region, the temperature profile shows a marked local minimum at a radial location of 6.5 mm or at a distance of 15 mm from the wall. Examination of the CO and CH_4 profiles shows maximum CO near the same radial portion and a low concentration of CH_4, i.e. of the order of 10 mole percent against about 90 mole percent at the center of the burner. This suggest the presence of a strong heat sink at this location. A similar irregularity in the temperature profile of a methane air counter-flow blue diffusion flame has been reported by Tsuji & Yamaoka (73). They also report that this irregularity corresponds roughly to the zone of negative heat release.

Another aspect suggested by this profile is that at this stage the combustion process may be approximated by a single reaction step, Spalding & Jain (69)

$$C_nH_{2n} + \frac{n}{2}O_2 \longrightarrow nCO + nH_2$$

for the cylindrical space enclosed by this radial location. Here CO is formed through pyrolysis of methane. In the area external to this radial location the combustion chemistry is essentially that of a CO-H_2-O_2 system.

It may be mentioned again that at this location the flame is relatively soot free.

Another concentration profile in Figure 3.4, which is worthy of note is that of oxygen. This profile shows that most of the oxygen originally present in fuel rich region at the 2.0 mm upstream location shown in Figure 3.3, has been consumed and that the maximum temperature zone is the major sink for oxygen, with the fuel-rich part of the profile exhibiting a very small gradient and a finite concentration of oxygen in the center. The O_2 profile at this location without any smoothing is presented in Figure 3.20, which shows a slight increase in O_2 concentration, just inside the maximum temperature zone, in the fuel-rich region. This is contrary to the findings of Wolfhard and Parker (81), who studied a CH_4-O_2 flat diffusion flame by spectroscopic means and concluded that O_2 does not reach the luminous carbon zone, but similar to the findings of Smith & Gordon (64) and Gordon, Smith & McNesby (26), who obtained profiles of O_2 similar to those obtained in the present work, in a CH_4 - air diffusion flame. Similar results are reported by Tsuji & Yamaoka (72,73) in a methane air counterflow diffusion flame in the forward stagnation region of a porous cylinder as well as in droplet studies (Aldred, Patel & Williams 1). On the contrary, methane profile drops to zero near the maximum temperature zone. The major implications of this O_2 profile are:

1. The reactants are mixing as a result of diffusion and hence the flame is truly a diffusion flame.

2. The chemical reaction rate in the maximum temperature zone, where the major energy release occurs is finite and as a consequence some oxygen can diffuse into the fuel zone. It may be noted here that in this particular flame this phenomenon may be helped by the flow field within the burner due to higher initial velocity of air stream.

The other profiles presented in Figure 3.4 do not need any particular interpretation and are as would be expected.

Figure 3.5 shows the temperature and species concentration profiles measured at a point 47.5 mm downstream of the burner inlet. At this location, in a narrow annular zone samples could not be taken due to soot formation and as mentioned earlier, the data have been graphically interpolated. This region is represented by dashed lines.

The nitric oxide concentration profile in this figure shows a similar character to that in Figure 3.4, namely, it exhibits a fairly sharp peak in the intense temperature zone, and this peak coincides with that of temperature and approximately with that of CO_2. The slopes of the NO profile also are similar to those in Figures 3.4. The concentrations of NO at this axial location when compared with those upstream reflect an accumulation of NO with the downstream flow of gases.

The temperature profile in Figure 3.5 shows an irregularity similar to that in Figure 3.4. However, the peak temperature is reduced from 3096°F at 17 mm to 3045°F at 47.5 mm downstream distance. This is most probably due to dilution. As in the case of peak of nitric oxide profile, the temperature profile peak shows a slight shift outwards. This is consistent with the general shape of the cylindrical diffusion flames.

The oxygen profile is similar to that in Figure 3.4 except that the slope is less steep. The fuel concentration profile seems to indicate that at this stage major position of fuel has already been transformed or consumed.

Further downstream, at 117.5 mm location, the temperature profile and concentration profiles, presented in Figure 3.6 show a general flattening of profiles indicating more mixing of the species in the burner. The temperature, nitric oxide and CO_2 profile peaks show an inward shift as compared to those in Figure 3.5 and results from the depletion of the fuel core. The virtual depletion of fuel is evident from the CH_4 concentration profile.

The nitric oxide peak is still fairly sharp and coincides approximately with that of CO_2 and temperature.

The peak nitric oxide concentration as well as general concentration profile of NO show an increase over the corresponding upstream concentrations presented in Figure 3.5 indicating further accumulation of NO.

The peak temperature value of 3012°F shows a further decrease compared to 3046°F in Figure 3.5.

The temperature and concentration profiles determined at a point 324 mm downstream are presented in Figure 3.7. This location is near the end of visible flame tip, the visible flame height being 16-1/4" (412 mm). The profile at this position were determined to get an idea of the end conditions. At this location, there was still a significant amount of soot in the central part of burner and the samples were drawn by using a probe of inner diameter of about 0.008" instead of usual inner diameter of 0.002". The samples were usually drawn at 1 mm radial intervals.

The profiles show, that all the fuel and most of the intermediate product CO have been consumed. The flattening of profile shows increased mixing and all peaks except that for O_2, are near the center. The N_2 profile has not been plotted as it is virtually constant at almost 80 mole percent. The NO concentration peak shows a decrease indicating increased mixing. The temperature peak also shows a significant decrease. The CO_2 profile indicates more complete combustion.

An examination of Figures 3.5 and 3.6 show that the annular zone where samples could not be taken due to excessive soot (represented by dashed lines) has increased and moved towards the center in moving from the 47.5 mm position to the 117.5 mm position. This and other profiles in these figures indicate, that at the 117.5 mm position, the fuel-rich region is composed mainly of soot and CO. Thus this would essentially represent a carbon combustion zone in which carbon is consecutively oxidized to CO and then to CO_2. The length over which the carbon combustion zone continues also indicates the relative slowness of the overall reaction rate of carbon combustion.

It is interesting to note that in Figures 3.4, 3.5 and 3.6 representing axial positions of 17, 47.5 and 117.5 mm, the points of peak nitric oxide concentration, as well as that of peak temperature coincide with nearly identical oxygen concentrations of about 3 mole percent.

Further, the concentration of oxygen in the center seems to fall in the region from 17 mm to 47.5 mm and then increase again from 47.5 mm to 117.5 mm. The higher concentration of O_2 in the center is most probably a residual effect of O_2 noticed upstream, where as at 117.5 it is due to diffusion into the fuel-rich region and small accumulation due to reduced reaction, a result of lower peak temperature.

Figures 3.8 through 3.13 and 3.14 through 3.19 show the experimental results for flame conditions B and C respectively. These conditions manifest lower overall equivalence ratios and high air/fuel velocity ratios as indicated in Table 3.1. These figures provide essentially the same information as in Figures 3.1 through 3.7 except for the following minor differences:

1. Peak temperatures decrease slightly with decreasing overall equivalence ratios and increasing air/fuel velocity ratios.

2. The peak concentration of nitric oxide follows the same trends as temperature.

3. Lowering the overall equivalence ratio and increasing the air/fuel velocity ratio tends to shift the maximum flame temperature surface towards the center.

4. The visible flame height decreases with decreasing overall equivalence ratio and increasing air/fuel velocity ratios. These values being 16-1/4", 14-1/4" and 13-3/4" for flame conditions A, B and C respectively.

3.3 Summary of Interpretation of Experimental Results

The interpretation of experimental results and the insight gained thereby can be summarized with reference to flame condition A, as follows:

A. The flame can be divided roughly into four zones in order:

   i. A small non-reactive space near the fuel tube mouth, where practically no energy releasing reactions take place. ($\leq$ 1.0 mm position for flame condition A)

ii. A premixed-like flame zone, in which the oxygen accumulated in the fuel-rich region, during the dead space, is consumed. (approximately around 6-10 mm for condition A)

iii. A true diffusion flame zone in which the energy release reactions are mainly confined to a narrow but finite annular zone. (extending to upstream of 17 mm and slightly downstream of 117.5 mm position for condition A)

iv. A carbon zone in which all of the original fuel has either been consumed or transformed to soot extends right up to the center, ending finally in a luminous tip of the flame.

B. In the true diffusion flame zone, nitric oxide is formed mainly in the narrow intense temperature region and diffuses both to the fuel-rich and oxygen rich regions. The slopes of concentration profiles suggest that formation of NO in the fuel-rich region is probably not significant.

C. The temperature profile shows an irregularity in the fuel region in the early part of the flame (17 mm and 47.5 mm positions). Other investigators have shown that this corresponds to an endothermic zone.

D. The concentration of O_2 is finite in fuel-rich region, a result of finite reaction rates.

TABLE 3.1

Burner Operating Conditions

Condition	Fuel Mass Flow Rate lbm/min	Air Mass Flow Rate lbm/min	Av. Fuel Velocity ft/sec	Av. Air Velocity ft/sec	Overall Eq. Ratio F/A	Air/Fuel Velocity Ratio 1/2
A	2.67×10^{-3}	7.95×10^{-2}	0.721	1.33	0.5755	1.841
B	2.67×10^{-3}	1.062×10^{-1}	0.721	1.779	0.433	2.47
C	2.67×10^{-3}	1.322×10^{-1}	0.721	2.2	0.351	3.05

TABLE 3.2

Type of determinations made at each axial location corresponding to each flame condition.

FLAME CONDITION	A			B			C		
Axial Position Downstream of Fuel Tube Mouth	Temp	NO	Other Species	Temp	NO	Other Species	Temp	NO	Other Species
0.5 mm	x	–	–	x	–	–	x	–	–
1.0 mm	x	–	–	–	–	–	–	–	–
2.0 mm	x	–	x	x	–	–	x	–	–
17.0 mm	x	x	x	x	–	x	x	–	–
47.5 mm	x	x	x	x	x	x	x	x	x
117.5 mm	x	x	x	x	x	x	x	x	x
324.0 mm	x	x	x	x	x	x	x	x	x

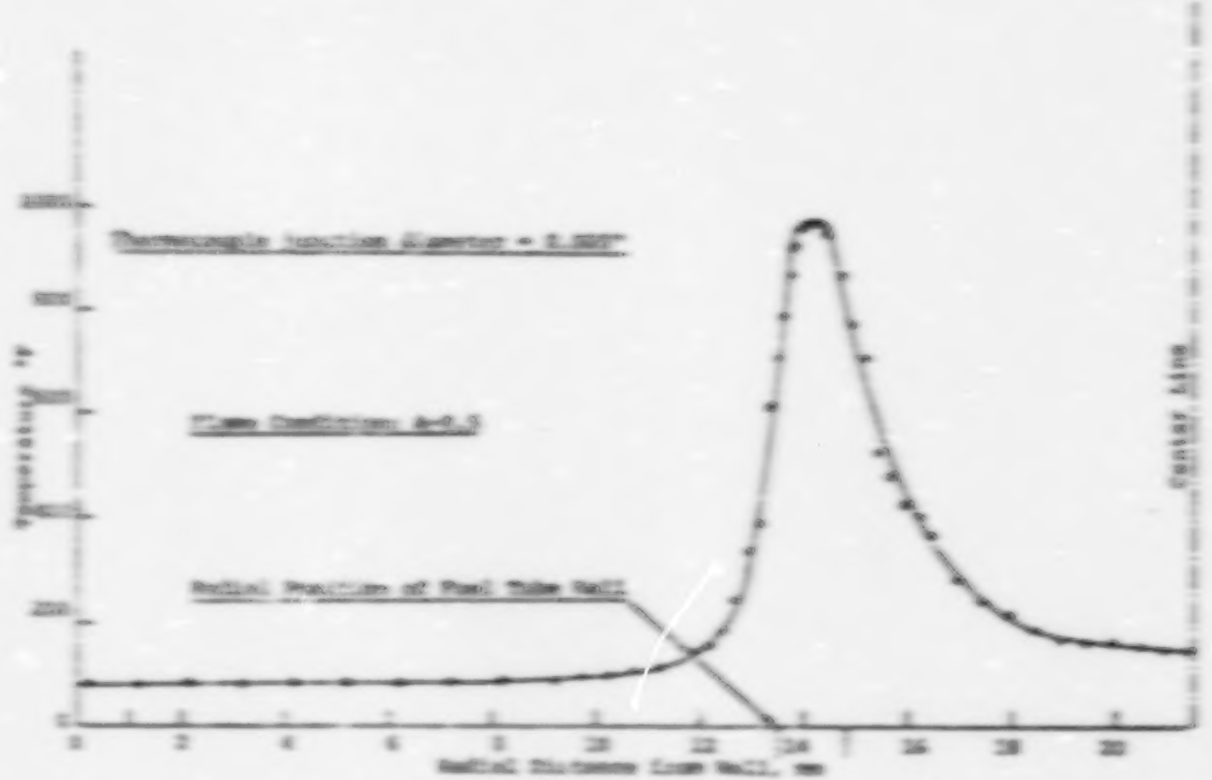

Figure 3.1: Temperature Profile 1.5 cm. above burner entrance. pressure, one atmosphere; fuel, methane

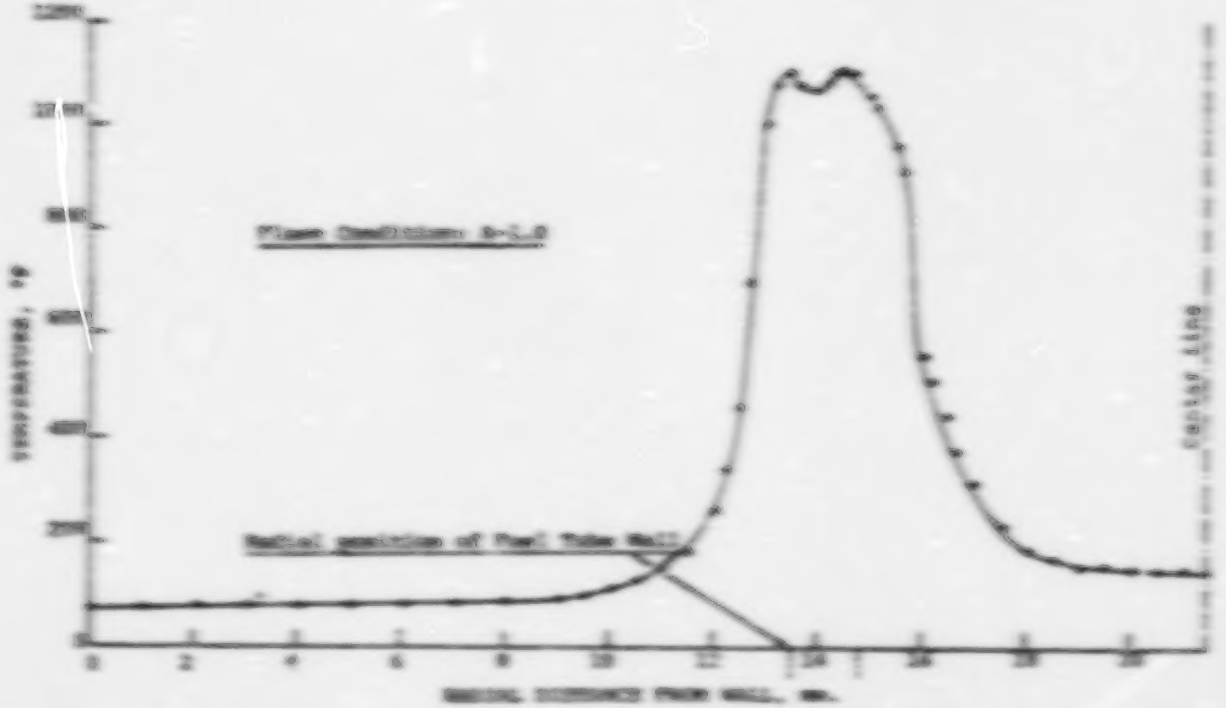

Figure 3.2: Temperature Profile 1.5 mm. above burner ambient; pressure, one atmosphere; fuel, methane

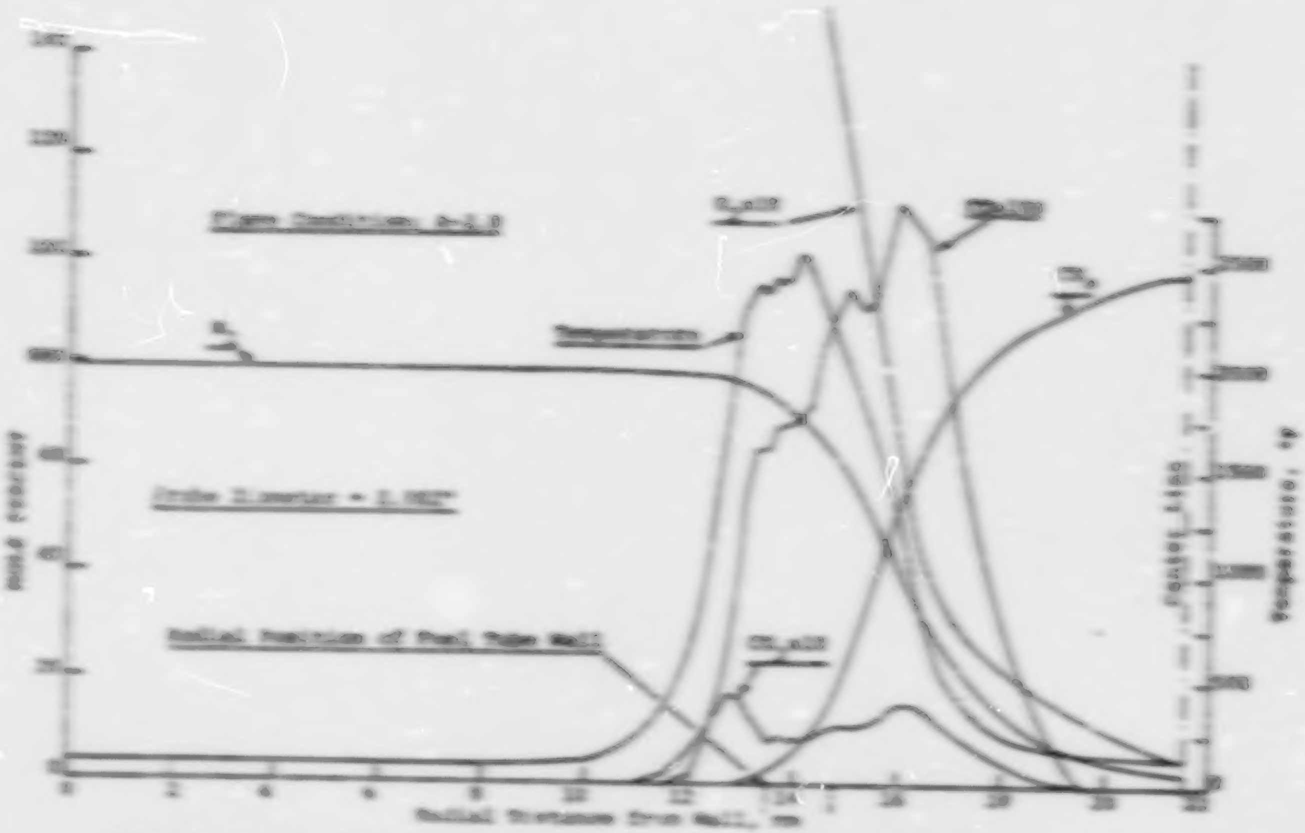

Figure 3.3: Temperature and Species Concentration Profiles 2.0 mm. above burner entrance; pressure, one atmosphere; fuel, methane

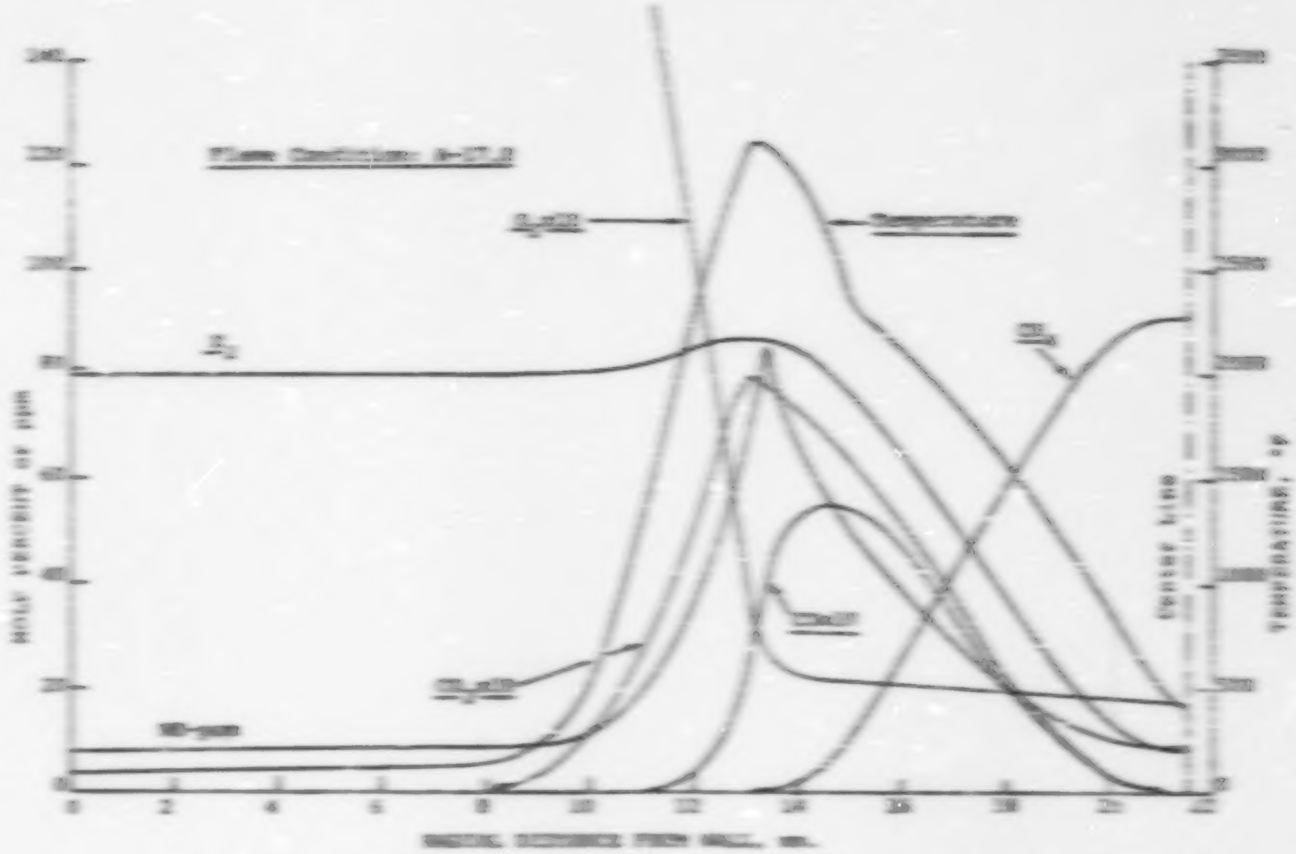

Figure 1.4: Temperature and Species Concentration Profiles 17.8 mm. above burner [illegible]; pressure, one atmosphere; fuel, methane

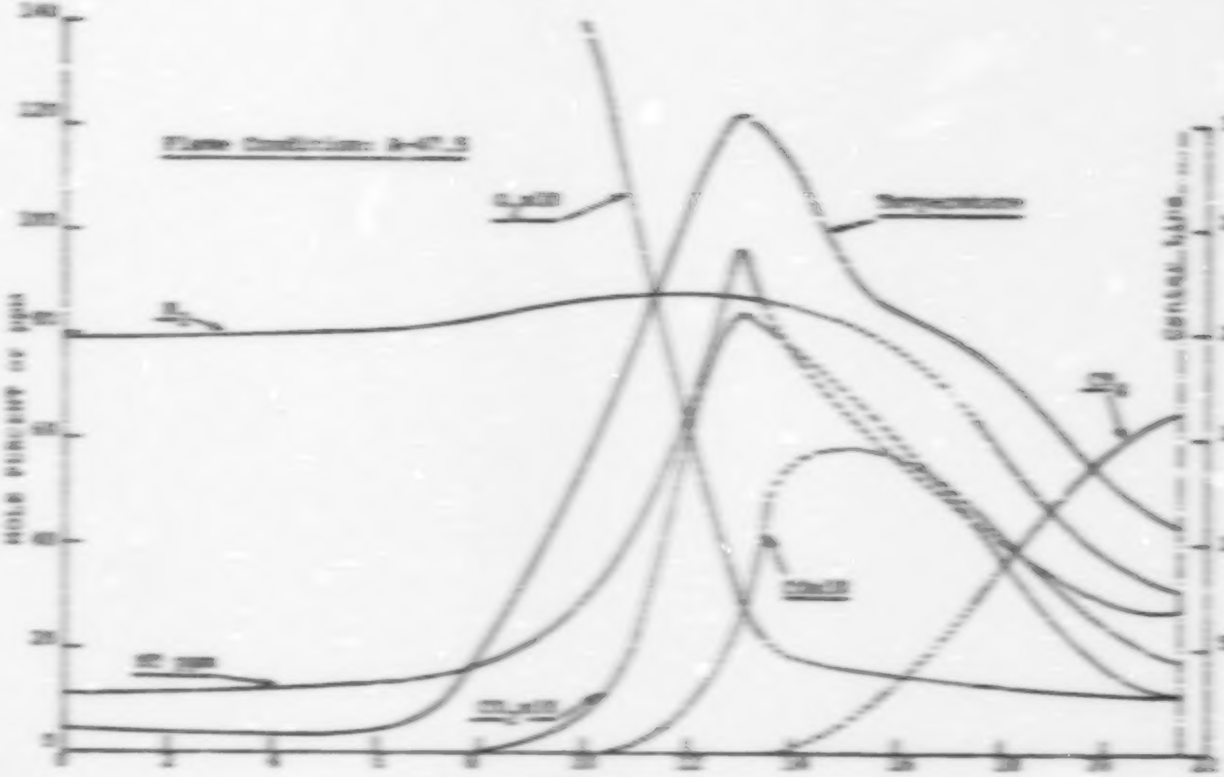

Figure 3.5: Temperature and Species Concentration Profiles 47.5 mm. above burner entrance; pressure, one atmosphere; fuel, methane

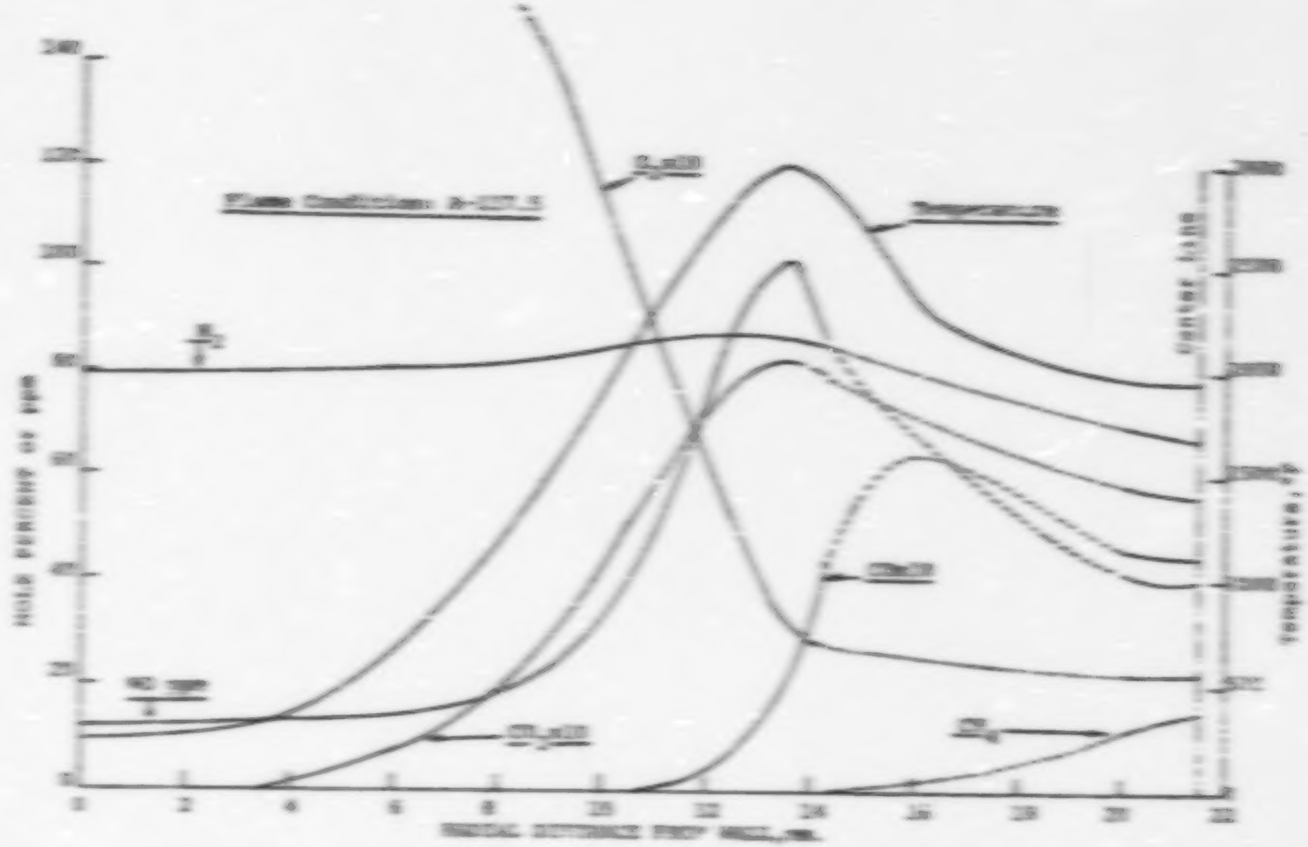

Figure 3.6: Temperature and Species Concentration Profiles 117.5 mm. above burner entrance; Pressure, one atmosphere; fuel, methane

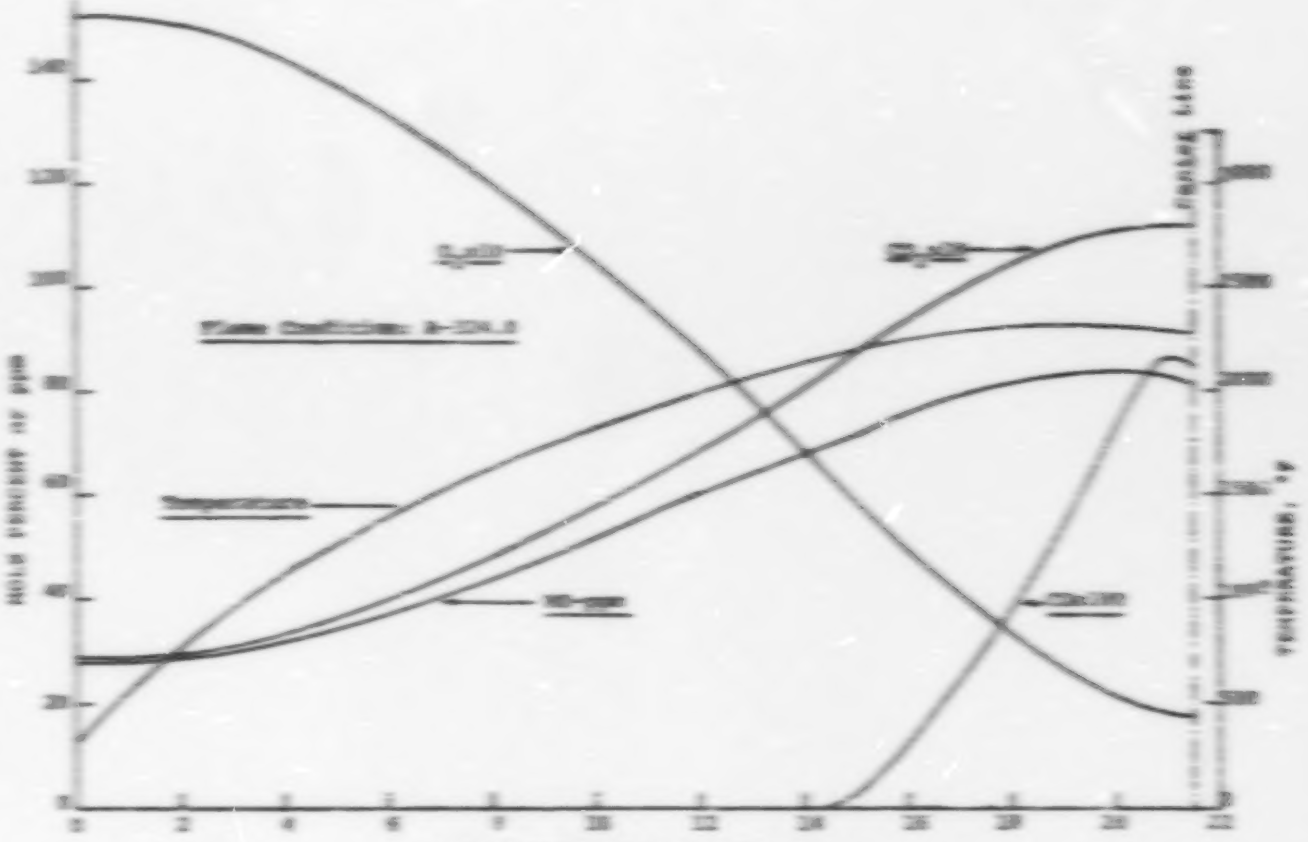

Figure 3.7: Temperature and Species Concentration Profiles 224.2 mm. above burner entrance; pressure, one atmosphere; fuel, methane

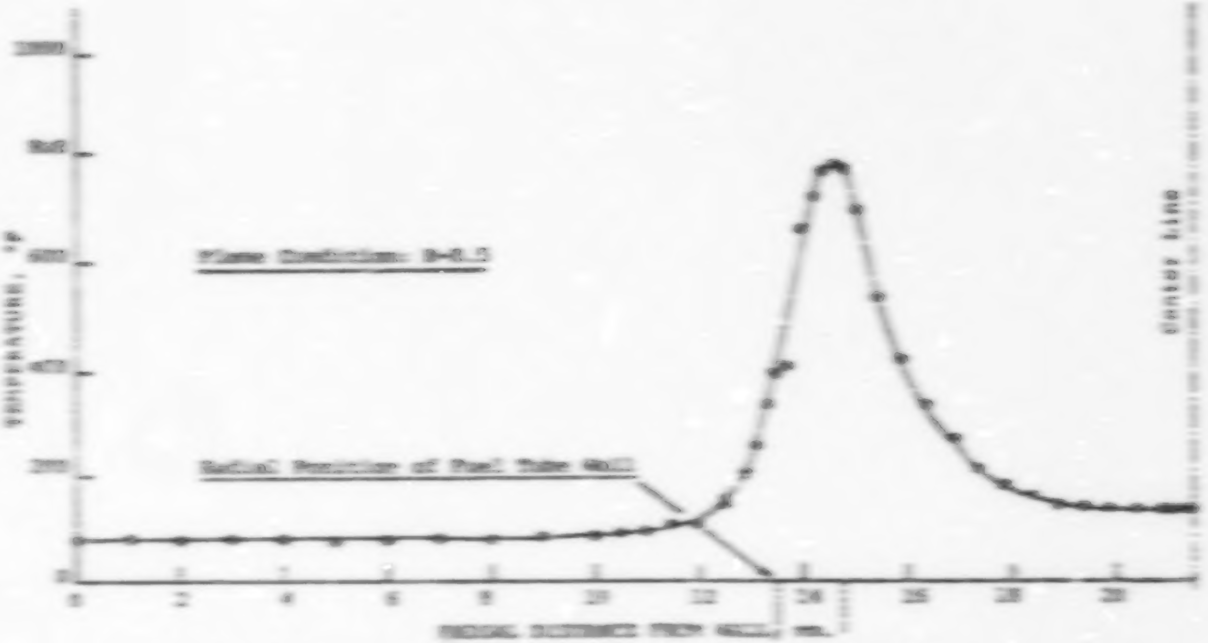

Figure 3.8: Temperature Profile, 2.5 cm. above burner entrance; pressure, one atmosphere; fuel, methane

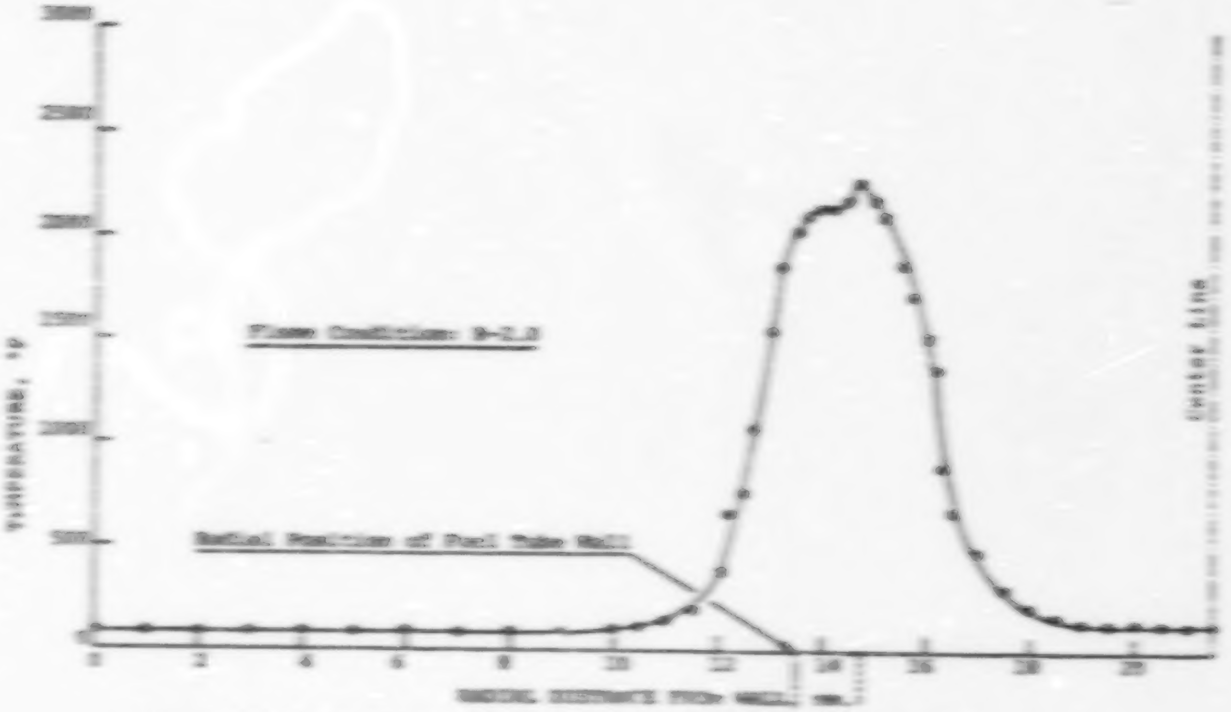

Figure 3.5: Temperature Profile, 2.0 mm. above burner entrance; pressure, one atmosphere, fuel, methane

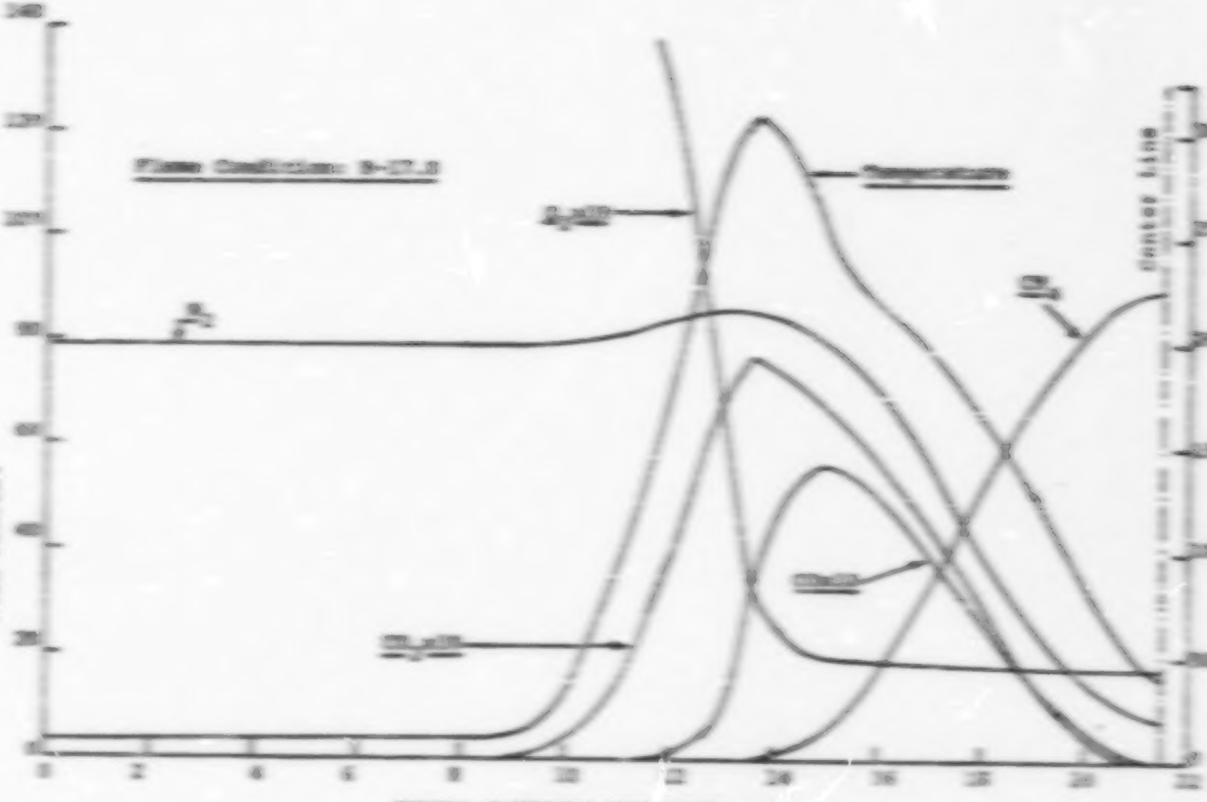

RADIAL DISTANCE FROM WALL, mm.

Figure 3.19: Temperature and Specie Concentration Profiles, 17.3 mm. above burner entrance; pressure, one atmosphere; fuel, methane.

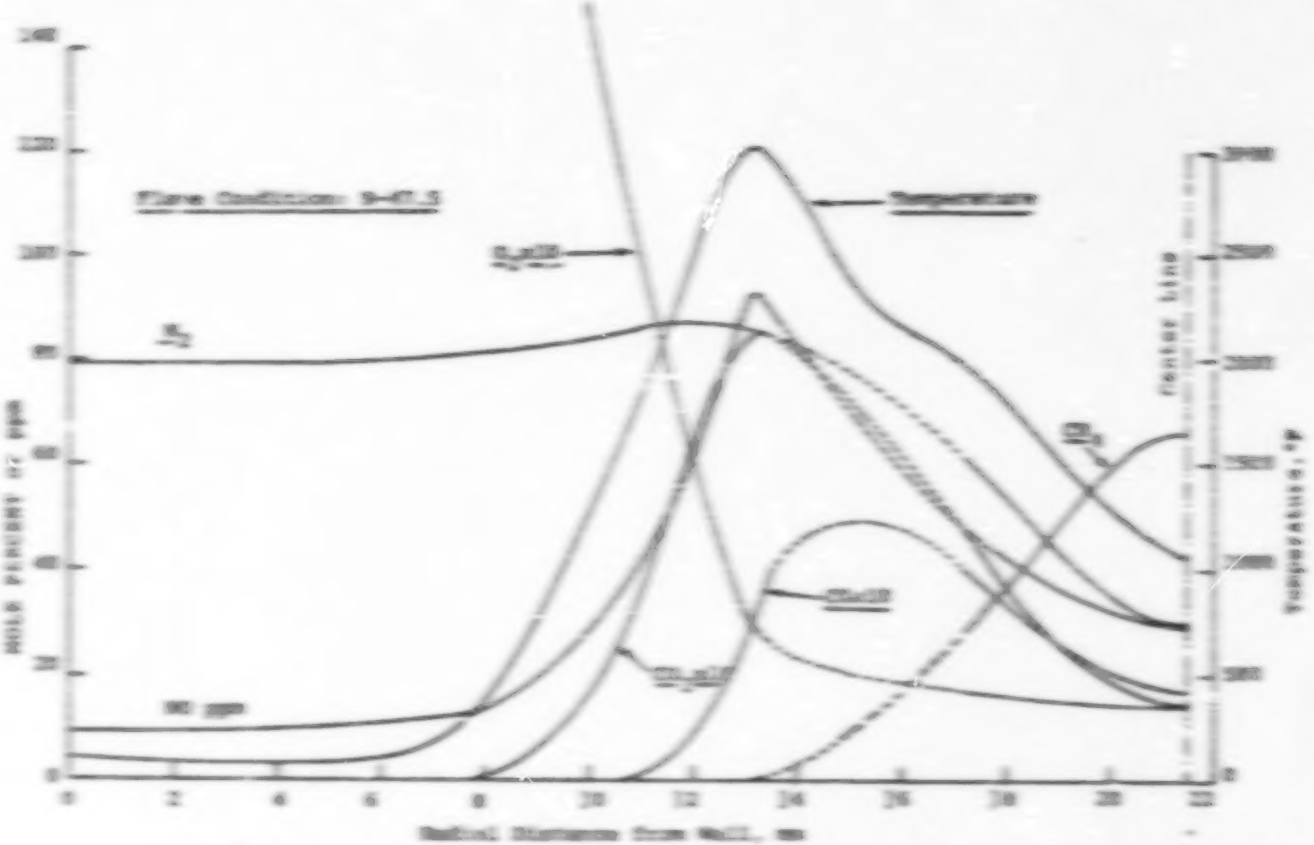

Figure 3.11: Temperature and Species Concentration Profiles 47.5 mm. above burner entrance; pressure, one atmosphere; fuel, methane

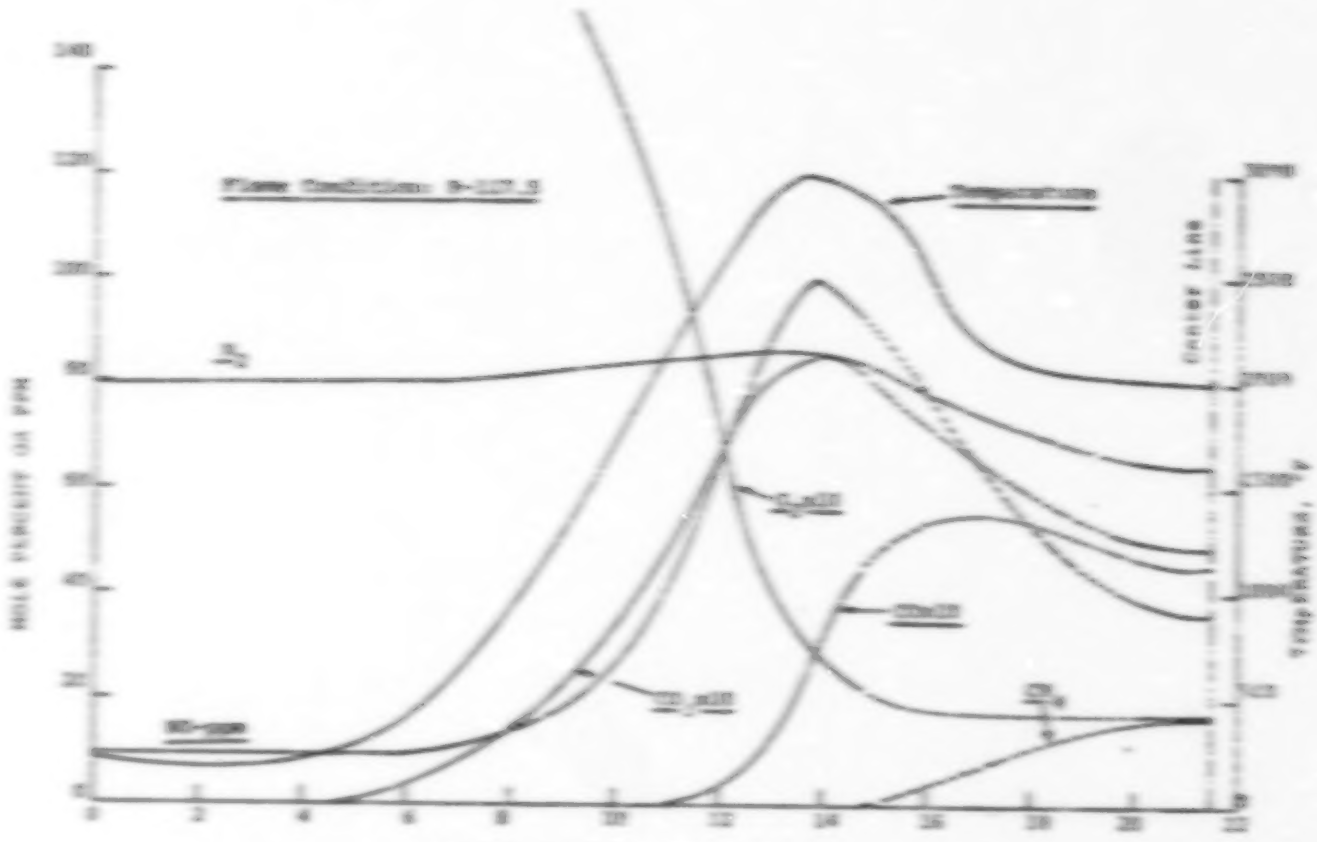

Figure 3.12: Temperature and Species Concentration Profiles, 127.5 cm. above burner entrance; pressure, one atmosphere; fuel, methane

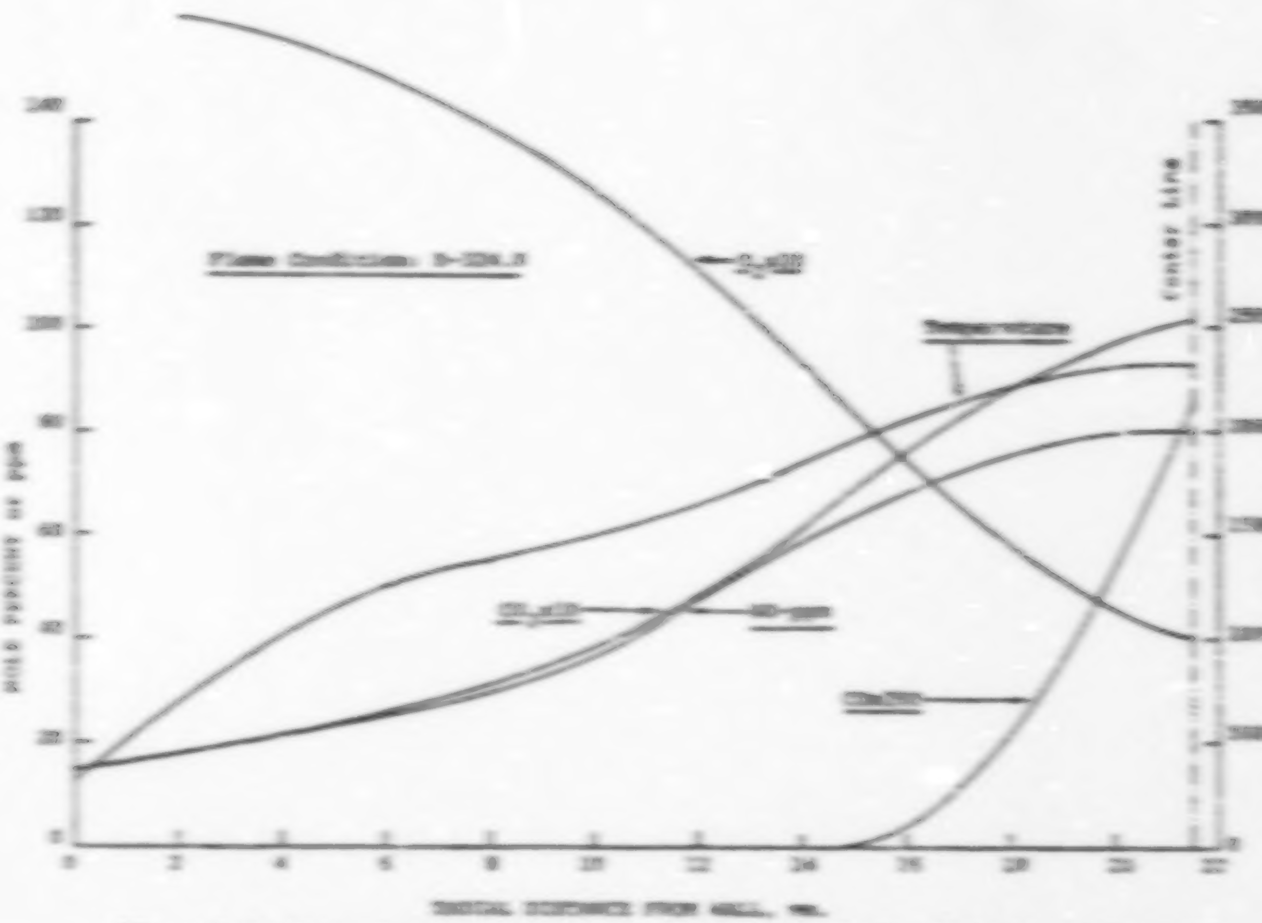

Figure 3.13: Temperature and Species Concentration Profiles, 124.0 cm. above burner entrance; pressure, one atmosphere; 5in², methane

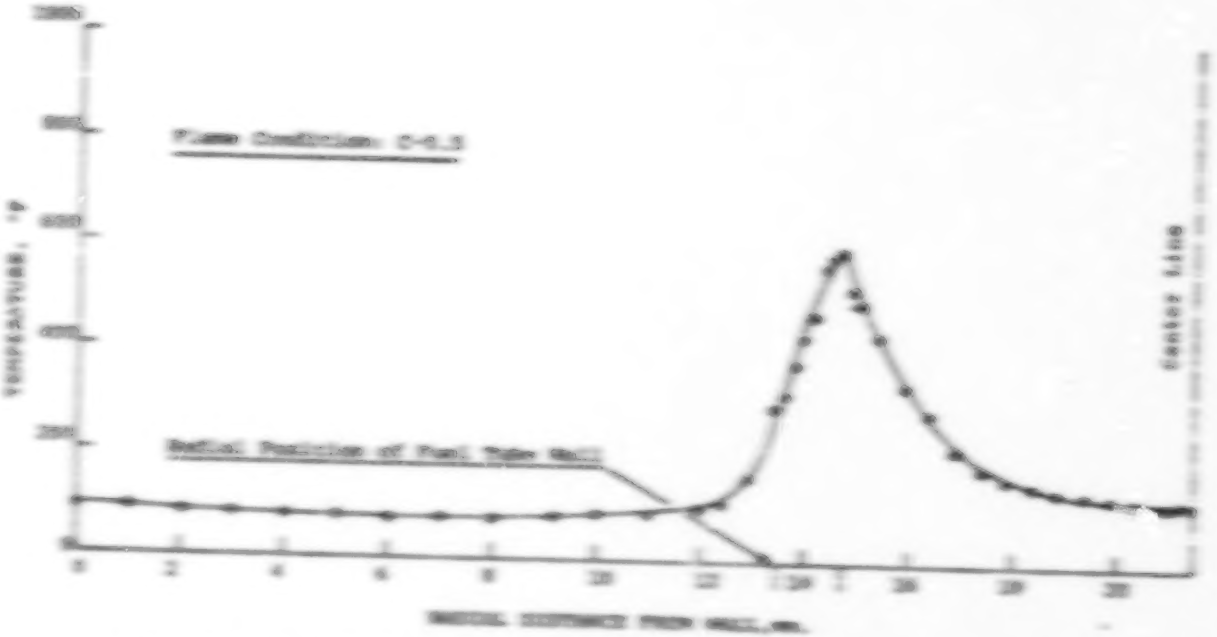

Figure 3.2A: Temperature Profile, 2.5 cm. above burner entrance; pressure, one atmosphere; fuel, methane

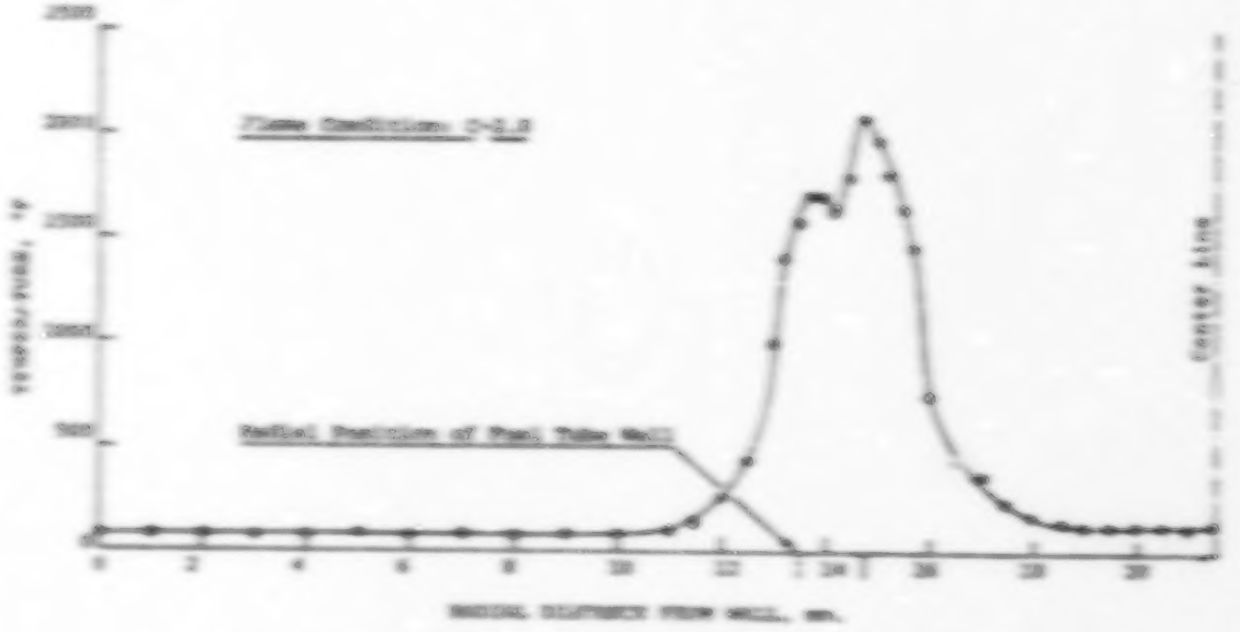

Figure 3.25: Temperature Profile, 2.5 cm. above burner entrance; pressure, one atmosphere; .1a/l, methane

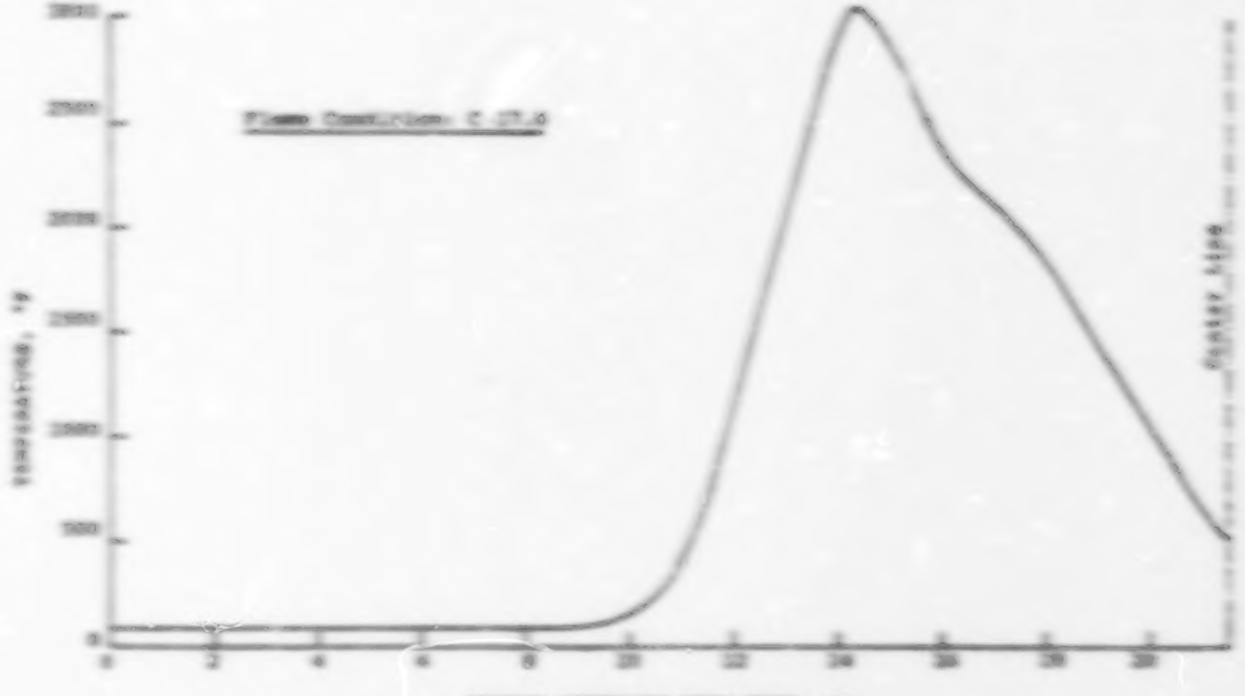

Figure 3.26: Temperature Profile, 17.3 mm. above burner entrance: pressure, one atmosphere; [illegible]

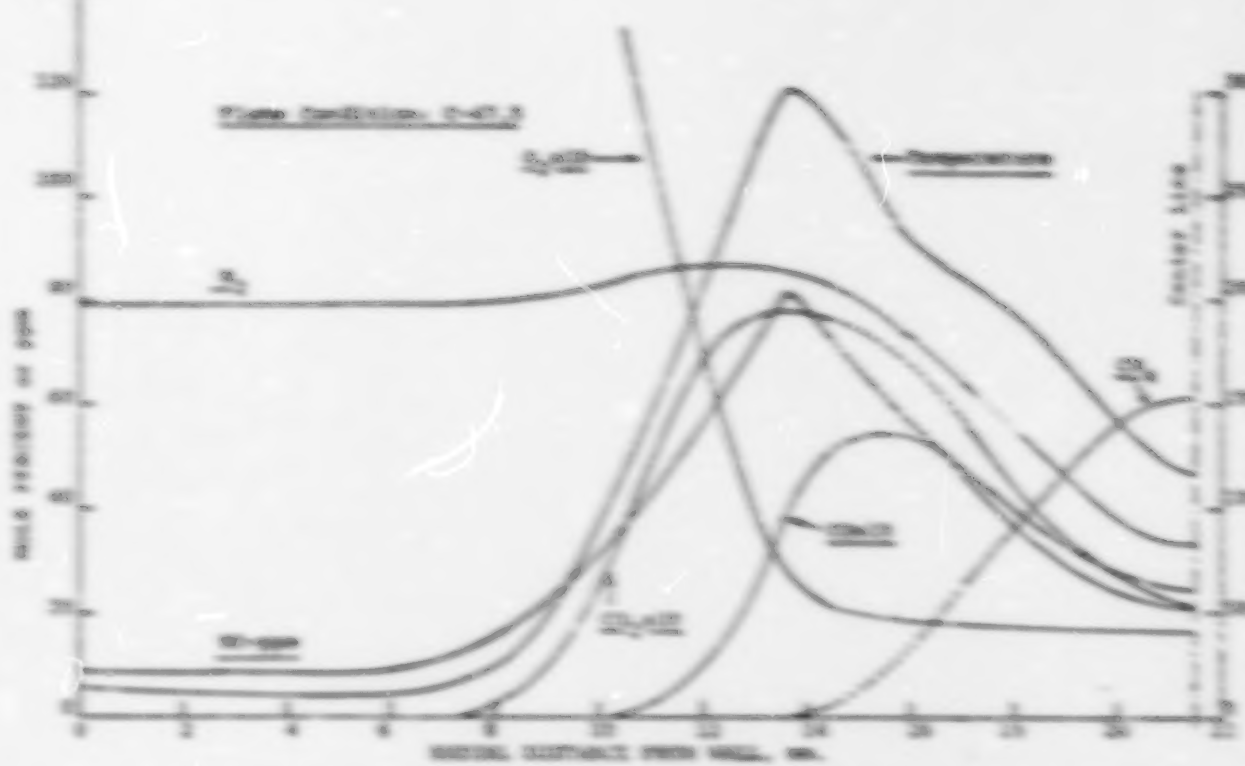

Figure 3.17. Temperature and Species Concentration Profiles, [illegible] cm. above burner; [illegible] pressure, one atmosphere; fuel, [illegible]

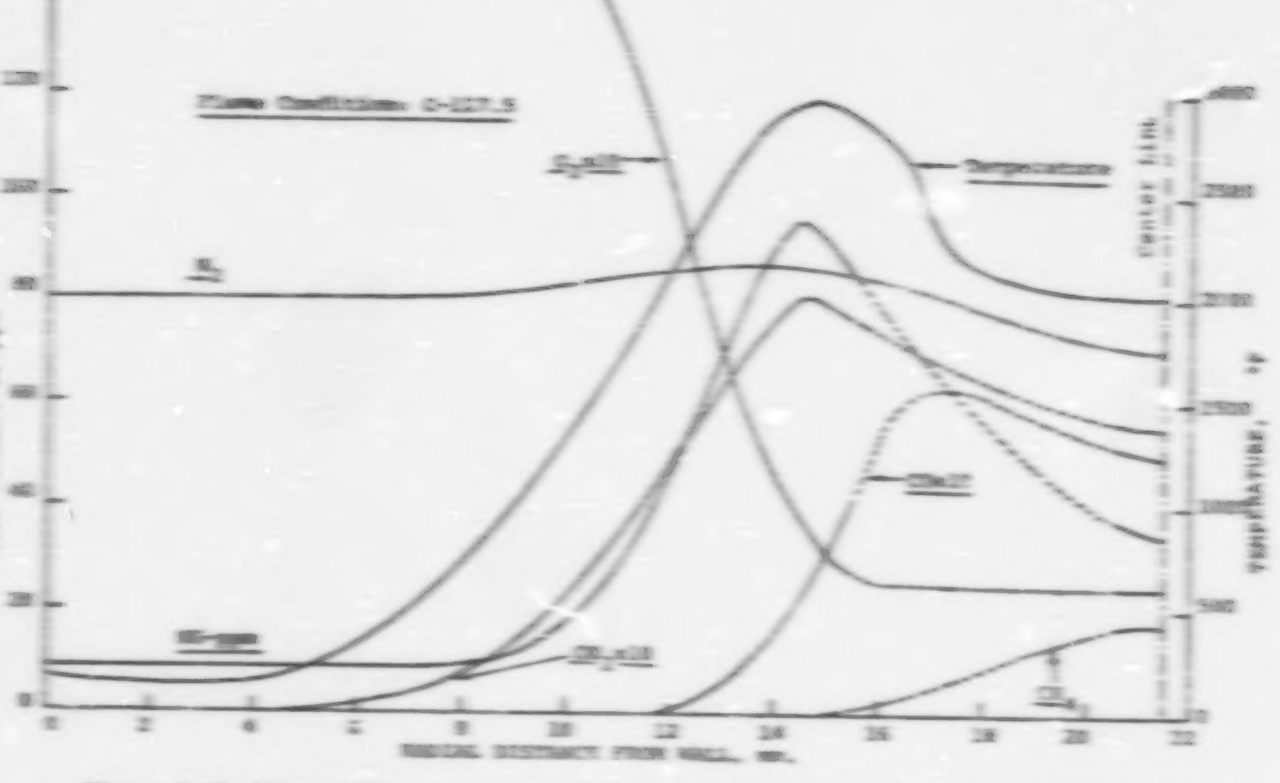

Figure 3.18: Temperature and Species Concentration Profiles, 127.5 mm. above burner entrance; pressure, one atmosphere; fuel, methane

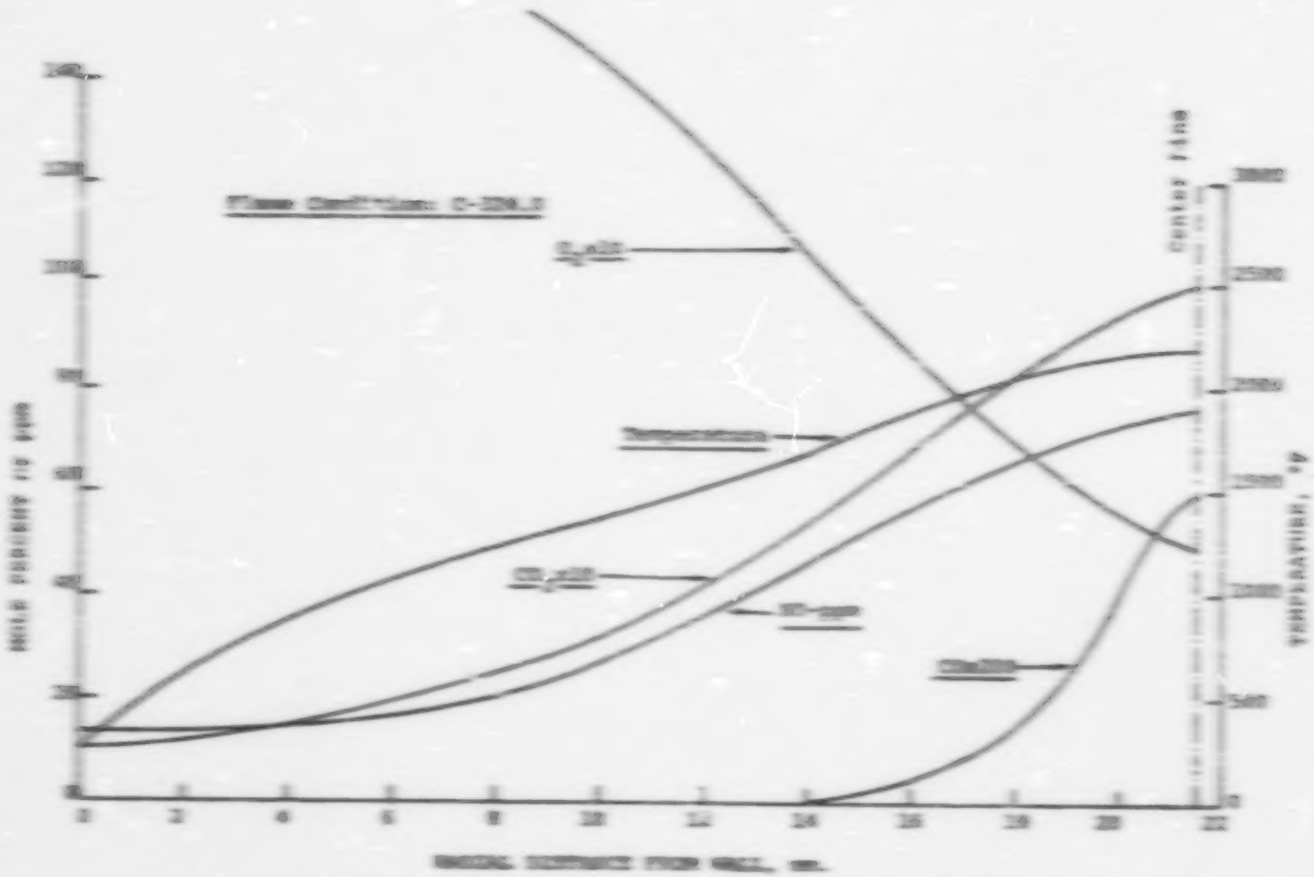

Figure 3.29: Temperature and Species Concentration Profiles, 224.2 cm. above burner entrance: pressure, one atmosphere: fuel, methane

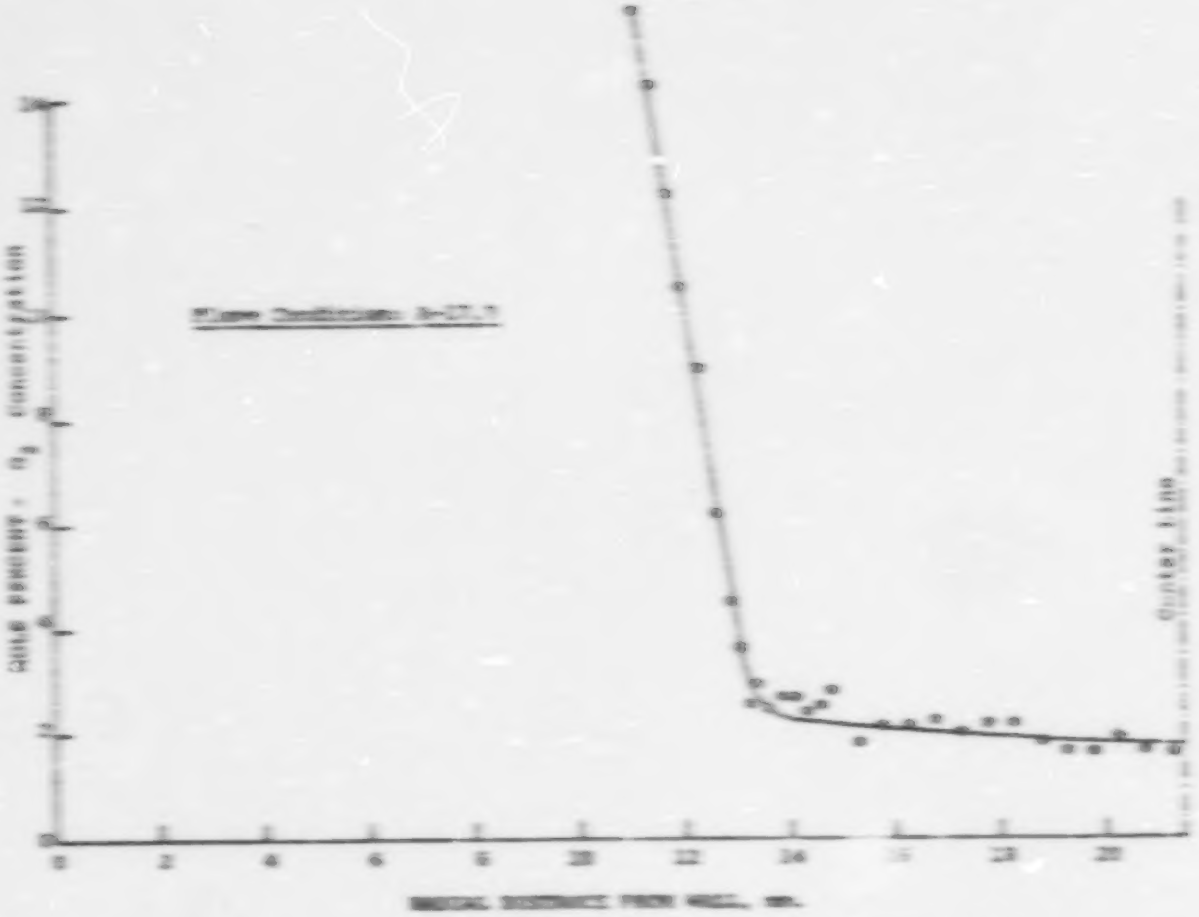

Figure 3.20: Oxygen Concentration Profile, 27.5 cm. above burner entrance

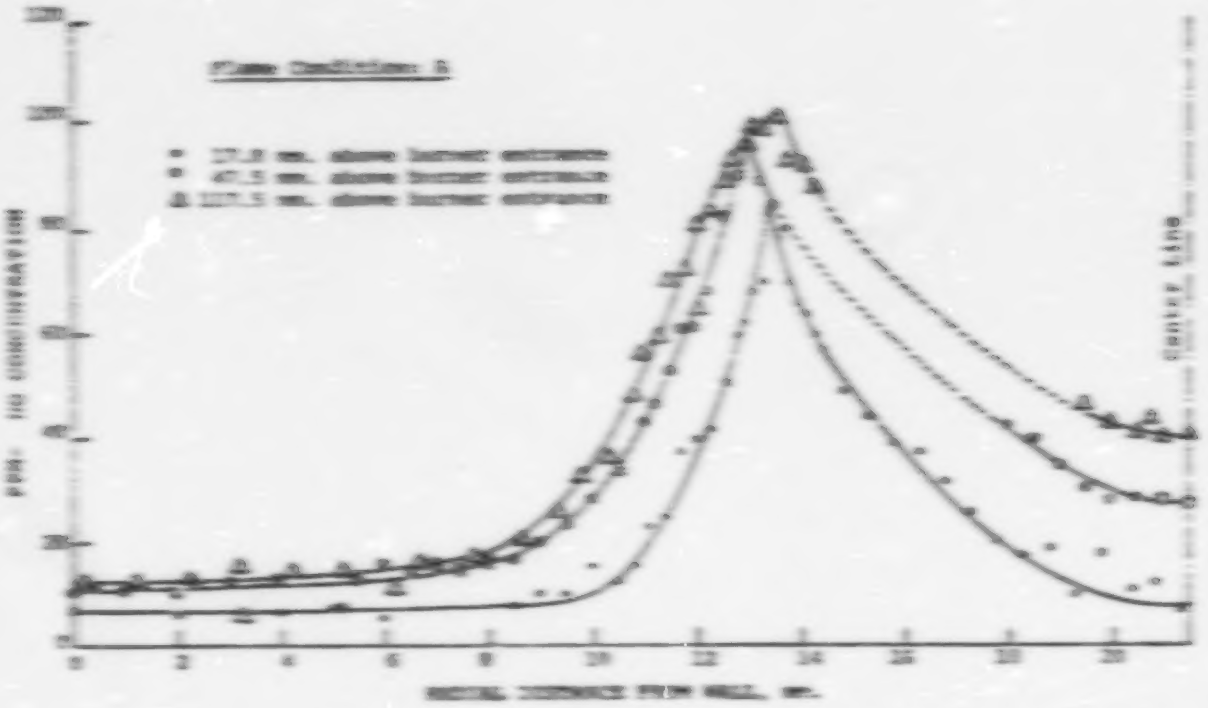

Figure 3.21: Comparison of NO Concentration Profiles at different axial locations

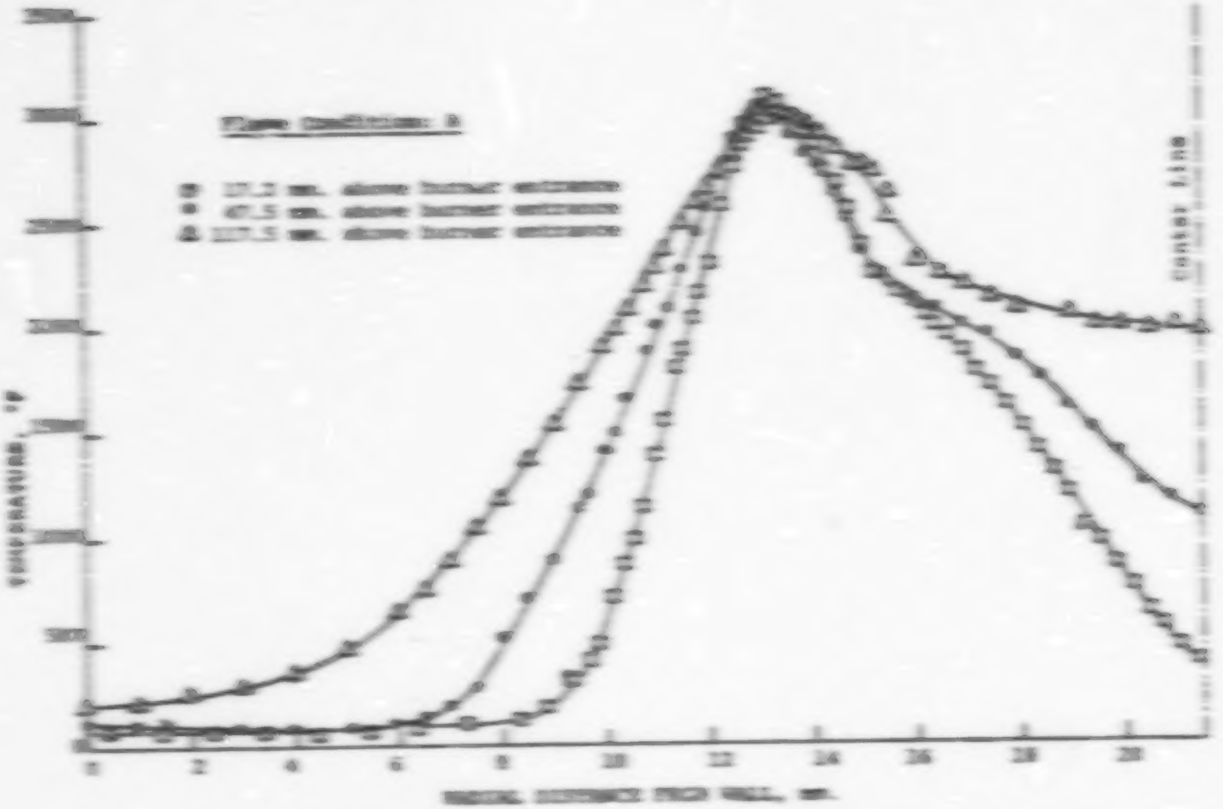

Figure 3.22: Comparison of Temperature Profiles at different axial locations

CHAPTER 4
THEORETICAL CONSIDERATION

4.1 Formation Kinetics of Nitric Oxide

The formation of nitric oxide has been studied extensively in the recent past in spark ignition engines (12,42,50,52) combustion bombs (51,63), shock tubes (7,8) and flow systems (66) and rate constants for important reactions have been determined. A review of the literature indicates that the following elementary reactions are relevent to the formation and decomposition of nitric oxide in general in combustion processes.

$$O + N_2 \rightleftharpoons NO + N \tag{1}$$

$$N + O_2 \rightleftharpoons NO + O \tag{2}$$

$$N + OH \rightleftharpoons NO + H \tag{3}$$

$$H + N_2O \rightleftharpoons N_2 + OH \tag{4}$$

$$O + N_2O \rightleftharpoons N_2 + O_2 \tag{5}$$

$$O + N_2O \rightleftharpoons NO + NO \tag{6}$$

$$N + O + M \rightleftharpoons NO + M \tag{7}$$

$$N_2 + O + M \rightleftharpoons N_2O + M \tag{8}$$

$$NO_2 + O \rightleftharpoons NO + O_2 \tag{9}$$

$$NO_2 + M \rightleftharpoons NO + O + M \tag{10}$$

out of these, the first two reactions from the Zeldovich mechanism were investigated in detail by Zeldovich & coworkers (67). This mechanism is generally adequate to account for nitric oxide formation in spark ignition engines, combustion bombs and shock tubes (7,8,42,51).

The two step Zeldovich mechanism

$$N_2 + O \rightleftharpoons NO + N \quad (1)$$

$$O_2 + N \rightleftharpoons NO + O \quad (2)$$

was thus used for calculating the formation rate of NO in the system under consideration here.

The reaction rate constants employed in this work were obtained from the literature (83) and are presented in the table below

Reaction	Rate Constant cm^3/mole-sec
$N_2 + O \rightarrow NO + N$	$7 \times 10^{13} \exp(-75{,}000/RT)$
$NO + N \rightarrow N_2 + O$	1.55×10^{13}
$O_2 + N \rightarrow NO + O$	$13.3 \times 10^{9} T \exp(-7080/RT)$
$NO + O \rightarrow O_2 + N$	$3.2 \times 10^{9} \exp(-39{,}100/RT)$

Making use of above reaction scheme, the rate of formation of nitric oxide in an elementary control volume is obtained as

$$\frac{d\,[NO]^{*}}{dt} = k_{1f}(T)\,[N_2]\,[O] + k_{2f}(T)\,[O_2]\,[N] - k_{1b}\,[NO]\,[N]$$
$$- k_{2b}(T)\,[NO]\,[O]$$

---

[*] [NO] stands for concentration of NO in moles/c.c.

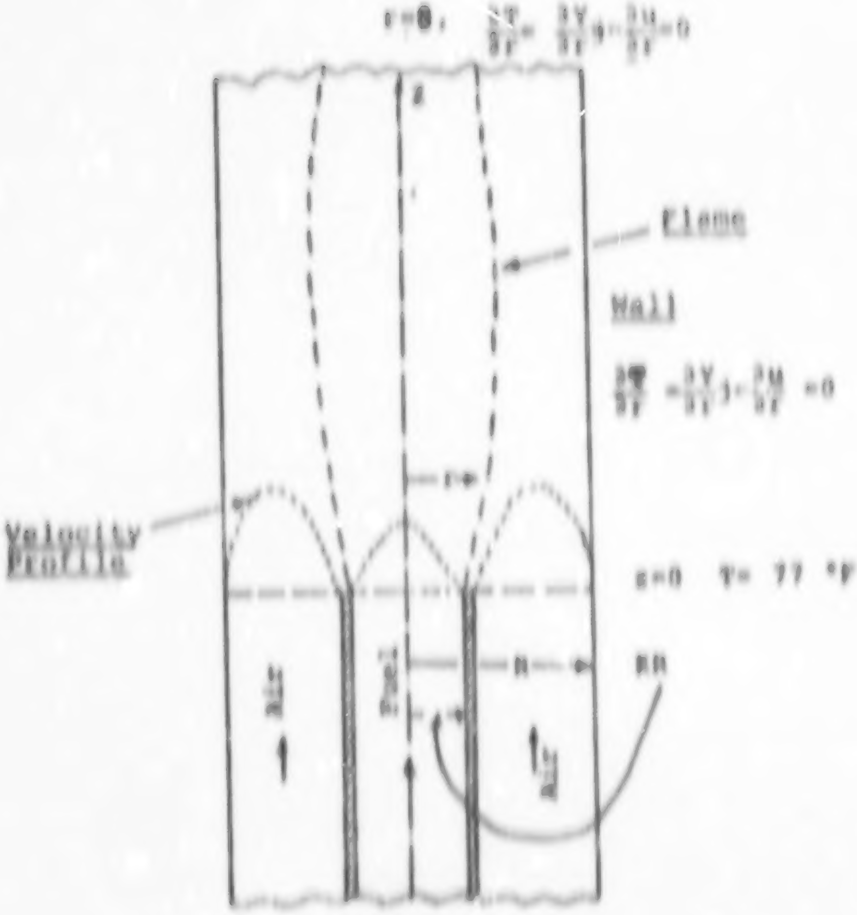
r=0, $\frac{\partial T}{\partial r}=\frac{\partial Y}{\partial r}i=\frac{\partial u}{\partial r}=0$
z
Flame
Wall
$\frac{\partial T}{\partial r}=\frac{\partial Y}{\partial r}i=\frac{\partial u}{\partial r}=0$
r
Velocity Profile
z=0 T= 77 °F
R
KR
Air
Fuel
Air

Figure 4.1: Schematic of Theoretical System Considered

$$= k_{1f}(T)[N_2][O] + k_{2f}(T)[O_2][N] - \{k_{1b}[N] + k_{2b}(T)[O]\}[NO \qquad (4.1)$$

Calculation of this rate of formation requires knowledge of instantaneous concentration of atomic and molecular oxygen and nitrogen i.e. $[O]$, $[O_2]$, $[N]$ and $[N_2]$ in the elementary control volume.

4.2 The System under Consideration

The theoretical system under consideration is shown schematically in Figure 4.1. Basically it involves steady mixing of laminar streams of two perfect reactive gases, with chemical reaction, resulting in a diffusion flame. Our interest is the study of the formation of nitric oxide in this chemically reactive system and determination of its concentration profiles.

The initial velocity profiles of fuel and air are parabolic and they are supplied at 77°F. The gradients of velocity, temperature and concentrations are taken as zero at the center and at the walls.

4.3 Calculation of Nitric Oxide Concentration Profiles

Nitric oxide formation kinetics as discussed in a previous section indicates that, the formation rate of nitric oxide can be calculated. However, as the flame under consideration is an axisymmetric two dimensional system with important gradients of species concentration, temperature and velocity, the eventual calculation of NO concentration will require more than integration of equation 4.1 above. In fact, this would require solution of conservation equation of NO involving convection, diffusion and generation of NO, i.e.,

$$\nabla \cdot (\rho \underline{V} Y_{NO} - \rho D_{NO} \nabla Y_{NO}) = R_{NO} = M_{NO} \frac{d[NO]}{dt} \qquad (4.2)$$

Solution of the above conservation equation would require knowledge of the velocity vector, density, diffusion coefficient, mass fraction of NO and its gradient, apart from the temperature and concentrations specified earlier. In other words a complete knowledge of the structure of the diffusion flame under consideration will be required to solve this conservation equation, so that the concentration field of NO can be established. Further, ideally, as the production and destruction of chemical species is coupled, the conservation equation for NO will have to be solved simultaneously with the governing differential equation for the structure of the flame, i.e. NO is a part of the structure of the flame.

A literature survey [42,46,51] shows that for premixed flames:

- Nitric oxide formation reactions are significantly slower than the combustion reactions providing energy release. Consequently nitric oxide is not formed in the flame front, but in the burnt gases after the passage of the flame front.
- The nitric oxide formation rate can be adequately approximated by the Zeldovich mechanism and the assumption that the concentrations of O, N, O_2 and N_2 are given by an equilibrium calculation at the temperature and pressure of the burnt gases.

The above information suggests that for approximate calculation of nitric oxide concentrations in diffusion flame, one could proceed as follows.

- Considering the Zeldovich mechanism and assuming that O and N are in equilibrium with O_2 and N_2, it is realized that due to extremely small concentration of O, N and NO as compared to those of N_2 and O_2, the amount of O_2 and N_2 consumed in this formation will be negligible. As such the formation of NO will have no appreciable effect on the structure of the flame itself.
- While the structure of the flame is insensitive to NO formation, the NO formation on the other hand is extremely sensitive to the structure of the flame due to its strong dependence on temperature and oxygen concentration.
- Thus, if one could establish the flame structure, without taking nitric oxide formation into account, but otherwise making the computations as accurately as possible, the nitric oxide concentration could then be evaluated by solving its conservation equation and using the appropriate values of velocity, temperature, concentrations and properties from the structure calculations.

This is the technique that has been used in this work and is essentially similar to that used in previous studies in combustion bombs (5).

13), spark ignition engines (42), turbine combustor models (32), and in droplet studies (9).

It should be noticed that "prompt NO" suggested by (18) and its possible explanation by consideration of hyper-equilibrium concentrations of O (7,8) have not been considered. A detailed discussion justifying the equilibrium assumption for O is given in Chapter 6.

The possibility of establishing flame structure purely from physical and chemical considerations was investigated. After working with a simplified kinetic model for methane combustion in diffusion flames it was concluded that the paucity of knowledge mainly in kinetics of methane combustion did not permit establishment of flame structure, well enough to predict NO, within a reasonable time and effort. Instead flame structure was established, by introducing experimental values for temperature and species concentration profiles into a computer programme which allowed calculation of flow field, completing the structure and finally the calculation of NO by the method outlined above. The inadequacy of existing information to establish correct structure is discussed in detail in Chapter 6.

4.4 Flame Structure

The term flame structure stands for the detailed knowledge of flow field, temperature and concentration profiles. Ideally, then, this flame structure as well as calculation of nitric oxide, can be described by following governing equations, representing steady laminar jet mixing of two reactive perfect gases. These involve convective and diffusive transport of mass, momentum, energy and chemical species and their generation due to chemical reaction. In addition the relations of transport properties, thermodynamic properties with respect to temperature, pressure and species concentrations would be required.

6.4.1 Generalized Equations

Conservation of Mass

This simply states the law of mass conservation

$$\nabla\cdot(\rho\underline{V}) = 0 \qquad (6.3)$$

Conservation of Momentum

$$\nabla\cdot(\rho\underline{V}\underline{V}) + \nabla p + \nabla\cdot(\underline{\tau}) = 0$$

In writing this equation, body forces have been assumed to be absent. Using the continuity equation this is reduced to

$$\rho\underline{V}\cdot\nabla\underline{V} + \nabla p + (\nabla\cdot\underline{\tau}) = 0 \qquad (6.4)$$

Conservation of Energy

Neglecting radiative heat transfer and viscous dissipation we can write the energy equation as

$$\nabla\cdot(\rho\underline{V}h' - k\nabla T - \rho\sum h_j D_j \nabla Y_j) = 0 \qquad (6.5)$$

It may be noted here that the assumption of neglecting radiative heat transfer is not correct and is introduced only for the sake of simplicity.

The effect of this assumption and as to how the error introduced can be compensated will be discussed in Chapters 5 and 6.

Viscous dissipation can be neglected as the velocities in the flame under consideration are small, so that this term will be negligible as compared to other terms.

Conservation of Species

Neglecting pressure and thermal diffusion terms, and using Fick's law we can write the equation for conservation of species as

$$\nabla \cdot (\rho \underline{V} Y_j - \rho D_j \nabla Y_j) = R_j \tag{4.6}$$

again by using the continuity equation this is reduced to

$$\rho \underline{V} \cdot \nabla Y_j - \nabla \cdot (\rho D_j \nabla Y_j) = R_j \tag{4.7}$$

where R_j is the rate of production of species j and is equal to

$$R_j = M_j \frac{d[C_j]}{dt}$$

The reaction rate term $\frac{d[C_j]}{dt}$ is usually evaluated with the kinetic rate equation of the form

$$\frac{d[C_j]}{dt} = \sum_{\substack{i=1 \\ \text{reaction}}}^{NR} \nu_{ji} \, k_f(i) \prod_{j=1}^{NS} C_j^{\nu'_{ji}} \tag{4.8}$$

where

ν_{ji} = is the stochiometric coefficient of species j in reaction i (-1 if specie j is a reactant, +1 if a product, and 0 if specie is not involved in reaction i)

ν'_{ji} = is the stochiometric coefficient of species j in reaction i (+1 or +2 if species j is a reactant and 0 if it is a product or not included in reaction i)

NR = is the total number of reactions considered

NS = is the total number of species considered.

The rate constants $k_i(T)$ according to chemical kinetics are a function of temperature only, and are written as

$$k_i(T) = Z_i \exp(-E_i/RT) \tag{4.9}$$

where the pre-exponential factor Z_i and activation energy E_i are obtained from the literature for reaction i.

The information available in the literature for the particular case considered will be discussed in detail later in this chapter.

4.4.2 Equations for the Particular System under Consideration

As mentioned earlier, the system under consideration is an axisymmetric two dimensional enclosed jet flame. Translating the general equations mentioned above to this particular system we can write,

Conservation of Mass

$$\frac{1}{r}\frac{\partial}{\partial r}(\rho v r) + \frac{\partial}{\partial z}(\rho u) = 0 \qquad (4.10)$$

Conservation of Momentum

$$\rho v \frac{\partial u}{\partial r} + \rho u \frac{\partial u}{\partial z} = \frac{1}{r}\frac{\partial}{\partial r}\left(r\mu \frac{\partial u}{\partial r}\right) + \frac{1}{r}\frac{\partial}{\partial z}\left(r\mu \frac{\partial u}{\partial z}\right)$$

$$- \frac{\partial p}{\partial z} \qquad (4.11) \text{ for z component}$$

$$\rho v \frac{\partial v}{\partial r} + \rho u \frac{\partial v}{\partial z} = \frac{1}{r}\frac{\partial}{\partial r}\left(r\mu \frac{\partial v}{\partial r}\right) + \frac{1}{r}\frac{\partial}{\partial z}\left(r\mu \frac{\partial v}{\partial z}\right)$$

$$- \frac{\partial p}{\partial r} \qquad (4.12) \text{ for r component}$$

Conservation of Species

$$\rho v \frac{\partial Y_i}{\partial r} + \rho u \frac{\partial Y_i}{\partial z} = \frac{1}{r}\frac{\partial}{\partial r}\left((r\rho D)_i \frac{\partial Y_i}{\partial r}\right) + \frac{1}{r}\frac{\partial}{\partial z}\left((r\rho D)_i \frac{\partial Y_i}{\partial z}\right)$$

$$+ R_i \qquad (4.13)$$

Conservation of Energy

$$\rho v \frac{\partial h'}{\partial r} + \rho u \frac{\partial h'}{\partial z} = \frac{1}{r}\frac{\partial}{\partial r}\left(r\frac{\lambda}{c_p}\frac{\partial h'}{\partial r}\right) + \frac{1}{r}\frac{\partial}{\partial z}\left(r\frac{\lambda}{c_p}\frac{\partial h'}{\partial z}\right)$$

$$+ \frac{1}{r}\frac{\partial}{\partial r}\left[r \sum_j \left(\frac{1}{Sc} - \frac{1}{Pr}\right) h_j \frac{\partial Y_j}{\partial r}\right]$$

$$+ \frac{1}{r} \frac{\partial}{\partial z} \Big] + \sum_i \left(\frac{1}{Sc} - \frac{1}{Pr} \right) h_i \frac{\partial Y_i}{\partial z} \Big]$$

(4.14)

Above equations are elliptic in nature and are difficult to solve.

A further assumption that can be made without losing much of the accuracy is the usual boundary layer assumption i.e.

- Momentum transfer in the axial direction is negligible as compared to momentum transfer in radial direction
- The radial component of momentum equation is negligible as compared to its axial component
- Axial heat conduction and species diffusion are negligible as compared to radial conduction and diffusion.

Incorporating these assumptions, the conservation equation can be rewritten as

Conservation of Mass

$$\frac{1}{r} \frac{\partial}{\partial r} (\rho v r) + \frac{\partial}{\partial z} (\rho u) = 0 \qquad (4.15)$$

Conservation of Momentum

$$\rho v \frac{\partial u}{\partial r} + \rho u \frac{\partial u}{\partial z} = \frac{1}{r} \frac{\partial}{\partial r} \left(r \mu \frac{\partial u}{\partial r} \right) - \frac{dp}{dz} \qquad (4.16)$$

Conservation of Energy

$$\rho v \frac{\partial h'}{\partial r} + \rho u \frac{\partial h'}{\partial z} = \frac{1}{r} \frac{\partial}{\partial r} \left(r \frac{\lambda}{c_p} \frac{\partial h'}{\partial r} \right)$$

$$+ \frac{1}{r} \frac{\partial}{\partial r} \left[r \sum_i \left(\frac{1}{Sc} - \frac{1}{Pr} \right) h_i \frac{\partial Y_i}{\partial r} \right] \qquad (4.17)$$

Conservation of Species

$$\rho v \frac{\partial Y_i}{\partial r} + \rho u \frac{\partial Y_i}{\partial z} = \frac{1}{r} \frac{\partial}{\partial r} \left(r \rho D_i \frac{\partial Y_i}{\partial r} \right) + R_i \qquad (4.18)$$

4.4.3 Reaction Rate Term R_i in the Species Conservation Equation for Methane Combustion

This term pertains to the rate of production (or destruction) of species in the species conservation equation and as explained earlier, ideally, will have a complicated form given by equations 4.7 - 4.9. The detailed kinetic scheme for methane combustion in diffusion flames is, however, not yet known. In the following, available information on kinetics of methane combustion is examined and various simplifications that can be introduced are considered.

4.4.3.1 Kinetics of Methane Combustion

The kinetics of methane combustion with oxygen as oxidant has been studied quite extensively in flames, flow reactors, shock tube stuties (20-25, 33, 66, 75, 76) and the reaction mechanism has been pretty well established for premixed flames, though there are differences about some elementary reactions relating to transition from CH_3 radicals to CO.

The complete mechanism can be broken down to four major parts.

i) Conversion of CH_4 to CH_3

ii) Formation of intermediates and CO from CH_3

iii) Conversion of CO to CO_2

iv) Chain branching and radical recombination reactions

A typical methane combustion mechanism used in shock tube studies (8) for premixed flames is as follows:

i) $CH_4 + M \rightleftharpoons CH_3 + H + M$ (11)

$CH_4 + OH \rightleftharpoons CH_3 + H_2O$ (12)

$CH_4 + O \rightleftharpoons CH_3 + OH$ (13)

$CH_4 + H \rightleftharpoons CH_3 + H_2$ (14)

ii) $CH_3 + O_2 \rightleftharpoons HCO + H_2O$ (15)

$CH_3 + O \rightleftharpoons HCO + H_2$ (16)

$HCO + OH \rightleftharpoons CO + H_2O$ (17)

$HCO + M \rightleftharpoons H + CO + M$ (18)

iii) $CO + OH \rightleftharpoons CO_2 + H$ (19)

iv) $H + O_2 \rightleftharpoons O + OH$ (20)

$O + H_2 \rightleftharpoons H + OH$ (21)

$O + H_2O \rightleftharpoons 2OH$ (22)

$$H + H_2O \rightleftharpoons H_2 + OH \qquad (23)$$

$$H + OH + M \rightleftharpoons H_2O + M \qquad (24)$$

The methane reaction mechanism used or postulated by other investigators are in fact quite similar to the one given above except for minor variations i.e. H_2CO is considered an important intermediate product (20-25).

In methane diffusion flames, it has been clearly demonstrated (Wolfhard & Parker, Gordon & Smith, Weinberg, Tsuji & Yamaoka) that pyrolysis of the fuel molecule is one of the most important reactions. Pyrolysis leads to the formation of intermediate hydrocarbons like C_2H_2, C_2H_4 and C_2H_6 and formation of carbon. Smith and Gordon (64) detected the above mentioned hydrocarbons, but apart from a rather uncertain trace of formaldehyde, found no sign of stable intermediate oxidation products. An examination of the reaction scheme presented above fails to take into account these hydrocarbons and formation of carbon and obviously cannot be expected to account for the reactions in a diffusion flame i.e. particularly in the fuel rich region.

Unfortunately, there is no known detailed mechanism for methane combustion in diffusion flames. This absence of a quantitative chemical mechanism for oxidation of hydrocarbons in general has thus been a stumbling block to the quantitative formulation in the theory of burning rates of fuels. As such, much ingenuity has gone into either completely avoiding or considerably simplifying the chemistry involved in formulation of these theories. Some of the common practices mentioned in the literature will be described briefly in the following, in decreasing order of their complexity.

4.4.3.2 Quasi-Global Combustion Mechanism

This approach used by Edelman & Fortune (14), proposes the reaction of fuel C_nH_m, directly with O_2 at an empirically determined finite rate to CO and H_2. The CO and H_2 then react via the known CO-H_2-O_2 chemistry. A typical scheme for methane is as follows:

$$\begin{array}{lcl}
CH_4 + 1/2\,O_2 & \longrightarrow & CO + 2H_2 \\
H + O_2 & \rightleftharpoons & OH + O \\
O + H_2 & \rightleftharpoons & OH + H \\
H + H_2O & \rightleftharpoons & H_2 + OH \\
O + H_2O & \rightleftharpoons & 2OH \\
H + H + M & \rightleftharpoons & H_2 + M \\
O + O + M & \rightleftharpoons & O_2 + M \\
H + OH + M & \rightleftharpoons & H_2O + M \\
CO + OH & \rightleftharpoons & CO_2 + H
\end{array}$$

Hammond & Mellor (29) assume the first reaction to be of infinite rate then follow a similar scheme.

A similar approach was first used by Spalding and Jain (69) in diffusion flame studies.

This approach has mainly been used in theoretical modeling of gas turbine combustion or flow reactors using plug flow or stirred reactor assumptions.

4.4.3.3 Global Reaction Rate

This approach used mainly in droplet studies numerical calculations (Lorrel, Wise & Carr, Brocco, Kassoy & Williams) assumes the combustion reaction to be completed in one step at a finite rate. For methane this would be

$$CH_4 + 2O_2 \rightarrow CO_2 + 2H_2O$$

with reaction rate of the form

$$-\frac{d\,CH_4}{dt} = A\,[O_2]^m\,[CH_4]^n \quad \exp(-E/RT)$$

The usual values for m and n are 1, indicating a second order reaction. A, the frequency factor and E, the activation energy are usually guessed or found by trial and error.

4.4.3.4 Infinite Reaction Rate

This is the classic Burke-Schumann assumption used in a number of diffusion flame and droplet combustion studies. This model assumes the existence of a flame sheet at which the fuel and oxidant combine in stochiometric proportions due to diffusion and burn instantaneously. The oxidant and fuel concentration at the flame surface are thus zero. This assumption coupled with a few others regarding transport properties eliminates the chemical reaction term from the species conservation equation thus facilitating solution of the equation.

4.4.3.5 Choice of Reaction Scheme

It can be readily appreciated that flame structure based on the flame sheet model will not give a reasonable prediction for NO as the concentration of O_2 will be zero in the fuel-rich region. It was therefore decided to try the next simplest approach employing a finite global reaction rate. As a point of reference, a solution was obtained for one of the flame conditions using the sheet model as well.

Based on the experience gained with the global reaction rate, it was felt that the even more complex schemes outlined earlier would not yield the desired accuracy in flame structure with a reasonable expenditure of time. As mentioned earlier, finally experimental temperature and species concentrations were introduced in the computer program and only the momentum equation was solved to establish the gas velocity field, thus establishing the structure. The equation for nitric oxide was solved simultaneously with the momentum equation to obtain NO profiles.

4.4.4 Thermodynamic and Transport Properties

Before the conservation equations discussed can be solved, certain auxiliary information in the form of data or equations is required to be specified:

i) Thermodynamic properties - density, specific heat and enthalpy of the system.

Transport properties - viscosity, thermal conductivity and diffusion coefficient.

4.4.4.1 Thermodynamic Properties

Density

Density is calculated from the equation of state for perfect gases, i.e.

$$p = \rho \frac{R}{\bar{M}} T$$

where $$\bar{M} = \sum_j X_j M_j \quad \text{or} \quad \frac{1}{\bar{M}} = \sum_j \frac{Y_j}{M_j}$$

Specific heats

Specific heats of individual species are available in the JANAF tables. However, it is more convenient to have polynomial fits for the numerical calculation by computer. Polynomial fits for O_2, N_2, CO_2, H_2 were taken from Newhall (49). For methane a polynomial fit over the denoted temperature range (298° - 3000°k) was made based on values in the JANAF table.

Specific heat for the mixture, on a mass basis, was calculated by the expression

$$c_p = \sum_i c_{pi} Y_i$$

Enthalpy of the System and Calculation of Temperature

The enthalpy of a fluid undergoing a simple chemical reaction of the type assumed, can be written as

$$h = \int_0^T c_p \, dT + Y_{fuel} \times HC$$

where HC stands for heat of combustion of fuel per unit mass.

The above definition of enthalpy involves the implicit assumption that absolute zero is the temperature of the base state.

Thus

$$h_O = \sum_j Y_j \, c_{pj \text{ at } T_O} \times T_O$$

and

$$h_F = \sum Y_j \, c_{pj \text{ at } T_F} \times T_F + Y_{fuel} \times HC$$

where subscripts O and F stand respectively for the conditions in the entering streams for oxidant and fuel.

The heat of combustion of methane can be evaluated from an enthalpy balance between the products and reactants, assuming that they combine according to stochiometric proportion. For a temperature of 537°R the value is

$$HC = 21571 \text{ BTU/lbm}$$

The choice of reaction temperature is not important as the heat of combustion is nearly independent of temperature. For example

$$HC = 21545 \text{ BTU/lbm at } 0°R$$

Owing to the above definition of enthalpy, the temperature at any point can be calculated by the following equation

$$T = \frac{h - Y_{fuel} \times HC}{\Sigma Y_i c_{pi} \text{ at } T}$$

Due to dependence of cp on temperature, the final temperature T is obtained by an iterative procedure, enthalpy h and fuel mass fraction, Y_{fuel}, being known, as they are dependent variables.

4.4.4.2 Transport Properties

Of the three transport properties required, data on viscosity of individual species is the best known and most reliable, and that on the diffusion coefficients in multicomponent mixture almost absent.

Therefore, in order to avoid complexities (which would even then not ensure significant accuracy over the approximation), Schmidt and Prandtl Numbers, Sc and Pr, were used. These are almost constant over a wide range of temperatures.

Mixture Viscosity

Viscosities of individual species were obtained from Krieth (41) and fitted as a function of temperature using Sutherland's Law as given by Reid & Sherwood (59)

$$\mu = \frac{bT^{3/2}}{S + T}$$

where b and S are constants determined from data.

The mixture viscosities were than calculated using Wilke's semi-empirical formula given by Bird et al (5)

$$\mu_{mix} = \sum_{i=1}^{n} \frac{x_i \mu_i}{\sum_{j=1}^{n} x_j \Phi_{ij}}$$

where

$$\Phi_{ij} = \frac{1}{\sqrt{8}} \left(1 + \frac{M_i}{M_j}\right)^{-1/2} \left[1 + \left(\frac{\mu_i}{\mu_j}\right)^{1/2} \left(\frac{M_j}{M_i}\right)^{1/4} \right]^2$$

where n is the total number of chemical species in the mixture. All other symbols have usual meaning.

Prandtl & Schmidt Numbers

$$Pr = \frac{\mu c_p}{\lambda} \text{ and } Sc = \frac{\mu}{\rho D}$$

were generally taken as 0.75, a value representative of conditions corresponding to laminar flows. Some calculations were also made with different Pr or Sc numbers to determine the effect of their value on final calculations. For the sake of simplicity Lewis number $Le = \frac{Sc}{Pr}$ was always taken to be one.

4.4.5 Incorporation of term Ri in the Species Conservation Equation- Flame Sheet Assumption

The species conservation equation

$$\rho v \frac{\partial Y_i}{\partial r} + \rho u \frac{\partial Y_i}{\partial z} = \frac{1}{r} \frac{\partial}{\partial r} \left(r \rho D_i \frac{\partial Y_i}{\partial r}\right) + R_i \quad (4.18)$$

is for species i. Thus the total number of equations would ordinarily be equal to the number of species considered.

In accordance with the choice of global reaction rate, finite or infinite, the reaction for methane can be written as

$$CH_4 + 2O_2 + 2 \times 3.76\,N_2 \rightarrow CO_2 + 2H_2O + 2 \times 3.76\,N_2 \qquad (4.19)$$

Thus the chemical species considered for structure of the flame are

CH_4 = 1
O_2 = 2
N_2 = 3
CO_2 = 4
H_2O = 5

The above chemical equation implies that

$$R_1 = \frac{R_2}{i}$$

where i is the number of mass units of oxygen required for stochiometric combustion with a single mass unit of fuel.

In the present case i is equal to 4.

Writing the differential equation for Y_1 and Y_2

$$\rho u \frac{\partial Y_1}{\partial x} + \rho v \frac{\partial Y_1}{\partial r} = \frac{1}{r} \frac{\partial}{\partial r} (r\rho D_1 \frac{\partial Y_1}{\partial r}) + R_1 \qquad (4.20)$$

and

$$\rho u \frac{\partial Y_2}{\partial x} + \rho v \frac{\partial Y_1}{\partial r} = \frac{1}{r} \frac{\partial}{\partial r} (r\rho D_2 \frac{\partial Y_2}{\partial r}) + R_2 \qquad (4.21)$$

respectively. Dividing equation (4.21) by i and subtracting it from equation (4.20) eliminates the source term and gives the following equation

$$\rho u \frac{\partial}{\partial z}\left(Y_1 - \frac{Y_2}{i}\right) + \rho v \frac{\partial}{\partial r}\left(Y_1 - \frac{Y_2}{i}\right) = \frac{1}{r}\frac{\partial}{\partial r}\left[r\rho\left(D_1 \frac{\partial Y_1}{\partial r} - D_2 \frac{\partial Y_2/i}{\partial r}\right)\right] \qquad (4.22)$$

A further simplification can be introduced by assuming equality of diffusion coefficients of fuel and oxygen and other species. The assumption, though not strictly correct is not very far from truth either, and is particularly desirable and convenient in view of other drastic assumption about chemical reaction and sparse knowledge about diffusion coefficients in multi-component reactive mixtures. i.e. $D_1 = D_2 = \ldots = D$ Further we define a fictitious species

$$\alpha = Y_1 - \frac{Y_2}{i} \quad \text{and assume } D_\alpha = D$$

Then we can reduce equation 4.22 to an equation in α

$$\rho u \frac{\partial \alpha}{\partial z} + \rho v \frac{\partial \alpha}{\partial r} = \frac{1}{r}\frac{\partial}{\partial r}\left(r\rho D \frac{\partial \alpha}{\partial r}\right) \qquad (4.23)$$

This is the classical way to introduce the flame sheet assumption first used by Burke & Schumann. Here a positive value of α indicates the fuel region and a negative value indicates the oxygen rich region.

$\alpha = 0 = Y_1 = Y_2$ defines the flame surface, at which the combustion takes place at stochiometric ratio.

Thus a single equation (4.23) in α would give both the fuel and oxygen concentration profiles. Equation (4.23) can be further modified to include other species in reaction equation (4.19) as well

Defining

$$f = \frac{\alpha - \alpha_O}{\alpha_F - \alpha_O}$$

where subscripts O and F stand for the conditions in the entering stream for oxidant and fuel, and

$$\alpha_O = -\frac{Y_{2,O}}{i}, \quad \alpha_F = 1 \qquad Y_{2,O} = 0{,}232 \text{ for air}$$

Equation 4,23 can be transformed to

$$\rho u \frac{\partial f}{\partial x} + \rho v \frac{\partial f}{\partial r} = \frac{1}{r} \frac{\partial}{\partial r} \left(r \rho D \frac{\partial f}{\partial r}\right) \qquad (4,24)$$

where f_{st} at the flame surface will correspond to

$$f_{st} = \frac{0 + \frac{Y_{2,O}}{i}}{1 + \frac{Y_{2,O}}{i}} = \frac{Y_{2,O}}{Y_{2,O} + i} \quad \text{and } f_O = 0 \quad f_F = 1$$

$f > f_{st}$ shall correspond to fuel region and

$f < f_{st}$ to oxidant region.

We further define

$$\beta = Y_1 + \frac{Y_4}{2{,}75}$$

$$\gamma = Y_1 + \frac{Y_5}{2{,}25}$$

where in β and γ, factors 2,75 and 2,25 are obtained from the stochiometric equation 4,19 in terms of mass fraction i.e.

$$R_1 = \frac{R_2}{4} = -\frac{R_4}{2{,}75} = -\frac{R_5}{2{,}25}$$

then it is obvious that

$$f = \frac{\beta - \beta_O}{\beta_F - \beta_O} = \frac{\gamma - \gamma_O}{\gamma_F - \gamma_O} = \frac{Y_3 - Y_{3,O}}{Y_{3F} - Y_{3,O}} = \frac{\alpha - \alpha_O}{\alpha_F - \alpha_O}$$

where $Y_{3,O} = 0.768$ $\qquad Y_{3,F} = 0$

$\beta_O = \gamma_O = 0$

$\beta_F = \gamma_F = 1$

and f has the uniform initial value of 1 in the fuel region and O in the oxidant region.

The boundary conditions for all species being the same i.e. at any axial position the radial gradients are zero at the center and at the walls, it is seen that a solution of equation 4.24 in f will give information about all species being considered in this case.

Global Finite Reaction Rate Assumption

It has been shown that equation 4.24 in f would provide complete information regarding the reactants, inerts and complete products of combustion according to the flame sheet model.

According to the global finite reaction rate assumption, the rate of disappearance of fuel is finite, and the relation

$$R_1 = \frac{R_2}{i}$$

holds due to stochiometry; the assumption, that the combustion occurs at stochiometric ratios being implicit.

Thus to introduce the finite reaction rate we add to the equation for Y_1 i.e. equation 4.20 to equation 4.24. Thus Y_1 would be calculated by equation 4.20 and the rest of the information could be obtained by equation 4.24.

It is convenient to do so, instead of using equations 4.20 and 4.21 with the finite reaction rate as it is easier to solve equations of the type 4.24 with no source term.

4.4.6 Simplification of Energy Equation

The energy equation 4.17

$$\rho u \frac{\partial h'}{\partial x} + \rho v \frac{\partial h'}{\partial r} = \frac{1}{r}\frac{\partial}{\partial r}\left(r \frac{\mu}{Pr}\frac{\partial h'}{\partial r}\right) + \frac{1}{r}\frac{\partial}{\partial r}\left[r \sum_j \left(\frac{1}{Sc} - \frac{1}{Pr}\right) h_j \frac{\partial Y_j}{\partial r}\right]$$

can be simplified by assuming Le = 1 or Sc = Pr which reduces the last term to zero. This assumption though strictly not true, is close to truth and is often adopted in combustion calculations (78). Further as the velocities in the system under question are low, the kinetic energy term in stagnation enthalpy

$$h' = h + \frac{V^2}{2}$$

can be neglected and the equation can be written in h instead of h', i.e.

$$\rho u \frac{\partial h}{\partial x} + \rho v \frac{\partial h}{\partial r} = \frac{1}{r}\frac{\partial}{\partial r}\left(r \frac{\mu}{Pr}\frac{\partial h}{\partial r}\right) \qquad (4.25)$$

Defining $\eta = \dfrac{h - h_O}{h_F - h_O}$ equation 4.25 can be written as

$$\rho u \frac{\partial \eta}{\partial x} + \rho v \frac{\partial \eta}{\partial r} = \frac{1}{r}\frac{\partial}{\partial r}\left(r \frac{\mu}{Pr}\frac{\partial \eta}{\partial r}\right) \qquad (4.26)$$

It can be seen that η will have a value of 1 in the fuel entry region and 0 in the oxidant entry region. The boundary conditions will be

$$\frac{\partial \eta}{\partial r} = 0 \quad \text{at } r = 0 \text{ and } r = R$$

It is seen that equation 4.26 in η is the same as equation 4.24 in f, Schmidt & Prandtl's number being equal

$$\rho u \frac{\partial f}{\partial x} + \rho v \frac{\partial f}{\partial r} = \frac{1}{r} \frac{\partial}{\partial r} \left(r \frac{\mu}{Sc} \frac{\partial f}{\partial r} \right) \qquad (4.24)$$

and have the same initial and boundary conditions.

Thus variable f can also provide information about h

$$f = \frac{h - h_O}{h_F - h_O} \quad \text{or}$$

$$h = f(h_F - h_O) + h_O$$

4.5 Final form of Differential Equations

In light of the preceding discussion we can write the differential equation in final form, with their respective boundary condition as

$$\frac{\partial}{\partial r}(\rho v r) + \frac{\partial}{\partial x}(\rho u r) = 0 \qquad (4.15)$$

$$\rho u \frac{\partial u}{\partial x} + \rho v \frac{\partial u}{\partial r} = \frac{1}{r} \frac{\partial}{\partial r} \left(r \mu \frac{\partial u}{\partial r} \right) - \frac{dp}{dx} \qquad (4.16)$$

with initial condition

$$z = 0$$

$$0 \leq r \leq kR \quad u = 2 \cdot u_{\text{fuel, av}} \left[1 - \left(\frac{r}{kR} \right)^2 \right]$$

$$kR \leq r \leq R$$

$$u = \frac{2 \cdot u_{\text{air, av}}}{\left(1 + k^2 - \frac{1-k^2}{\ln (1/k)} \right)} \left[1 - \left(\frac{r}{R}\right)^2 + \frac{1-k^2}{\ln (1/k)} \ln \left(\frac{r}{R}\right) \right]$$

and boundary condition

$$r = R \quad u = v = 0$$

$$r = 0 \quad \frac{\partial u}{\partial r} = 0 \quad v = 0$$

$$\rho u \frac{\partial f}{\partial z} + \rho v \frac{\partial f}{\partial r} = \frac{1}{r} \frac{\partial}{\partial r} \left(r \frac{\mu}{Sc} \frac{\partial f}{\partial r} \right) \qquad (4.24)$$

Initial condition

$$0 \leq r \leq kR \qquad f = 1$$

$$kR \leq r \leq R \qquad f = 0$$

Boundary condition

$$\frac{\partial f}{\partial r} = 0 \qquad \text{at } r = 0 \ \& \ r = R$$

$$\rho u \frac{\partial Y_i}{\partial z} + \rho v \frac{\partial Y_i}{\partial r} = \frac{1}{r} \frac{\partial}{\partial r} \left(r \frac{\mu}{Sc} \frac{\partial Y_i}{\partial r} \right) + R_i \qquad (4.25)$$

Initial condition

$$0 \leq r \leq kR \qquad Y_1 = 1$$

$$kR \leq r \leq R \qquad Y_1 = 0$$

Boundary condition

$$\frac{\partial Y_1}{\partial r} = 0 \qquad \text{at } r = 0 \ \& \ r = R$$

The major assumptions in arriving at these equations have been

i) Diffusion coefficients of all species at any point is the same i.e. $D_j = D$

ii) Lewis' number is unity

iii) Fuel is destroyed by a single step chemical reaction and rate of destruction is finite

iv) Radiation losses have been neglected.

The solution of the above equations will give the structure of the flame. The nitric oxide profile can then be calculated by adding the equation

$$\rho u \frac{\partial Y_{NO}}{\partial z} + \rho v \frac{\partial Y_{NO}}{\partial r} = \frac{1}{r} \frac{\partial}{\partial r} \left(r \frac{\mu}{Sc} \frac{\partial Y_{NO}}{\partial r} \right) + R_{NO} \qquad (4.27)$$

with initial conditions

$$0 \leq r \leq R \qquad Y_{NO} = 0$$

and boundary condition

$$\frac{\partial Y_{NO}}{\partial r} = 0 \qquad r = 0 \text{ or } r = R$$

Simultaneous solution of equations presented in section 4.5 will give us the desired calculated concentration profiles of NO.

CHAPTER 5
COMPUTATIONAL PROCEDURES

5.1 Introduction

The equations presented in Chapter 4 are nonlinear, second order partial differential equations with source terms and have to be solved numerically. The most common technique used for numerical solution of these types of equations is that of finite differences. Two computer programs based on this technique by Gosman etal (28) and Patankar & Spalding (58), for the solution of elliptic and parabolic form of equations respectively, became available to this author successively in above order. It was felt that these programs could be used directly with modifications to suit this particular problem.

Solution of governing equations was first attempted by using the program for solution of the elliptic form of equations (Gosman etal). Experience showed that because of the nature of the equations, excessive amounts of time would be required to achieve a reasonable degree of sophistication and accuracy.

It seemed that the solution of the parabolic type of equations by the method of Patankar & Spalding (58) would meet the needs. The expectation was justified by subsequent experience, however, as mentioned earlier, lack of sufficient knowledge in chemical kinetics did not allow proper establishment of flame structure from first principles.

Finally it was decided to use experimental values to establish the flame structure. This was achieved by suppressing the solution of species conservation and energy equations in solution of the parabolic form of equations and instead experimental values for temperature and specie concentration were introduced. Momentum and NO conservation equations were then solved by the computer program to get the desired results.

5.2 Computation by Solution of Elliptic Form of Equation

Gosman etal (28) have published a monograph "Heat and Mass Transfer in Recirculating Flows" in which a generalised development of a computer program for solving elliptic equations has been described.

These equations are basically the same, as derived earlier and given by equations 4.10 through 4.14, along with various simplifications introduced later and the relations for properties. In order to apply a generalized method, equations are transformed or combined into more convenient form. The momentum equations in the radial and axial directions are combined to eliminate the pressure terms and most of the velocity terms. Performing this operation results in a new variable, vorticity (ω). In cylindrical geometry, it is convenient to replace ω as the dependent variable by ω/r. A second manipulation normally undertaken is to introduce the stream function ψ, defined by

$$\rho u r = \frac{\partial \psi}{\partial r} \quad \& \quad \rho v r = -\frac{\partial \psi}{\partial z}$$

into the continuity equation and into the other governing equations where ever velocity appears. The preceding manipulation results in elimination of the continuity equation and equations for the following dependent variables are obtained

- Stream function ψ
- Vorticity variable ω/r
- Stagnation enthalpy h'
- Species conservation equation for component j, Y_j

The equations for each of these dependent variables have a similar structure. For axi-symmetric flow, the general form is represented by

$$a_\theta \left[\frac{\partial}{\partial z}\left(\theta \frac{\partial \psi}{\partial r}\right) - \frac{\partial}{\partial r}\left(\theta \frac{\partial \psi}{\partial z}\right)\right] - \frac{\partial}{\partial z}\left[b_\theta \frac{\partial}{\partial z}(c_\theta \theta)\right]$$

$$- \frac{\partial}{\partial r}\left[b_\theta \frac{\partial}{\partial r}(c_\theta \theta)\right] + d_\theta = 0 \quad (5.1)$$

Values of a_θ, b_θ, c_θ, d_θ are given in Table 5.1 for each of the dependent variables, θ, considered.

Comparing the general form of equation 5.1 with system of equations 4.10 through 4.14 readily shows that this program could be used with minor modifications.

The finite difference formulation of these equations is covered in the above referred monograph and will not be discussed here.

TABLE 5.1

Values of a_ϕ, b_ϕ, c_ϕ, and d_ϕ in Equation 5.1

ϕ	a_ϕ	b_ϕ	c_ϕ	d_ϕ
ψ	0	$\frac{1}{\rho r}$	1	$-\omega$
$\frac{\omega}{r}$	r^2	r^2	μ	$-r^2\left\{\frac{\partial}{\partial z}\left(\frac{u^2+v^2}{2}\right)\frac{\partial\rho}{\partial r}\right.$ $\left.-\frac{\partial}{\partial r}\left(\frac{u^2+v^2}{2}\right)\frac{\partial\rho}{\partial z}\right\}$
h'	1	$r\sigma_h$	1	$-\frac{\partial}{\partial z}\left[\mu r\left\{\left(1-\frac{1}{Pr}\right)\frac{\partial V^2/2}{\partial z}\right.\right.$ $\left.\left.+\sum_j\left(\frac{1}{Sc}-\frac{1}{Pr}\right)h_j\frac{\partial V_j}{\partial z}\right\}\right]$ $-\frac{\partial}{\partial r}\left[\mu r\left\{\left(1-\frac{1}{Pr}\right)\frac{\partial V^2/2}{\partial r}\right.\right.$ $\left.\left.+\sum_j\left(\frac{1}{Sc}-\frac{1}{Pr}\right)h_j\frac{\partial V_j}{\partial r}\right\}\right]$
V_j	1	$r\sigma_j$	1	$-rR_j$

The algebric equation resulting from the finite difference formulation are solved for the complete grid by an iterative technique of successive substitution.

5.2.1 Computational Details

Solution with the Burke-Schumann (Flame Sheet) Assumption

Solution was obtained, for flame condition A, described in Chapter 3 by solving equations for Ψ, ω/r, f and Y_{NO}. As was demonstrated in Chapter 4, the equations for the dependent variable f is the same as for Y_j, with $R_j = 0$. With the flame sheet assumption the dependent variables f replaces dependent variables Y_1, Y_2, Y_3, Y_4, Y_5 and h.

To minimize computational time and still effectively cover the area of steep gradients, a non-uniform grid was tried. This led to convergence problems. The final adopted grid was uniform and 14 x 19 in size and is shown schematically in Figure 5.1.

As is seen from Figure 5.1, this grid is very course, particularly in the Z direction where the step size is 1". As expected NO values were very low, of the order of 10^{-9} mole percent, partly due to the characteristic of structure due to flame sheet assumption and partly due to very large steps.

In order to account for radiation losses in this solution, it was argued that since in this model energy release takes place at a surface only, a reduction in enthalpy to correspond with the experimental

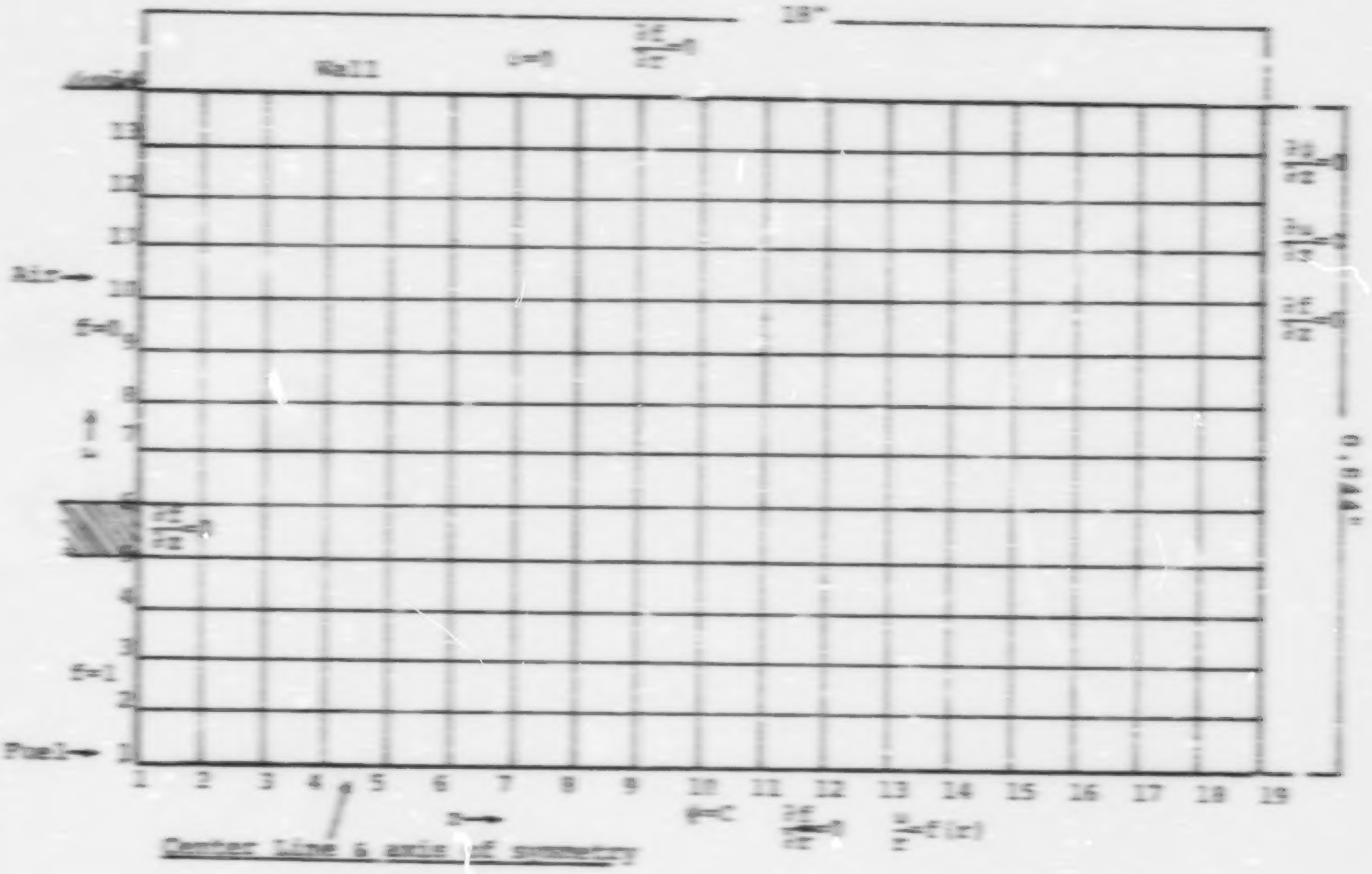
18"
Wall
u=0
$\frac{\partial f}{\partial r}=0$
Ambient
Air→
f=0
r↑
$\frac{\partial f}{\partial z}=0$
f=1
Fuel→
1
2
3
4
5
6
7
8
9
10
11
12
13
1
2
3
4
5
6
7
8
9
10
11
12
13
14
15
16
17
18
19
z→
φ=C
$\frac{\partial f}{\partial r}=0$
$\frac{u}{r}=f(r)$
$\frac{\partial u}{\partial z}=0$
$\frac{\partial v}{\partial z}=0$
$\frac{\partial f}{\partial z}=0$
0.044"
Center Line & axis of symmetry

Figure 5.1: Grid and Boundary Conditions for solution of elliptic form of equations

temperature would account for the radiation loss. However this sort of correction can be applied only when the specific heat of the mixture is supposed to be constant and independent of temperature. In case of variable specific heat, temperature also depends on the number of species considered.

The complete results for this calculation are presented in Chapter 6, where no adjustment was made for radiation loss, the value of Schmidt Number used was 0.75 and apart from NO all the five species i.e. CH_4, O_2, N_2, CO_2 and H_2O were considered.

Experience showed that any attempt to increase the nodes in the grid to increase accuracy would result in an undesirable amount of computer time.

5.2.2 Attempted Solution with Finite Global Reaction Rate

Solution for flame condition A, was attempted by solving equations for ψ, ω/r, f, Y_1 and Y_6 with the same grid of 14 x 19.

The rate of reaction of fuel was expressed as

$$R_1 = M_1 \frac{dC_1}{dt} = A\,[O_2]^m\,[CH_4]^n\,e^{-(E/RT)}$$

m and n were taken to be 1, and values of A and E were varied in the following range

$A = 10^{12} - 10^{15}$ cc/gm mole-sec

$E = 15{,}000 - 40{,}000$ cal/gm mole

One additional requirement for obtaining a solution according to the finite global reaction rate assumption is an ignition condition, a mathematical analogue of the spark to start combustion. This requirement dictates either an additional initial condition for the energy equation or an additional term in the energy equation. This requirement was circumvented by imposing the temperature profile at the first calculated downstream position from the solution with flame sheet model.

However, in a limited number of trials with varying A and E, no convergence could be obtained. At very high activation energy values, the mathematical analogue of ignition could not be sustained and a pure diffusion solution was obtained. At low activation energy, it resulted in instability.

At this stage this program was not considered worth pursuing any further.

5.3 Computation by Solution of Parabolic Form of Equations

Patankar and Spalding (58) have published a monograph "Heat and Mass Transfer in Boundary Layers" in which a generalised development of a computer program for the solution of parabolic equations has been described.

The equations presented in section 4.5, arrived at by adopting the boundary layer assumptions are parabolic and thus can be solved by this method. In order to simplify computations several manipulations are made and these equations are transformed to more convenient form. The manipulations are:

- Introduction of the stream function, Ψ, which is defined such that it is constant along a stream line, so that

  $$z = \text{fixed} \quad d\Psi = \rho u r dr$$

- $z - \Psi$ coordinates, the Von-Mises coordinate system is adopted instead of the usual z, r system, i.e. the independent variable r is replaced by stream function Ψ as the cross stream variable

- The cross stream variable is non-dimensionalized as

  $$\omega = \frac{\Psi - \Psi_I}{\Psi_E - \Psi_I}$$

  where Ψ_I is the value of the stream function at the inner boundary, i.e. the axis of symmetry in this case and Ψ_E is the value of the stream function at the external boundary, i.e. the wall in this case. These are defined as

  $$\frac{d\Psi_I}{dz} = -r_I \dot{m}_I''$$

  $$\frac{d\Psi_E}{dz} = -r_E \dot{m}_E''$$

where $\dot{m}''$ stands for the rate of mass transfer and the subscripts I and E stand for internal and external boundaries i.e. axis of symmetry and wall in this case.

These manipulations result in elimination of continuity equation and differential equation for the following variables

- Stream velocity u
- Stagnation enthalpy, h'
- Mass fraction of specie j, Y_j

The equation for each of these dependent variables has a similar structure. For axisymmetric flow, the general form is represented by

$$\frac{\partial \theta}{\partial x} + (a + b\omega)\frac{\partial \theta}{\partial \omega} = \frac{\partial}{\partial \omega}\left(c\frac{\partial \theta}{\partial \omega}\right) + d \qquad (5.2)$$

where

$$a = r_I \dot{m}_I'' / (\psi_E - \psi_I)$$

$$b = (r_E \dot{m}_E'' - r_I \dot{m}_I'') / (\psi_E - \psi_I)$$

and

$$c = r^2 \rho u \cdot \mu / \left[(\psi_E - \psi_I)^2 \ \Gamma\right]$$

Here θ stands for the dependent variable and d is the term on the right hand side which does not contain $\frac{\partial \theta}{\partial \omega}$. Table 5.2 gives the particular expression for d and Γ given in definition of c above.

Again the finite difference formulation for this general equation will not be discussed here.

TABLE 5.2

Value of d and f in Equation 5.2

ϕ	d	f
u	$-\frac{1}{\rho u}\frac{dp}{dx}$	1
h'	$\frac{\partial}{\partial\omega}\left\{\frac{r^2\rho u\mu}{(\psi_E-\psi_I)^2}\left(1-\frac{1}{Pr}\right)\frac{\partial(u^2/2)}{\partial\omega}\right\}$	Pr
V_j	$R_j/(\rho u)$	Sc

The finite difference equations finally arrived at are solved by simple successive substitution formulae, which permit step by step progress of solution as against iteration for the solution of the complete grid.

5.3.1 Computational Details

Solutions were obtained for flame condition A based on the flame sheet assumption and the global finite reaction rate. In the case of the global finite reaction rate assumption, the ignition condition was provided by imposing a temperature profile at the first downstream calculated axial position; the temperature profile at that position having been obtained by the flame sheet model previously.

5.3.1-1 Grid Size & Selection

As mentioned earlier, the independent space variables in this scheme are x and ω, the non-dimensional stream function as the cross stream variable. Thus, the grid specifies the initial values of stream lines and all the downstream calculations are performed along these stream lines. This feature results in divergence of stream lines in the areas where temperatures are high. In order to effectively cover the region of steep gradients, non-uniform grids are required. Two grids with 35 and 49 intervals were tried. Most of the calculations were performed with 49 internal grids. However, both the grids gave similar results. Another feature of this program is that no finite thickness of fuel tube wall can be introduced, as that would induce reverse flow and negative velocities. Therefore, in calculation, wall radius was reduced slightly to have the actual mass flow rates.

5.3.1.2 Forward Step

As recommended by Patankar and Spalding (58), the forward step was taken as proportional to the outer radius. The constant of proportionality used was 0.05 and this resulted in a downstream distance of about 1 mm or less per step.

5.3.1.3 Prandtl and Schmidt Number

As it has been already assumed that both Prandtl and Schmidt are equal, henceforth the term Schmidt-Number would stand for both.

It is normally expected that the solution obtained based on the flame sheet model predicts the gross structure fairly well. Thus it was reasoned that the solution should be able to predict the temperature at the symmetry axis, at various axial locations fairly close to the experimental values.

Calculations performed with Sc = 0.75 indicated lower central temperatures. Various values of Sc were tried and it was found that Sc = 0.5 gave the results closest to experimental ones. The reason for this value of Sc = 0.5 was not investigated; as later it turned out that this solution technique was not used for final calculations.

5.3.2 Reaction Rate

The constants A and E in the reaction rate expressions were varied in the following range.

$$A = 10^{12} - 10^{16} \quad \frac{cc}{gm\ moles\text{-}sec}$$

$$E = 30,000 - 40,000 \text{ cal/gm mole}$$

The reaction rate term was calculated by two methods

i) Reaction rate was calculated in the straight forward manner

$$\text{i.e.,} \quad -\frac{d[CH_4]}{dt} = A\,[CH_4]^m\,[O_2]^n\,e^{(-E/RT)}$$

$[CH_4]$ and $[O_2]$ were calculated from Y_1 and Y_2 where Y_1 is a dependent variable and Y_2 is calculated from a combination of Y_1 and f.

ii) The program formulation allows the source term to be expressed as a linear function of the dependent variable. Patankar & Spalding (58) express the above term for concentrations as

$$[CH_4][O_2] = [CH_4]_u\,[O_2]_u \cdot \frac{(Y_1 - Y_{1,b})}{(Y_{1,u} - Y_{1,b})}$$

for the forward interval.

Here $Y_{1,b}$ is the value of Y_1 which will prevail if reaction proceeds as far as possible, while the variable α remains unchanged; hence we have

$$\alpha_U < 0 \quad Y_{1,b} = 0$$

$$\alpha_U > 0 \quad Y_{1,b} = \alpha_U$$

The subscript U stands for the upstream values in the calculations.

Based on the above relations $Y_{1,b}$ is expressed as

$$Y_{1,b} = \frac{|\alpha_U| + \alpha_U}{2}$$

This procedure is mainly intended to prevent excessive reaction rate.

In results, these methods are referred to as Reaction Mode 1 and Reaction Mode 2 respectively. It might be mentioned here that Reaction Mode 2 seems to slow down the reaction rate at high temperuture as compared to Reaction Mode 1. For most of the calculations Reaction Mode 2 was used.

Experience with various activation energy values showed that with E = 35,000 or above, the reaction did not sustain and with E = 30,000 the reaction rate was excessive. The corresponding value of A in these calculations was 10^{14}. These calculations indicated that an appropriate value of E would lie between 30,000 and 35,000 cal/gm mole. However, a few further calculations to find the appropriate value by trial and error, indicated that it would be a long search and that this type of rate expression gave rise to some physically impossible results mentioned below, for acceptable values of activation energy which would at least sustain the reaction mathematically.

All the physically impossible situations can be attribuied to excessive reaction rate, which result in excessive depletion of fuel and oxidant. These situations and the solutions adopted or attempted to avoid them are described below.

5.3.2.1 Excessive Temperature

It will be recalled that at any point temperature is calculated by using the following expression

$$\sum_j Y_j c_{pj} (T) \times T = h - Y_f \times HC = h_s$$

where h_s is the notation for $h - Y_f \times HC$, and values of h, Y_f and Y_j's are obtained as direct solution of equations or from other dependent variables e.g. f, m etc. It is to be noticed that the energy equation with h as a dependent variable has no source term, as such, the value of h is determined by flow field and the values of exchange coefficients with no regard to chemical reaction. In case of excessive reaction rate, a very low value of Y_f is obtained resulting in an excessive value of h_s, which gives a very high temperature value, sometimes more than adiabatic flame temperature.

It will be recalled that

$$f = \frac{h - h_O}{h_F - h_O} \quad \text{and } f_{st} = \frac{0.232}{0.232 + 6} = 0.05846$$

thus $h_{st} = f_{st}(h_F - h_O) + h_O$ and at $f = f_{st}$ $Y_1 = 0$

thus $h_a = h_{st}$ is the maximum possible value of h_a

To correct this situation due to excessive reaction i.e. in the event of $h_a > h_{st}$ at any point, the value of $(h_a - h_{st})/HC$ is added to the calculated value of Y_1 to get its proper value. The values of Y_2 etc are accordingly modified.

This manipulation effectively brings the chemical reaction rate in line with the diffusion and conduction phenomena which are more predominant.

5.3.2.2 Negative Values of Oxygen Mass Fraction

The above situation was sometimes encountered even after introduction of the preceding correction. This being a physically impossible situation all negative values of Y_2 were made zero.

The above correction still left much to be desired in the calculated oxygen profile as compared to the experimentally obtained oxygen profile. Various methods attempted to correct the O_2 profile did not prove fruitful.

Another approach was tried to get calculated O_2 penetration in the fuel rich region, to correspond to the experimental values. Kassoy &

Williams (37) have concluded for droplet studies, that an increasingly large amount of oxidiser penetrates the flame as n increases above 1.0 in the following comparable expression

$$-\frac{d[CH_4]}{dt} = A[CH_4]^m [O_2]^n e^{(-E/RT)}$$

Various values of $n > 1$ were tried in calculations, but that too failed to give desirable results.

5.3.3 Final Comments about this Method

It was concluded that trial and error search for the proper rate expression (if there is one), which will give reasonable O_2 profiles will be long, and though it may be possible to predict NO trends correctly, it will not lead to any further meaningful conclusion due to lack of knowledge of chemical kinetics, particularly in formation and destruction of carbon and the thermal radiation from it. This aspect is discussed more completely in Chapter 6.

In Chapter 6, a few selected results are given for indicative purposes only. In these calculations only three species CH_4, O_2, N_2 were considered apart from NO.

5.4 Computation Using Experimental Results

In this method, basically the program described in Section 5.3 was used with modifications. Thus only the differences from the method described in Section 5.3 will be discussed here. The following approach is discussed with reference to flame condition A, but is true in general as well. The differences in detail will be indicated wherever appropriate.

5.4.1 General Outline of Approach

From the discussion in Chapter 3, it can be recalled that the flame can be roughly divided into four zones i.e. non-reactive space near the base, premixed like region, diffusion controlled region and the carbon dominated zone. The most interesting part of the flame is the diffusion controlled region and the experimental measurements at 17 mm, 47.5 mm and 117.5 mm downstream positions, are in this region.

The measurements at 0.5 mm, 1 mm and 2 mm downstream positions are either in the non-reactive space or on the boundary of the non-reactive space and the premixed like region.

An examination of profiles at 17 mm, 47.5 mm and 117.5 mm positions in Figures 3.4 - 3.6 shows, that change in all profiles is quite regular, except for the fact that the maximum temperature surface seems to more away from the center, between the 17 mm and 47.5 positions, and seems to move towards the center between 47.5 mm and 117.5 mm positions. This indicates, that if the concentration of a species or temperature at a particular location with coordinates (r_1, z_1) was desired $(17 < z_1 < 47.5)$, then a linear interpolation of the form

$$T_{r_1, z_1} = T_{r_1, 17} + (T_{r_1, 47.5} - T_{r_1, 17}) \times (z_1 - 17) / (47.5 - 17.0)$$

would give a reasonable value of the desired concentration or temperature, which will not be very far from the true value. The same logic could also be applied to values between 47.5 mm and 117.5 mm positions. However, it would seem that this scheme will not be applicable to axial positions between 2 mm and 17 mm as well as between the 117.5 mm and 324 mm position, particularly because the shapes of O_2 profiles at the 2mm and the 324 mm positions are dissimilar to those at 17 mm, 47.5 mm and 117.5 mm, and also because the value of peak temperature at a given plane goes through a maximum somewhere between 2 mm and 17 mm, most probably between 6 mm and 10 mm. Thus an extrapolation of temperature or species concentration based on values of 47.5 mm and 17 mm, could perhaps be valid up to 10 mm position.

The preceding argument suggests that, it is possible to approximate reasonably well the values of temperature and specie concentrations at any point between 10 mm and 117.5 mm downstream positions by interpolation or extrapolation of experimental values.

Thus to establish the structure of the flame, apart from information derived from the experimental data, only the knowledge of flow field is required.

It is generally recognized that a solution obtained by using the flame sheet assumption predicts gross structure of the flame fairly well and this includes the flow field. This solution was thus used to establish the flow field up to the 10 mm downstream position. This involved simultaneous solution for equations of dependent variables u, σ, h and Y_6. At the 10 mm position solution of equations with dependent variables σ and h was suppressed, instead, experimental values of temperature and species concentrations were introduced. For flame condition C, the position where experimental values were introduced was 30 mm, as no detailed experimental data is available for the 17 mm position. Downstream of the position, where experimental values are introduced, only equations for the dependent variables u and Y_6 are solved. However, NO calculations immediately downstream of the position of introduction, e.g. 10 mm for flame condition are not valid, because calculated values preceding to 10 mm are based on a structure established by the flame sheet assumption. In order to have a meaningful comparison with experimental values, experimental concentrations of NO are introduced at the 17 mm position for flame conditon A and the NO concentration profiles are calculated at the 47.5 mm and 117.5 mm positions. For flame conditions B & C the experimental values of nitric oxide are introduced at the 47.5 mm position and profiles are calculated for the 117.5 mm position only.

5.4.2 Introduction of Experimental Data in the Computer Program

The experimental data reported in Chapter 3 is in tabular form for a particular axial position and gives a concentration or temperature at a particular radius for that particular position. However, it is easier to have this data in form of a function which can be readily evaluated in a computer program. Polynomial fits were obtained for concentration profiles with radius as the independent variable. Wherever it was not possible to obtain a single polynomial fit for the complete profile, the polynomial fits were obtained for different interconnecting parts of the profile. These fits were obtained by using POLWOT Subroutine on DATACRAFT 6024 computer of Engineering Computing Laboratory of University of Wisconsin.

The experimental values of temperature reported in Chapter 3 are direct thermocouple readings with no correction for radiation or conduction losses. However, in order to use these temperatures to establish flame structure, these corrections have to be applied. The theoretical analysis involved in determining a radiation correction is well known. In the present calculation, the following equation mentioned by Fristrom & Westenberg (23) has been used,

$$Tg - Tc = \frac{\epsilon \sigma d\,(Tc^4 - Tw^4)}{2\lambda}$$

where

Tg is the desired gas temperature in K°

Tc is the thermocouple temperature in K°

Tw is the wall temperature in K°

d is the diameter of thermocouple in cm

σ is the Stephan-Boltzmann Constant in C.G.S. units

λ is the thermal conductivity of gas at gas temperature in C.G.S units

and ε is the emissivity of thermocouple.

The value of λ was taken to be that of nitrogen at approximately 2000°K i.e. $\lambda = 10^4$ erg cm^{-1} K^{-1} Sec^{-1} and the emissivity value was taken as 0.4, and independent of temperature. The use of emissivity value of 0.4 is justified in Chapter 6.

The polynomial fits for temperature profiles were obtained in a manner similar to that described for concentration profiles.

Experimental temperature and concentration profiles for O_2, CH_4 and N_2 were thus introduced.

5.4.3 Final Remarks

Calculations were made for each condition only up to the 120 mm downstream position. For the purpose of calculation of properties, CH_4, O_2 and N_2 values determined by $Y_{N_2} = 1 - Y_{CH_4} - Y_{O_2}$ were used. For NO calculations actual values of N_2 were used.

The results of these calculations are presented in Chapter 6.

CHAPTER 6
RESULTS AND DISCUSSION

6.1 Presentation of Results

Experimental results are presented in Chapter 3. The equations developed in Chapter 4 and method of solution involving experimental values described in Article 5.4, along with the Zeldovich mechanism for formation of nitric oxide, are used to calculate the concentration profiles of nitric oxide for all flame conditions. The calculated concentration profiles were integrated within the program to determine the mass or moles of nitric oxide flowing through a plane downstream of fuel tube mouth. Using the same computed flow field, the experimental nitric oxide profiles were integrated to obtain similar results for purpose of comparison. The experimental nitric oxide profile for flame condition A at the 324 mm downstream position, was integrated using the flow field at that position, established by the solution of the elliptic form of equation involving Burke-Schumann assumptions.

The calculated NO concentration profiles are compared with experimental NO concentration profiles in Figures 6.1 and 6.4. Solid lines represent the results of theoretical calculations of NO, based on experimental data for structure of the flame, as discussed in Chapter 4 and 5. Experimental curves in dashed lines are reproduced from the results presented in Chapter 3. The corresponding flame conditions and axial positions for the profiles are indicated on each figure. Figure 6.5 shows a plot of the calculated rate of formation of nitric oxide against radius, for flame condition A at axial positions of 47.5 and 117.5 mm. The other relevent information regarding the flames at various axial positions, i.e. temperature and other specie concentration profiles have been presented in Chapter 3.

The comparison of integrated values of calculated and experimental NO profiles is presented in Table 6.1. Table 6.2 presents the integrated values of experimental NO profiles for all axial position of flame condition A.

A few selected theoretical results obtained by methods of solution described in Articles 5.2 and 5.3 are presented. These solutions are based both on the Burke-Schumann assumption of infinite reaction rate and also upon an assumed finite global reaction rate as discussed in Chapter 4. The purpose of presenting these results is not to draw conclusions with regard to formation of nitric oxide, but merely to illustrate, that present insufficient knowledge of reaction kinetics of methane in diffusion flames does not permit calculation of flame structure in sufficient detail to yield meaningful conclusions with regard to nitric oxide formation.

Figures 6.6 through 6.9 present the calculated results corresponding to flame condition A, obtained by the solution of the elliptic form of the equations using the Burke-Schumann assumption as outlined in Article 5.2. Figures 6.10 and 6.11 show the calculated results corresponding to flame condition A, obtained by solution of the parabolic form of the equation using the finite reaction rate assumption, as outlined in Article 5.3.

6.2 Inadequacy of Kinetic Models for Combustion in Diffusion Flames

In Chapters 4 and 5 it was mentioned that based on experience with the global finite reaction rate assumption, it was felt that the present state of knowledge of reaction kinetics in diffusion flames was insufficient to permit establishment of flame structure accurate enough to calculate nitric oxide formation meaningfully. This insufficient knowledge is particularly in the area of carbon formation and destruction and fuel pyrolysis. Due to this insufficiency it appears that even if the more sophisticated kinetic models mentioned in Article 4.3.3.1 were used, they would not be adequate to accomplish this objective as these mechanisms do not include reactions involving pyrolysis products, particularly carbon.

In the following, it is intended to examine the effect of absence of these reactions on three aspects of diffusion flame structure which have maximum bearing on the calculation of nitric oxide.

6.2.1 Temperature

Fuel pyrolysis and the formation of carbon represent a heat sink in the fuel-rich region of the diffusion flame, partly because these reactions are endothermic and partly due to radiation losses from the carbon particles.

This affects both the temperature profile in general and the maximum temperature in the reaction zone i.e. non-inclusion of carbon and pyrolysis reactions in theoretical analysis predicts the maximum temperature zone to be farther from the flame center than indicated by the experimental determination. This effect on the temperature profile distorts the flow field and due to the nature of NO kinetics predicts peak nitric oxide at a position farther from the center than measured experimentally. The maximum temperature obtained is also affected, as it depends not only on the heat of combustion of fuel, but also on the composition and heat capacity of the mixture in the reaction zone. Absence of carbon reactions along with insufficient knowledge of transport properties in reactive mixtures does not allow correct calculation of correct maximum temperature.

The differences between the theoretical and experimental positions of peak temperature and peak nitric oxide concentration and general shape of temperature profiles particularly in the fuel-rich region is evident from a comparison of Figures 3.5 - 3.6 and 6.10 - 6.11, respectively. For example, Figure 3.5 for flame condition A at the 47.5 mm position shows the measured peak temperature at 8 mm radius or 13.5 mm from the wall, whereas the calculated position for maximum temperature is 10 mm radius or 11.5 mm from the wall as shown in Figure 6.10.

Further, Figures 3.4 through 3.7 shows that peak temperature decreases slightly with downstream distance. The global finite reaction rate model will, on the contrary, predict constant peak temperature, and it is not certain that with more complex schemes this sort of effect can be predicted.

6.2.2 Oxygen Concentration Profile

Figures 3.4 through 3.6 indicate a finite concentration of oxygen in the fuel-rich region, as determined experimentally. The calculated O_2 profile, based on globabl finite reaction rate are presented in Figures 6.9 and 6.10. As mentioned in Chapter 5, it was realised that for the global finite reaction rate assumption estimation of reaction rate constants leading to proper oxygen profiles would be a lengthy process. However, it may be possible to do so with a quasi-global reaction rate scheme by adjusting the reaction rate of the initial step involving conversion of fuel to CO and H_2.

6.2.3 Flow Field

The flow field is greatly affected by changes in fluid velocity and density which in turn are affected by temperature changes. It thus follows from the preceding discussion of calculation of correct peak temperatures and temperature profiles that the flow field will also be affected by non-inclusion of complete kinetics.

The above discussion relates to flames in which carbon is generated and destroyed. However, it is sometimes possible to have blue diffusion flames under controlled conditions (72,73). In such cases it may be possible to complete the reaction scheme by including reactions involving C_2H_2, C_2H_4 and C_2H_6, the principle products of fuel pyrolysis in methane diffusion flames (64,73) along with their oxidation schemes and the reactions for the premixed flame discussed in Chapter 4. Such a scheme might be adequate to predict the flame structure for blue diffusion flames.

In diffusion flames involving carbon, the reaction scheme without carbon may not be able to predict the structure adequately.

6.3 Discussion of Assumptions

Two major assumptions are made in establishing the flame structure and then calculating the concentration profiles of nitric oxide in accordance with the Zeldovich mechanism.

1) The emissivity of the thermocouple is taken as 0.4, and experimental temperatures are corrected on that basis for radiation losses. The corrected temperatures are then used in the establishment of flame structure.

2) The concentration of molecular and atomic oxygen are assumed to be in equilibrium with each other at the measured local temperature.

These assumptions are discussed in detail in the following:

6.3.1 Emissivity of the Thermocouple

As discussed in Chapter 2 a Pt-Pt-10% Rh thermocouple of 0.001" diameter wire and 0.005" diameter junction was used to measure experimental temperatures. This thermocouple was coated with silica, as recommended by Fristrom & Westenberg (23) to avoid catalytic effects. The measured temperatures are reported in Chapter 3.

In order to get correct temperatures it is necessary to introduce a correction for thermocouple radiation and conduction losses. Due to the very small diameter of the wire and the orientation of the thermocouple, as described in Chapter 2, conduction losses were estimated to be negligible. The expression for correction of radiation losses given in Chapter 5 requires knowledge of the thermal conductivity of gases and emissivity of the thermocouple. The thermal conductivity of gases is usually assumed to be that of nitrogen and a value of $\lambda = 10^4$ ergs/cm-k°-sec recommended by Fristrom and Westenberg (23) was adopted.

The emissivity of pure platinum can be found in the literature and has a value of about 0.2 at 2100°k (35). However, silica coating adds an uncertainity into the value of emissivity of the thermocouple. The usual practice in premixed flame temperature measurements is to assume the maximum recorded temperature as the adiabatic flame temperature and calculate the emissivity of the thermocouple on that basis.

Theoretical analysis of diffusion flames by Zeldovich (86) indicates that in the absence of radiation losses, the peak temperature should be equal to the adiabatic flame temperature for a stochiometric mixture. However, due to radiation losses, this peak temperature would be less than the adiabatic flame temperature. Unfortunately this difference cannot be estimated on the basis of this simplified analysis.

Wolfhard & Parker (61) measured diffusion flame temperatures in H_2-O_2 and CH_4-O_2 flames by the sodium line reversal method and report for H_2-O_2 flame as follows:

> "The temperature attained a rather flat maximum at 2800°C. This agrees very closely with the calculated value for a stochiometeric mixture of H_2 and O_2, allowing for dissociation but not for external heat losses. It appears therefore that diffusion flames are quite as hot as premixed flame."

Regarding CH_4-O_2 flat diffusion flame they report:

> "The maximum temperatures (by Na line-reversal method) is close to theoretical."

Other investigators, Smith & Gordon (64) and Tsuji & Yamaoka (73) have reported only direct thermocouple readings. In one droplet study (77) it is reported that the maximum temperature does not correspond to that expected for stochiometric combustion but agrees more with the value expected for rich limit combustion.

Above information indicates that the maximum temperature encountered in a diffusion flame is slightly less than the adiabatic flame temperature for stochiometric combustion.

In the flame under consideration, it was reported in Chapter 3 that the peak temperature decreases with downstream distances. The maximum recorded temperature is 3096°F for flame condition A at the 17 mm downstream position. However, upstream of the 17 mm position i.e. around 6-10 mm from the fuel tube mouth, the premixed like condition exits in the in the combustion zone. Also in this zone, radiation losses are very small. Therefore it can be expected that the peak profile temperature in this zone will be maximum i.e., ~ 3096°F. The peak temperature at 10 mm position was estimated by straight line extrapolation of the peak temperatures at the 67.5 mm position and that at the 17 mm position, as shown in Figure 6.12 and estimated to be 3107°F.

The adiabatic flame temperature for stochiometric combustion of methane was calculated by using a previously developed computer program by the author. This program, described in principle in the Appendix (D) uses previously develope subroutines SPECY 1 and SPECY 2 by Newhall (49).

The adiabatic flame temperature of equivalence ratio 1 was calculated to be 4003°R (2223°K). The estimated temperature at the 10 mm position, 3107°K (1961°K), was considered equal to 2203°K arbitrarily, i.e. slightly less than the adiabatic flame temperature, as indicated in the literature. This indicates a maximum radiation correction of 222°K. The emissivity is then calculated to be 0.4, using equation (1) discussed in Chapter 5.

For the purpose of comparison, some calculations were made for flame condition A, 47.5 mm position, assuming the emissivity to be 0.2, 0.36, 0.4 and 0.448. This comparison is shown in Figure 6.13. The emissivity value of 0.2 corresponds to that of platinum and the value of

0.448 was obtained by assuming that the maximum recorded temperature of 3096°F (1976°K) was equal to the adiabatic flame temperature. The emissivity value of 0.36 was taken only for the purpose of comparison.

The comparison presented in Figure 6.13 indicates the NO profile corresponding to 0.4 emissivity to be closest to experimental one. This value was thus used in further calculations already presented in Figures 6.1 through 6.4. It may be added here that for the results presented in Figure 6.13, a higher value for concentration of N_2

$$X_{N_2} = 1 - X_{CH_4} - X_{O_2}$$

was used, instead of the actual N_2 concentration. This accounts for the difference in curves corresponding to Sc = 0.75 in Figures 6.1 and 6.13.

6.3.2 Equilibrium Atomic Oxygen Concentration

It is well known that in combustion reactions a finite time is required for the species to equilibrate and atomic oxygen is no exception. However, the time periods for which non-equilibrium or hyper-equilibrium concentration of atomic oxygen are present i.e. relaxation time, is known to be very short. Shahed (62) calculated this time to be of the order of 0.1 m sec. for a premixed H_2-Air system. Martney (46) performed similar calculations and reported similar results for a CH_4-Air system. They also showed that this time was very short as compared to that for nitric oxide equilibration and assumed in their subsequent calculations for NO, using the Zeldovich mechanism, that atomic oxygen was in equilibrium with molecular oxygen.

Fenimore (18) reported that in the vicinity of the reaction zone in hydrocarbon-air flames, particularly rich ones, the nitric oxide formation rate exceeds those predicted by the Zeldovich mechanism and the assumption that O was in equilibrium. Fenimore termed the rapidly formed nitric oxide "prompt NO" and postulated that it was formed by some reactions other than those in the Zeldovich mechanism and most probably involving some fuel derived species.

In shock tube studies of H_2-O_2-N_2 and CH_4-O_2-N_2 mixtures Bowman (6) and Bowman & Seery (8), observed that nitric oxide formation rates were found to exceed rates indicated by the Zeldovich mechanism and the equilibrium assumption. However, observed rates were consistant with the Zeldovich mechanism without the equilibrium O assumption. In these cases values of O concentrations were determined from complete chemistry of combustion and were found to be several orders higher than equilibrium for a short time. The effect of this hyper-equilibrium O is found to be more important in case of rich flames.

With the above background, it would seem that non-equilibrium O concentration in the initial stages may be important in premixed flames, however, it is not quite clear that the same is true for diffusion flames.

The possibility of importance of non-equilibrium O in the diffusion flame under consideration was examined. Due to the following reasons, it was concluded that non-equilibrium concentration of atomic oxygen will not be important.

6.3.2.1 Experimental Data

As mentioned earlier, Fenimore (18) found more "prompt NO" in premixed flames of fuel-rich mixtures than in stochiometric or somewhat fuel-lean mixtures. Now, where as a premixed flame can be controlled to react at a predetermined, fuel/air equivalence ratio, a diffusion flame chooses its local equivalence ratio depending upon a muliplicity of factors, chiefly, the reactants diffusing to form whatever mixture is fastest burning. It is often assumed that in case of overventilated diffusion flames combustion occurs in the reaction zone in stochiometric proportions. However, from one side of the reaction zone to another, the equivalence ratio practically varies from zero to very large values. The rich equivalence ratios at which Fenimore observed more "prompt NO" would exist in such a case near the reaction zone and towards the fuel-rich region.

Figure 3.4 showing experimental nitric oxide concentration profile against radius or distance from the wall, at 17 mm downstream position for flame condition A, is particularly interesting and informative from this point of view. This shows a very sharp NO peak corresponding to the temperature profile peak. If there was any "prompt NO" being formed, by above reasoning, it would be noticed in the fuel-rich region, very close to the reaction zone and the profile will show a flat plateau or another smaller peak in that region. The absence of a platesu, another peak and the regular diffusion like profile in the fuel-rich region all indicates that NO is being formed only in the reaction zone.

The other NO profiles at the 47.5 mm and the 117.5 mm positions for flame condition A, in Figures 3.2 and 3.6, give similar information, but not as clearly as the one at 17 mm, because a part of the profiles had to be graphically interpolated. Nitric oxide profiles for flame conditions B & C also give similar information.

Similarly, as non-equilibrium O effects are also noticeable at rich equivalence ratios, these effects would normally show in the same locations as discussed for "prompt NO".

Based on the arguments presented earlier, it would seem that non-equilibrium O effects are not important.

6.1.2.2 Time Scales Involved

In those studies in which non-equilibrium effects have been considered important, it is agreed that, the time period during which these effects are important are very small i.e. 0.1 to 0.2 m secs. In shock tube studies, it practically amounts to a step input of temperature to the system. Similar is the case for premixed flames in which reactants are are converted into products, very quickly in the reaction zone and corresponding energy release and increase in temperature occurs in a very small period of time.

In the case of diffusion flames, though the main part of energy is released in the reaction zone, due to dominance of transport effects, the rise of temperature for a particular element is gradual. This is not exactly true in the case of the premixed like zone but true for the diffusion region. Due to this gradual increase of temperature, the time for which non-equilibrium conditions will persist, will be shorter than for the step input of temperature.

Moreover, in general, in diffusion flames the rate of burning in terms of number of moles of oxygen per cm^3 per sec undergoing reaction, is much smaller than that in premixed flames. Wolfhard and Parker (82) estimate this rate for an ethylene oxygen flame to be nearly five orders lower than that of the corresponding pre-mixed gas flame. This would further reinforce the argument that the time scale of non-equilibrium O will be much smaller as compared to the overall rate of reaction.

Another factor, which further supports this idea is as follows. It is well known that dilution of reactive species by inert species reduces non-equilibrium processes. An examination of complete profiles for flame condition A, in Figures 3.4 through 3.6 reveals that in the reaction zone i.e. the high temperature region, there are about 94 mole percent of inerts i.e. N_2 and CO_2 in terms of energy release reactions which is much larger than the usual 79 mole percent (roughly) in premixed flames. This would thus indicate that non-equilibrium processes will be of shorter duration.

Thus, in diffusion flames, where as the time scales of the overall combustion reaction are much larger than those in premixed flames, the relaxation time for atomic oxygen are much shorter than those in premixed flames. This coupled with experimental observation indicates that it is reasonable to consider atomic oxygen in equilibrium with molecular oxygen for the purpose of calculating nitric oxide formation.

It may be added here that, in an atmospheric burner (31), a simple model which takes into account non-uniformities of flow, but assumes that when most of the NO is being formed oxygen atoms are in equilibrium, predicts NO formation quite adequately.

6.4 Discussion of Nitric Oxide Formation in Diffusion Flames

Experimental results presented in Chapter 3 lead to the conclusion that in the diffusion flame region, nitric oxide is formed in a narrow region corresponding to the high temperature zone and diffuses into both fuel-rich and oxidant rich regions. Figure 6.5 showing the plot of the calculated rate of formation of nitric oxide against radius for flame condition A, at 47.5 and 117.5 mm positions matches the above description.

As discussed in Article 6.3, the maximum temperature encountered in the flame can be reasonably taken to be slightly less than the adiabatic flame temperature for stochiometeric combustion. Further it is reasonable to regard non-equilibrium atomic oxygen concentrations as important in the present system. Making use of these conclusions, the kinetics of nitric oxide formation discussed and the method of calculation outlined in Chapter 5. The resulting profiles were presented in Figures 6.1 through 6.4 and compared with experimental values. These figures show reasonable agreement between theory and experiment, except in the fuel-rich region where calculated concentrations are higher than the experimental values. This discrepancy may be due to insufficient knowledge of transport properties in reactive mixtures and the uncertainity in the flow field. The upstream region was determined by using an idealized model i.e. Burke-Schuman assumption. Usage of a constant emissivity value, independent of temperature, in temperature correction calculations, also contributes to this discrepency.

Table 6.1 shows the comparison between integrated theoretical and experimental profiles indicating the mass or number of moles of NO flowing per sec. through an axial plane. This comparison indicates the percentage difference on the basis of experimental values, to be maximum of the order of 29% and a minimum of the order of 6%.

It can thus be concluded that in diffusion flames concentration of nitric oxide can be adequately predicted using a reaction mechanism consisting of the following two elementary reactions

$$N_2 + O \rightleftharpoons NO + N$$

$$O_2 + O \rightleftharpoons NO + O$$

in the NO conservation equation, provided the structure of the flame can be properly established in terms of flow field, temperature and species concentration.

Experimental results further indicate that significant amounts of nitric oxide are formed in the premixed zone. Table 6.2 illustrates this point quantitatively for flame condition A and indicates that about 26% of the total amount of NO is formed in this region. In practical combustion system involving droplet combustion, this premixed like zone would roughly correspond to wake combustion. Hence, in such a system, both the diffusion combustion around the droplet and wake combustion would be important sources of nitric oxide formation.

6.4.1 Effect of Residence Time

Figure 6.14 shows a plot of man of NO flowing/sec through various axial positions against the residence times calculated for the same positions, for flame condition A. This data is given in Table 6.2. An examination of this plot reveals that in the diffusion region the rate of addition of nitric oxide with respect to residence time is almost constant. The inital high rate corresponds to the premixed like region.

6.4.2 Comparison with NO Formed in Premixed Flames

In order to compare the amount of nitric oxide formed in diffusion flames and premixed flames at the same overall equivalence ratios the following calculations were made.

- Making use of the adiabatic flame temperature program outlined in Appendix (D), the equilibrium adiabatic flame temperature and equilibrium mole fraction of nitric oxide were calculated for equivalence ratio of 0.5755.
  These values were 2918°R and 0.137×10^{-2} respectively.

- Making use of Zeldovich mechanism, equilibrium assumption for O and N, the mole fraction of NO at 310 m sec time was calculated at a temperature of 2918°R and corresponding concentration by integrating the rate equation.
  The value obtained was 0.49×10^{-6}.

- The value of NO given in Table 6.2 for flame condition A position 324 mm was converted in mole fraction to compare with above values.
  This value was found to be 0.487×10^{-4}.

This comparison indicates that the amount of nitric oxide formed in this diffusion flame is less than its equilibrium value. Further, for the same residence time this diffusion flame generates a larger quantity of NO than an equivalent premixed flame.

This is explained by the fact that where as in diffusion flames maximum temperatures attains values near to the adiabatic flame temperature for stochiometeric combustion i.e. about 4000°R, the temperature of premixed flame would be 2918°R uniformly.

6.4.3 Effect of Air-Fuel Velocity Ratio and Overall Eq. Ratio

Experimental measurements and theoretical calculations were made for three flame conditions A, B and C. In all these conditions, the fuel velocity and mass flow rate were constant and air velocity and mass flow rates were varied, giving different air to fuel velocity ratios. The experimental concentration profiles showed a lower value of NO and overall lower value NO concentration with increasing air to fuel velocity ratio and decreasing overall equivalence ratio. However, integration of these profiles at 117.5 mm position, to calculate the total man of NO flow up through that axial plane, presented in Table 6.1, shows approximately the same amount of mass of NO flowup through 117.5 mm position for all the three conditions. This indicates that the total amount of NO formed will be the same for all three conditions and that velocity ratio in this equivalence ratio range has no significant effect.

However, the preceding indication regarding the effect of air-fuel velocity ratio and overall equivalence ratio on total quantity of NO formed is not conclusive. The reason being that the total amounts of NO formed in flame conditions B and C have not been calcuated, as it would have involved excessive time and cost in computation.

6.5 Conclusions

1. Nitric oxide is formed in diffusion flames in the high temperature zone and diffuses towards both the fuel-rich and oxidant-rich regions.

2. The nitric oxide concentration profile can be adequately predicted by using a simple kinetic mechanism consisting of the following two reactions:

$$N_2 + O \rightleftharpoons NO + N$$

$$O_2 + N \rightleftharpoons NO + O$$

   This presupposes that the flame structure can be properly established.

3. It is estimated that the atomic oxygen concentration can be taken to be in equilibrium with molecular oxygen in the above calculation and that hyper-equilibrium concentrations of O are not important.

4. There seems to be no evidence of formation of extra NO, not explained by the reaction mechanism used.

5. A significant part of the nitric oxide is formed in the early stages of the premixed type combustion in this flame.

6. A comparison of the total amount of NO formed in diffusion flame with that in an equivalent premixed flame, for the same residence time, indicates that diffusion flames generate much more NO.

7. The total amount of NO formed does not seem to have any relation with the air-fuel velocity ratio or overall equivalence ratio in the range considered.

8. The present knowledge of combustion kinetics in diffusion flame is insufficient to establish flame structure well enough to calculate NO properly.

TABLE 6.1

Integrated values of calculated and experimental NO profiles in terms of mass and number of moles of nitric oxide flowing through a particular axial plane of burner per sec.

Flame Conditions	Axial Position mm	NO - Kg/sec x 10^{-8} (1) Cal.	Exp'l	NO - Kg moles/sec x 10^{-10} (2) Cal.	Exp'l	Total Mass Kg/sec x 10^{-4}	N_2 moles/sec x 10^{-5}	%Diff. between calculated & experimental $\frac{(1)-(2)}{(2)} \times 100$
A	47.5	1.2784	1.2068	4.3777	4.0560	6.211	2.1467	5.9
A	117.5	2.1698	1.7284	7.5744	5.7612	6.211	2.1429	25.5
B	117.5	2.3034	1.7802	7.8573	5.9341	6.1175	2.0332	29.3
C	117.5	2.1181	1.8495	7.1797	6.1650	9.966	3.4960	14.56

TABLE 6.2

Integrated values of experimental NO profiles for flame condition A in terms of mass of NO flow/sec through an axial plane.

Axial Position	Calculated Residence Time m sec	NO-Kg/sec	Fraction* Total Amount of NO
17	31.505	0.1184×10^{-8}	0.256
47.5	78.179	1.2166×10^{-8}	0.35
117.5	156.83	1.7284×10^{-8}	0.55
324	300-320**	3.04×10^{-8}	1.00

* Fractions are calculated, taking the mass of NO at 324 mm position to be 1.00

** This is a rough estimation only

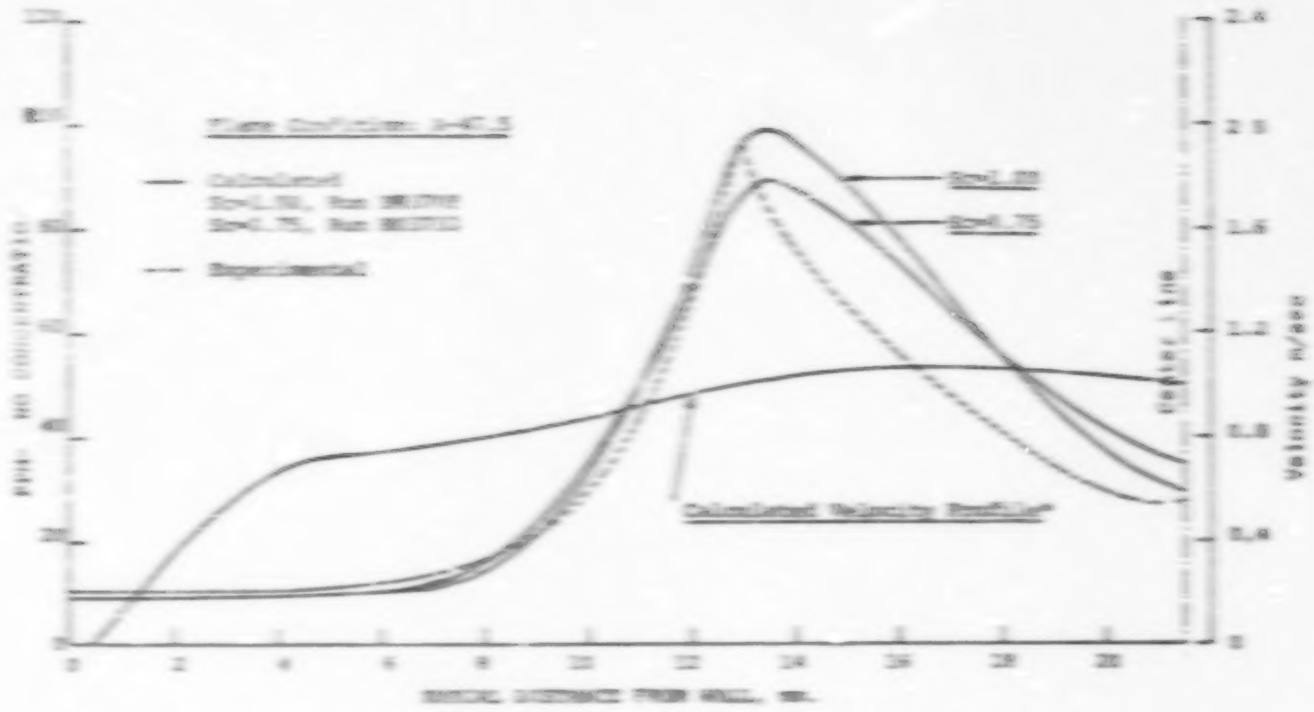

Figure 6.1: Calculated and Experimental NO Concentration Profiles 47.5 mm. above burner entrance

*In these calculations fuel tube wall thickness could not be introduced (see 5.3 and 5.4) as such, in order to have the actual mass flow rate zero velocity is shown slightly away from the wall.

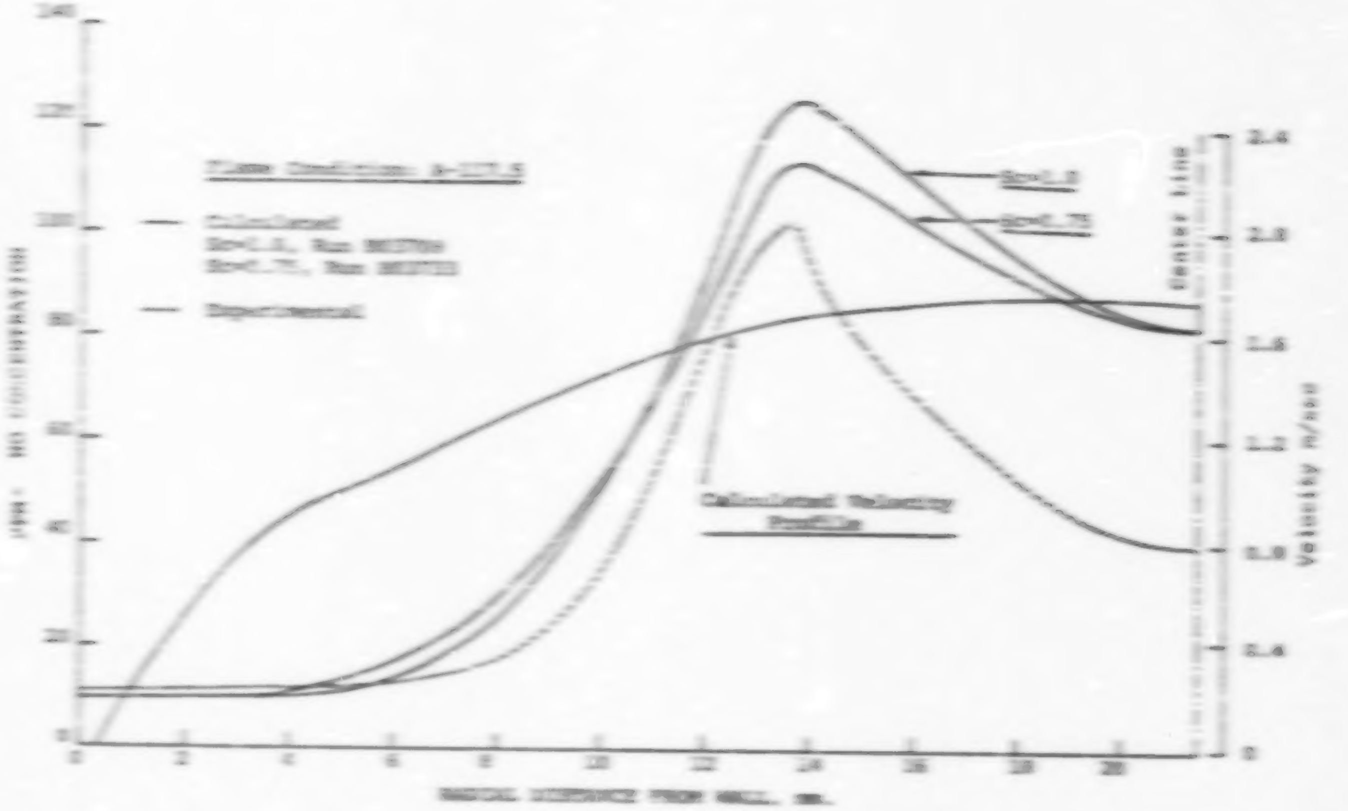

Figure 6.2: Calculated and Experimental NO Concentration Profiles at 117.5 mm. above burner surface

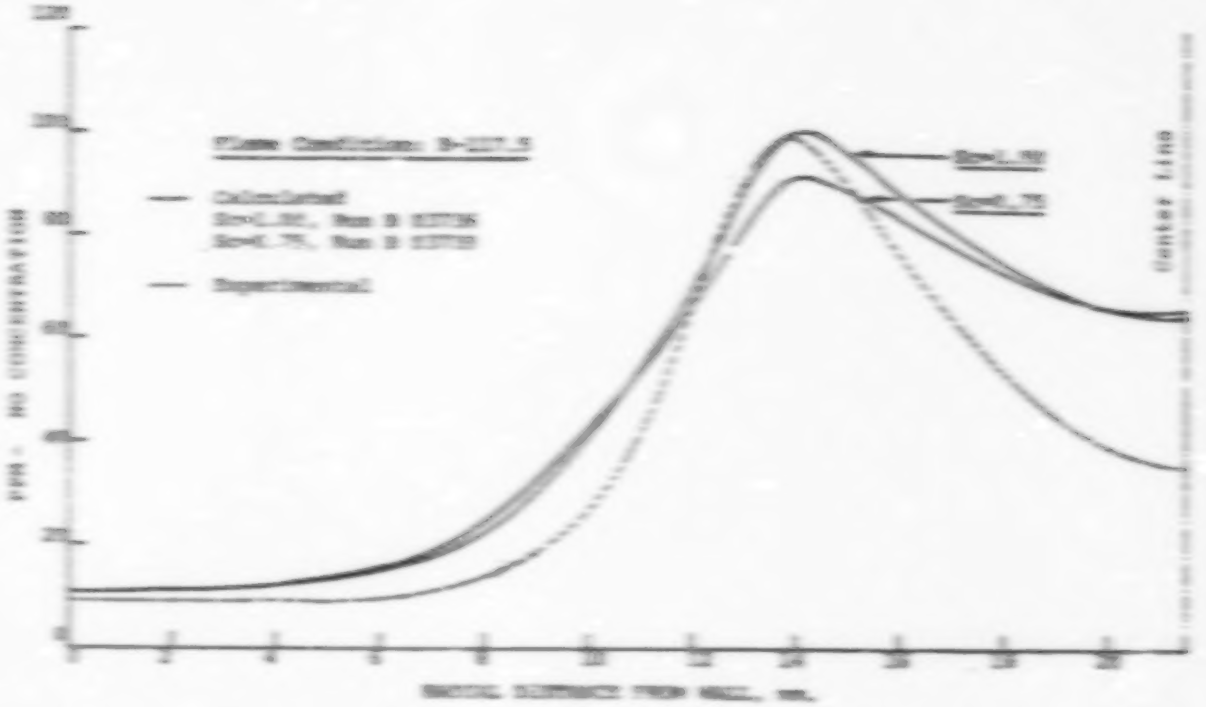

Figure 4.3: Calculated and Experimental NO Concentration Profiles 227.5 mm. above burner entrance

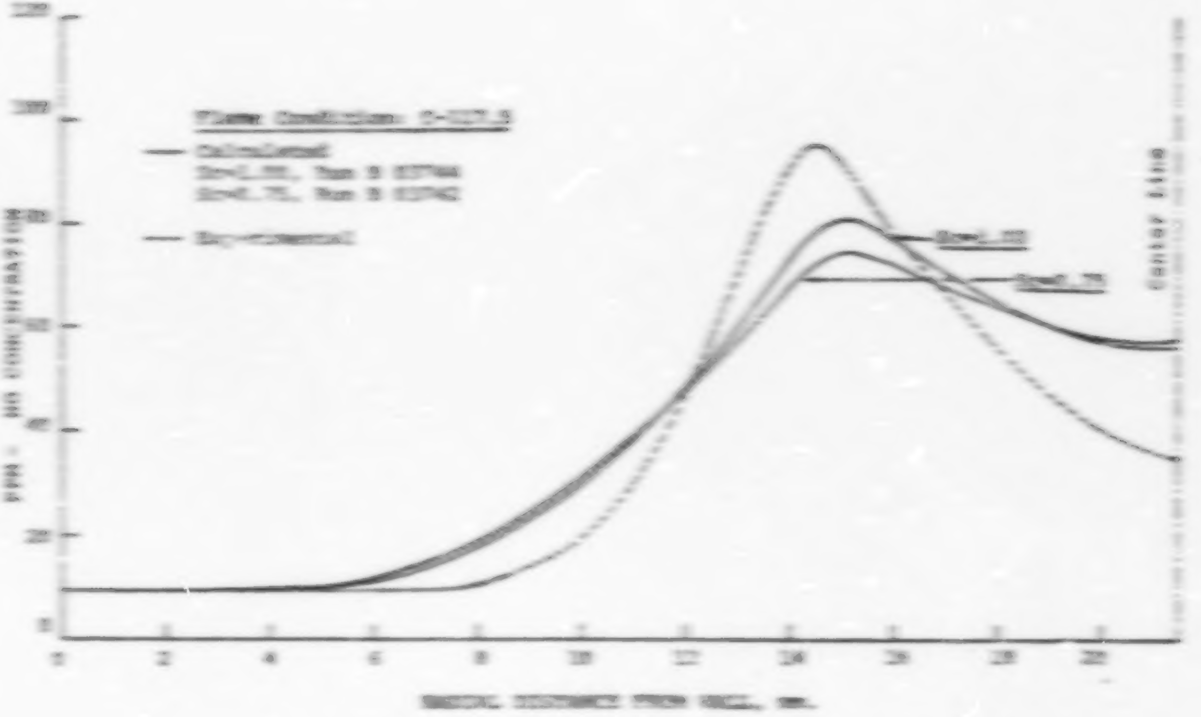

Figure 6.4: Calculated and Experimental NO Concentration Profiles 117.5 mm. above burner entrance

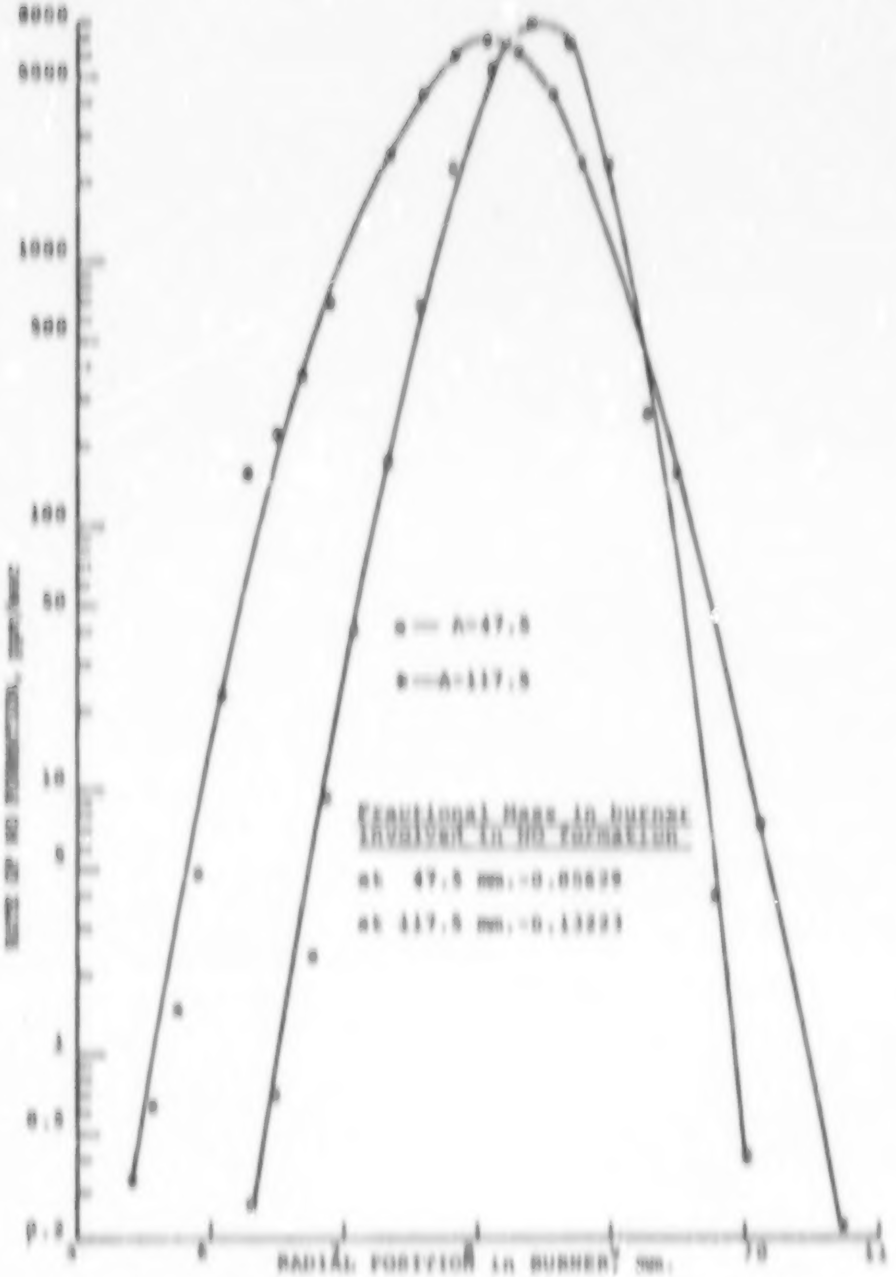

Figure 6.1. Calculated rate of formation of NO at two axial locations for Flame Condition A

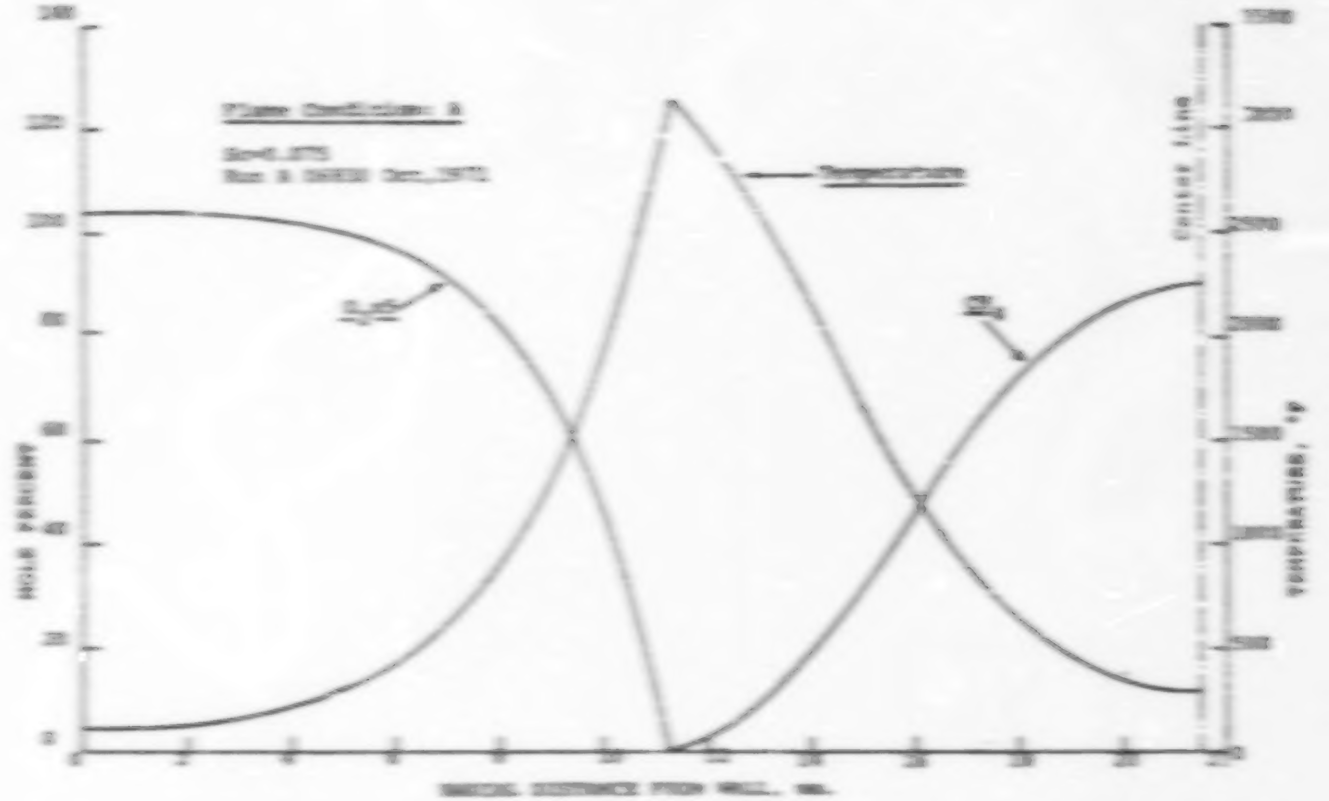

Figure 6.6: Calculated Temperature and Species Concentration Profiles 1" (25.4 mm.) above burner exit plane using Flame Sheet assumption

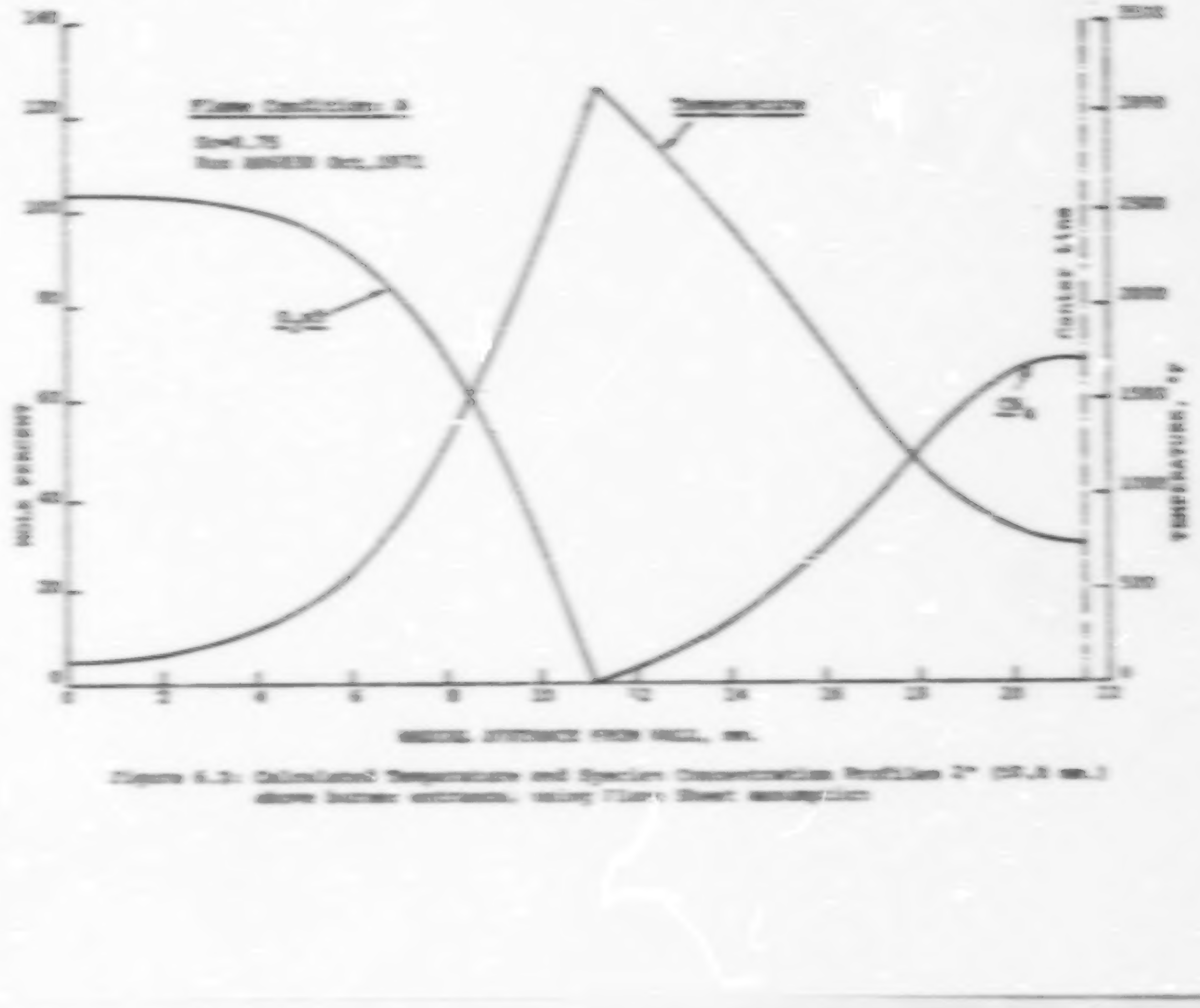

Figure 6.3: Calculated Temperature and Species Concentration Profiles 2" (50.8 mm.) above burner entrance, using Flame Sheet assumption

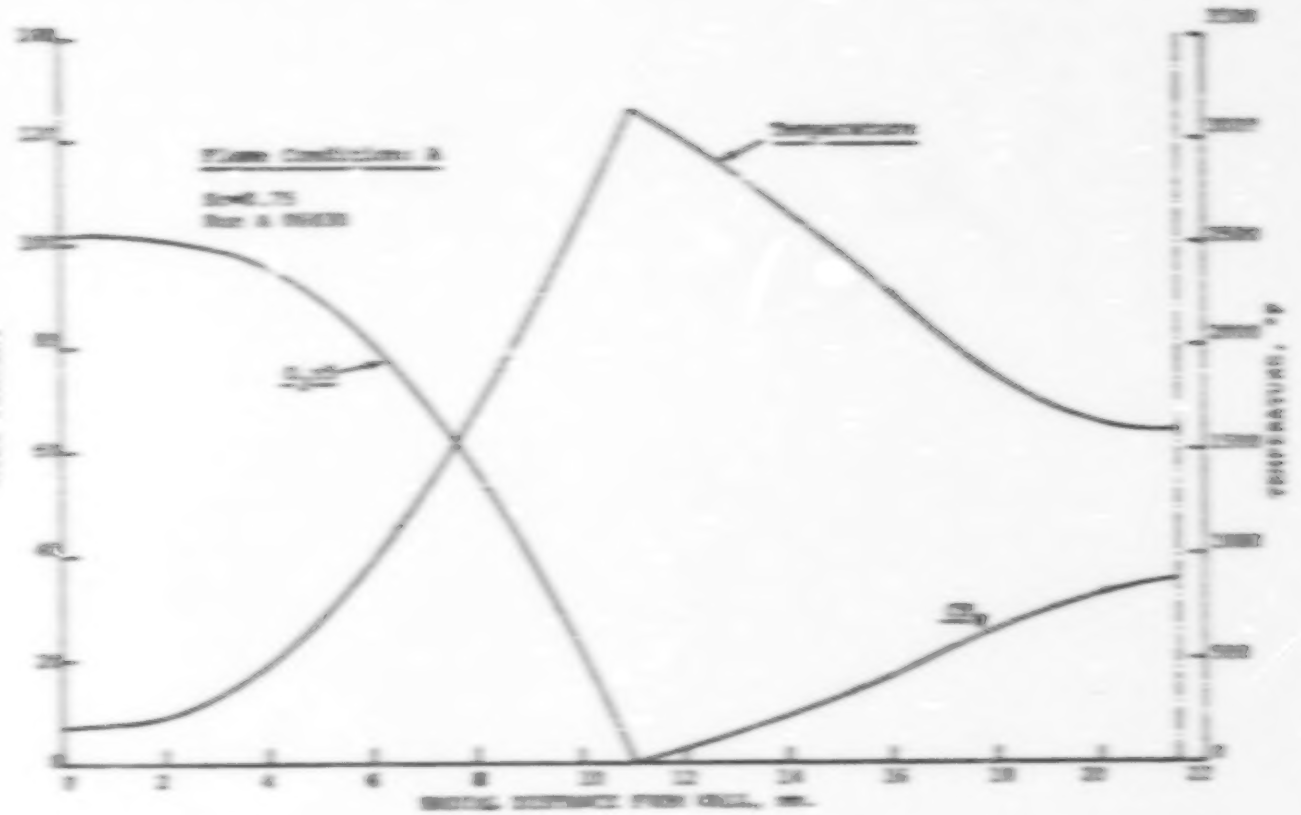

Figure 4.8: Calculated Temperature and Species Concentration Profiles 5" (127.0 mm.) [illegible] using Flame Sheet assumption

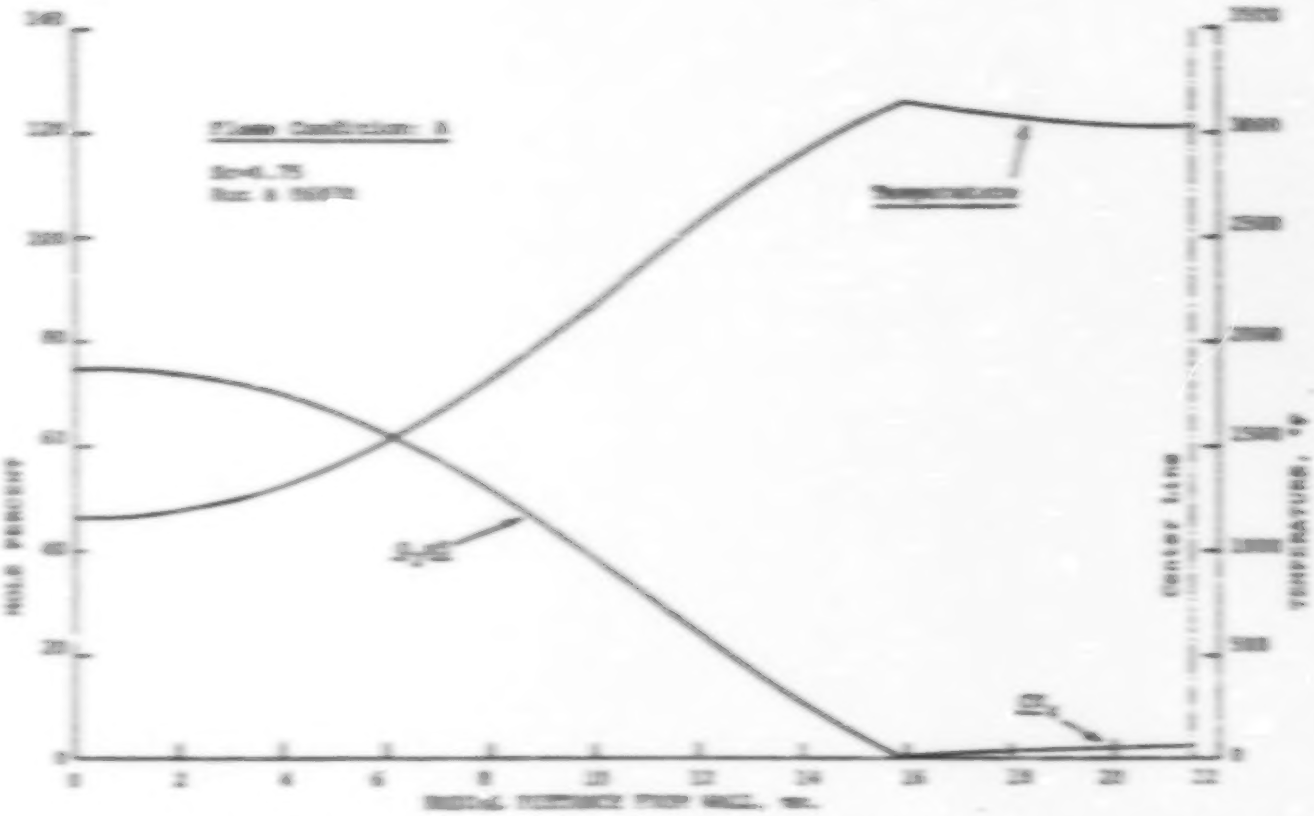

Figure 4.3c: Calculated Temperature and Species Concentration Profiles 17" ([illegible] mm.) above burner entrance: using flame sheet assumption

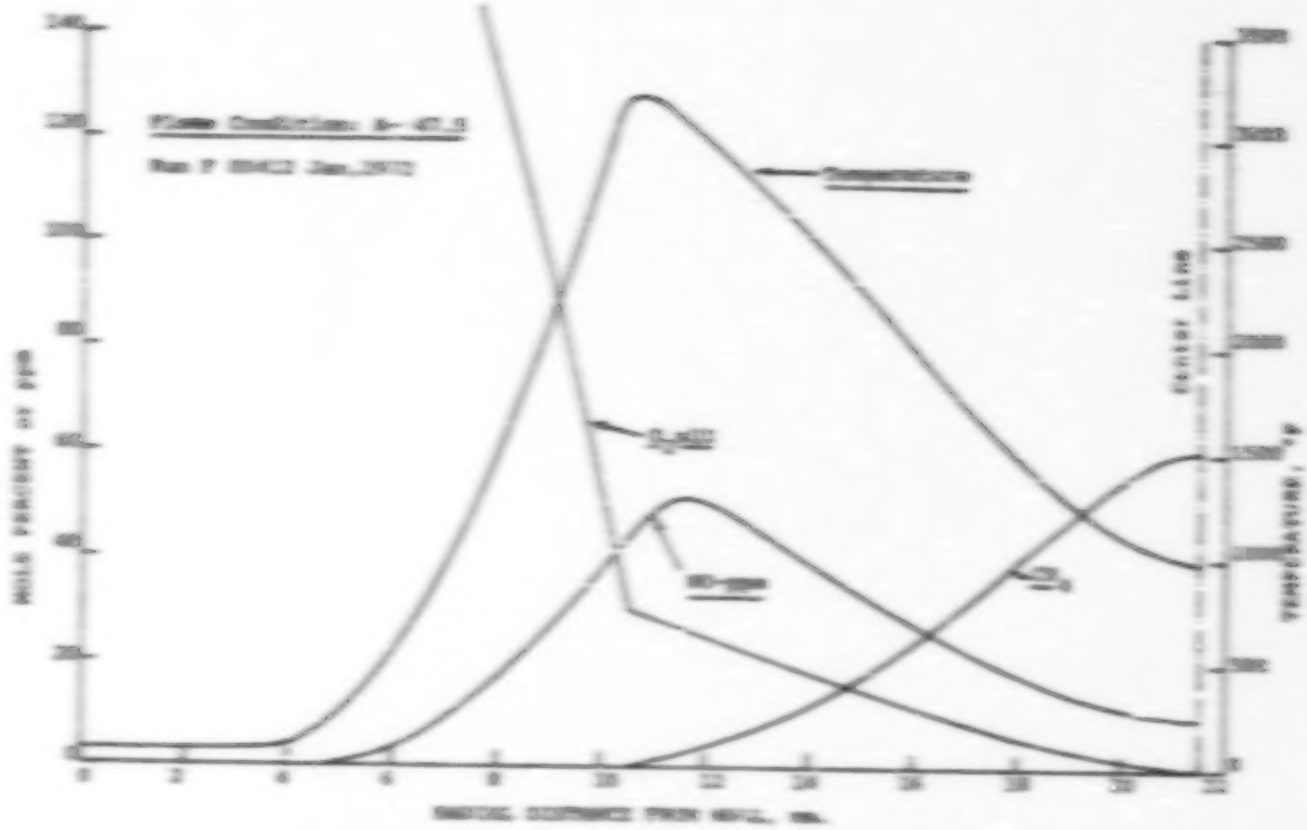

Figure 4.20: Calculated Temperature and Species Concentration Profiles 47.5 mm. above burner entrance; using Fictive Global Reaction Rate

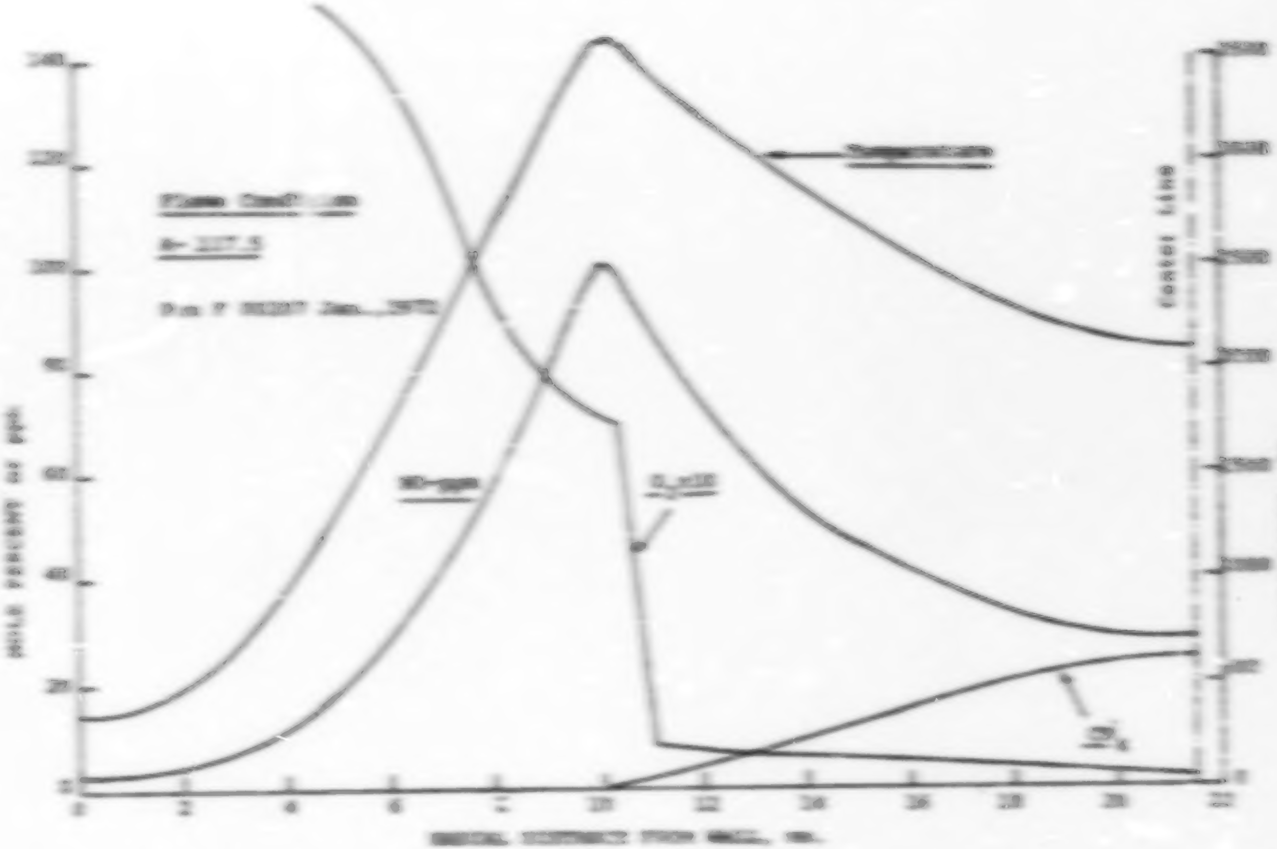

Figure 6.31: Calculated Temperature and Species Concentration Profiles 137.5 cm. above burner entrance: using Finite Global Reaction Rate

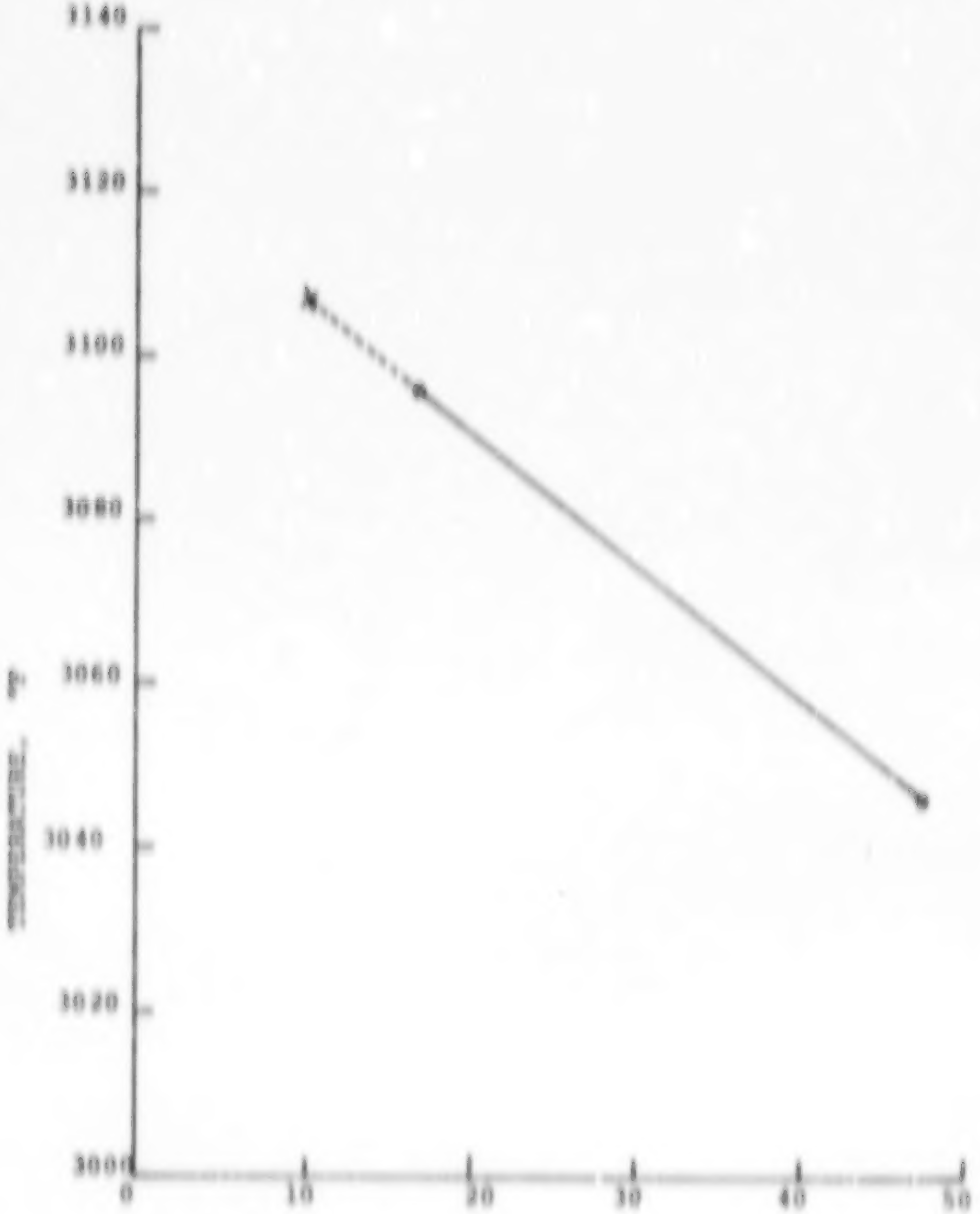

Figure 6.12: Extrapolation of maximum temperature at 10.0 mm. axial location; Flame Condition A

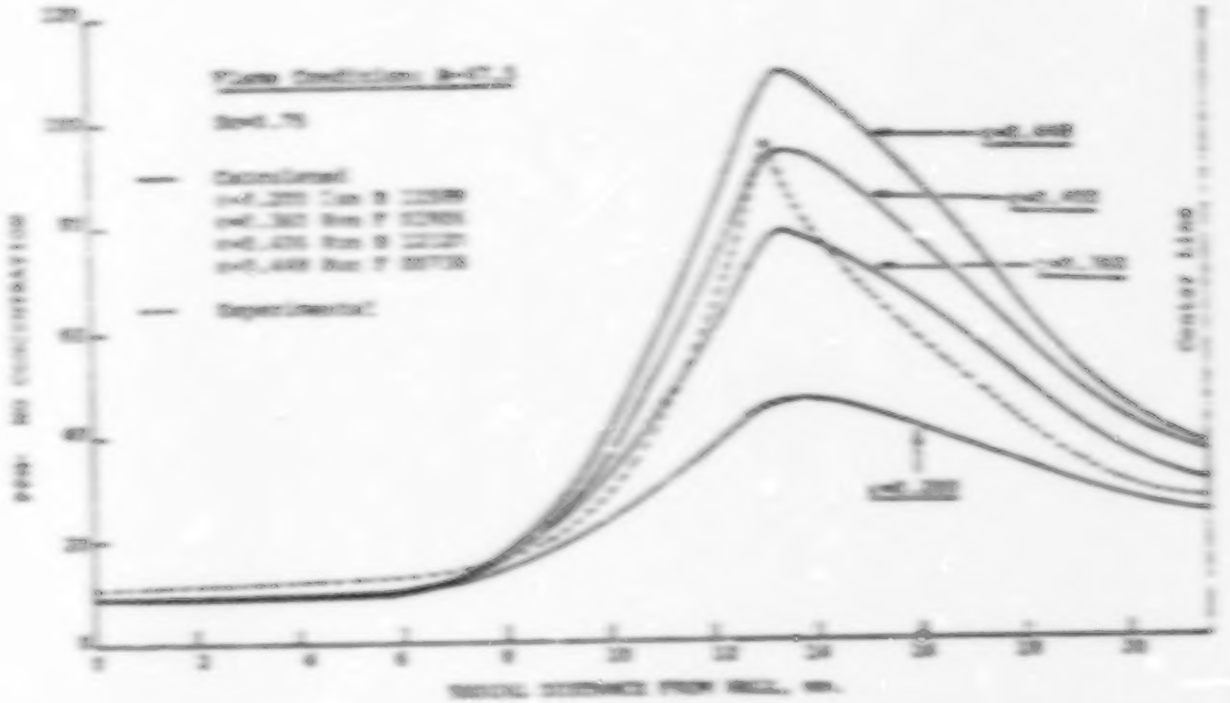

Figure 4.23: Calculated NO Concentration Profiles 47.5 mm. above burner entrance using different emissivity values for temperature correction

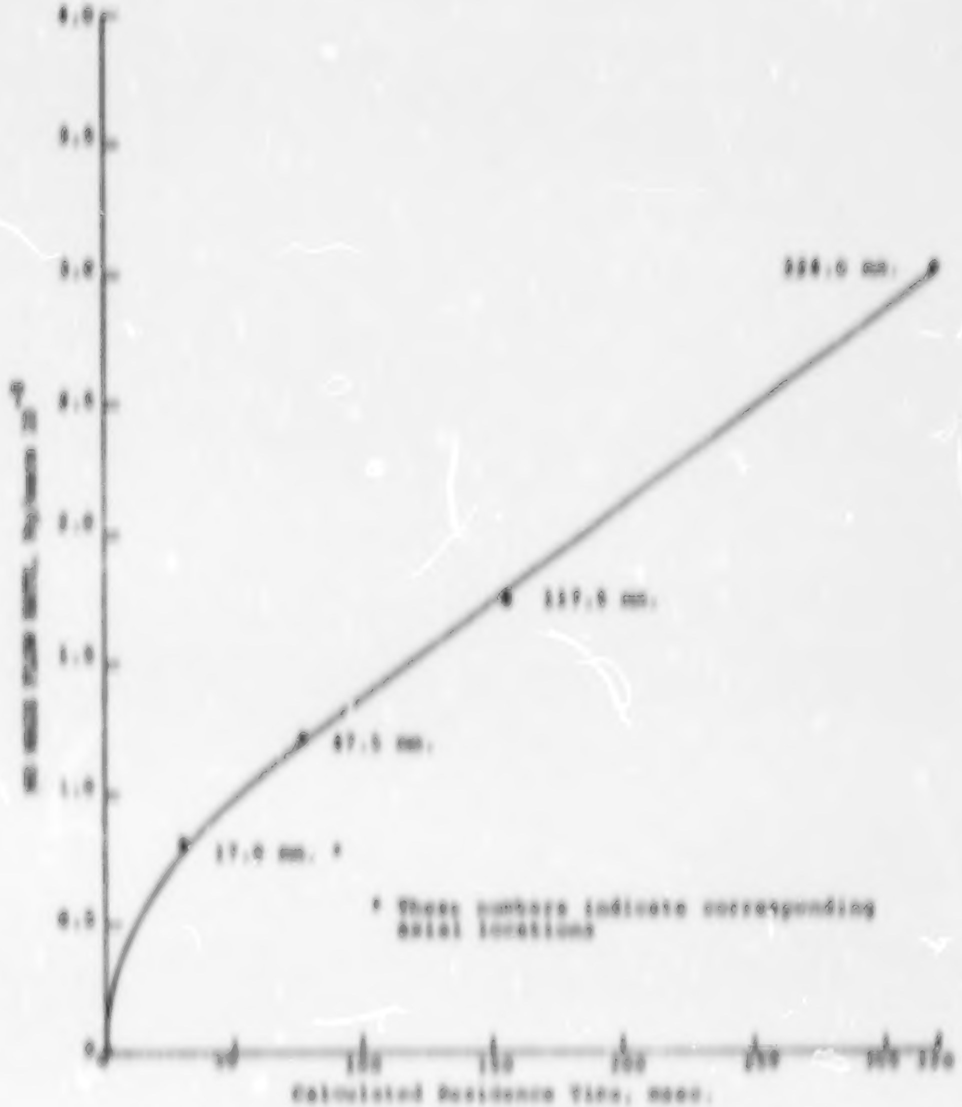

Calculated Residence Time, msec.

Figure 6.16: NO Mass Flow Rate: Residence Time History; Flame Condition A

REFERENCES

1. Aldred, J. W., Patel, J. C. and Williams, A., "The Mechanism of Combustion of Droplets and Spheres of Liquid n-Heptane," Combustion and Flame, 17, 139-148 (1971).

2. American Society of Testing Materials, D1607-69, 1969 Book of ASTM Standards, Part 23.

3. Barr, J., "Length of Cylindrical Laminar Diffusion Flames," Fuel, Jan. 1956, pp. 51-59.

4. Bascom, R. C., Broering, L. C., and Wulfhorst, D. E., "Design Factors that Affect Diesel Emissions," SAE Paper 710485, SAE SP 365, 1971.

5. Bird, R. B., Stewart, W. E., and Lightfoot, E. N., "Transport Phenomena," John Wiley & Sons, 1960.

6. Bowman, C. T., "Investigation of NO Formation Kinetics in Combustion Processes: The Hydrogen-Oxygen-Nitrogen Reaction," Combustion Science and Technology, 1971, Vol. 3, pp. 37-45.

7. Bowman, C. T., "An Experimental and Analytical Investigation of the High-Temperature Oxidation Mechanisms of Hydrocarbon Fuels," Combustion Science and Technology, 1970, Vol. 2, pp. 161-172.

8. Bowman, C. T. and Seery, D. J., "Investigation of NO Formation Kinetics in Combustion Processes: The Methane-Oxygen-Nitrogen Reaction," Emissions from Continuous Combustion Systems, Plenum Press, 1972, pp. 123-133.

9. Bracco, F. V., "NO Formation in Droplet Diffusion Flames," Paper 71-29 presented at the Western States Section/Combustion Institute Fall Meeting, Irvine, California, Oct. 25-26, 1971.

10. Burke, S. P. and Schumann, T. E. W., "Diffusion Flames," Industrial and Engineering Chemistry, Vol. 20, No. 10, pp. 998-1004, Oct. 1928.

11. Campau, R. M. and Neerman, J. C., "Continuous Mass Spectrometric Determination of Nitric Oxide in Automobile Exhaust," SAE Transactions, Vol. 75 (1967), paper 660116.

12. Caretto, L. S., Muzio, L. J., Sawyer, R. F. and Starkman, E. S., "The Role of Kinetics in Engine Emission of Nitric Oxide," Combustion Science and Technology, 1971, Vol. 3, pp. 53-61.

13. Cornelius, W. and Wade, W. R., "The Formation and Control of Nitric Oxide in a Regenerative Gas Turbine Burner," SAE Paper 700708 (1970).

14. Edelman, R. B. and Fortune, O. F., "A Quasi Global Chemical Kinetic Model for Finite Rate Combustion of Hydrocarbon Fuels with Application to Turbulent Burning and Mixing in Hypersonic Engines and Nozzles," Paper 69-86 presented at the 7th AIAA Aerospace Science Meeting, New York, January 1969.

15. Eyzat, P. and Guibet, J. C., "A New Look at Nitrogen Oxides Formation in Internal Combustion Engines," SAE Transactions, Vol. 77 (1968), paper 680126.

16. Fay, J. A., "The Distribution of Concentration and Temperature in a Laminar Jet Diffusion Flame," Journal of Aeronautical Sciences, Oct. 1954, pp. 681-89.

17. Fenimore, C. P., "Chemistry in Premixed Flames," Pergamon Press, 1964.

18. Fenimore, C. P., "Formation of Nitric Oxide in Premixed Hydrocarbon Flames," Thirteenth Symposium (International) on Combustion, The Combustion Institute, Pittsburgh, 1971, pp. 373-379.

19. Fenimore, C. P., Hilt, M. B. and Johnson, R. H., "Formation and Measurement of Nitrogen Oxides in Gas Turbines," ASME Paper 70-WA/GT-3 (1970).

20. Fenimore, C. P. and Jones, G. W., "Consumption of Oxygen Molecules in Hydrocarbon Flames Chiefly by Reaction with Hydrogen Atom," Journal of Physical Chemistry, Vol. 63, pp. 1834-38, 1959.

21. Fenimore, C. P. and Jones, G. W., "Formation of Carbon Monoxide in Methane Flames by Reaction of Oxygen Atoms with Methyl Radicals," Journal of Physical Chemistry, Vol. 65, pp. 1532-36, 1961.

22. Fenimore, C. P. and Jones, G. W., "Rate of Reaction of Methane with H Atoms and OH Radicals in Flames," Journal of Physical Chemistry, Vol. 65, 2200-03, 1961.

23. Fristrom, R. M. and Westenberg, A. A., "Flame Structure," McGraw-Hill, 1965.

24. Fristrom, R. M., Grunfelder, C. and Favin, S., "Methane Oxygen Flame Structure. I. Characteristic Profiles in a Low-Pressure, Laminar, Lean, Premixed Methane-Oxygen Flame," Journal of Physical Chemistry, Vol. 64, pp. 1386-92, 1960.

25. Fristrom, R. M., Grunfelder, C. and Favin, S., "Methane-Oxygen Flame Structure. III. Characteristic Profiles and Matter and Energy Conservation in a One-Twentieth Atmosphere Flame," Journal of Physical Chemistry, Vol. 65, pp. 587-90, 1961.

26. Gordon, A. S., Smith, S. R. and McNesby, J. R., "Study of the Chemistry of Diffusion Flames," Seventh Symposium (International) on Combustion, Butterworth & Co., London, 1959, pp. 317-326.

27. Groth, R. H. and Calabro, D. S., "Evaluation of Saltzman and Phenoldisulfonic Acid Methods for Determining NO_x in Engine Exhaust Gases," Journal of Air Pollution Control Association, Vol. 19, No. 11, Nov. 1969, pp. 884-87.

28. Gosman, A. D., Pun, W. M., Runchal, A. K., Spalding, D. B. and Wolfshtein, M., "Heat and Mass Transfer in Recirculating Flows," Academic Press, London, 1969.

29. Hammond, D. C. and Mellor, A. M., "A Preliminary Investigation of Gas Turbine Combustion Modeling," Combustion Science and Technology, 1970, Vol. 2, pp. 67-80.

30. Haupt, C. G., "Exhaust Emission by a Small Gas Turbine," SAE paper 680463, 1968.

31. Heywood, J. B., "Discussion of paper, 'Emissions from Gas-Turbine Combustors,' by N. J. Friswell," Emissions from Continuous Combustion Systems, Plenum Press, 1972, pp. 175-179.

32. Heywood, J. B., Fay, J. A. and Linden, L. H., "Jet Aircraft Pollutant Production and Dispersion," AIAA Journal, May 1971, pp. 841-850.

33. Higgin, R. M. R. and Williams, A., "A Shock Tube Investigation of Combustion of Lean Methane and n-Butane Mixtures with Oxygen," Twelfth Symposium (International) on Combustion, The Combustion Institute, Pittsburgh, 1969, p. 579.

34. Hottel, H. C. and Hawthorne, W. R., "Diffusion in Laminar Flame Jets," Third Symposium on Combustion, Flame and Explosion Phenomena, pp. 254-66, Williams & Wilkins, Baltimore, 1969.

35. Hottel, H. C. and Sarofim, A. F., "Radiative Transfer," McGraw-Hill, New York, 1967.

36. JANAF Interim Thermochemical Data Tables," by the Joint Army-Navy-Airforce Thermochemical Panel.

37. Kassoy, D. R. and Williams, F. A., "Liquid Droplet Combustion with Finite Rate Chemistry," Paper No. 68-131, presented at AIAA 6th Aerospace Sciences Meeting, New York, Jan. 22-24, 1968.

38. Khan, I. M., Greeves, G. and Probert, D. M., "Prediction of Soot and Nitric Oxide Concentration in Diesel Engine Exhaust," Institution of Mechanical Engineers Transactions, London, 1971, p. 205.

39. Khan, I. M., Wang, C. H. T. and Langridge, B. E., "Effect of Air Swirl on Smoke and Gaseous Emissions from Direct-Injection Diesel Engines," SAE Paper 720102, 1972.

40. Khan, I. M., and Wang, C. H. T., "Factors Affecting Emission of Smoke and Gaseous Pollutants from Direct Injection Diesel Engines," Symposium on Pollution Control in Transport Engines, Institution of Mechanical Engineers, London, November 1971.

41. Kreith, F., "Principles of Heat Transfer," 2nd ed., International Textbook Company, 1965.

42. Lavoie, G. A., Heywood, J. B., and Keck, J. C., "Experimental and Theoretical Study of Nitric Oxide Formation in Internal Combustion Engines," Combustion Science and Technology, 1970, Vol. 1, pp. 313-326.

43. Lieberman, A. "Composition of Exhaust from a Regenerative Turbine System," Journal of Air Pollution Control Association, March 1968, Vol. 18, No. 3.

44. Lorell, J., Wise, H. and Carr, R. E., "Steady-State Burning of a Liquid Droplet. II. Bipropellant Flame," The Journal of Chemical Physics, Vol. 25, No. 2, Aug. 1956, pp. 325-331.

45. Lozano, E. R., Melvin, W. W. and Hochheiser, S., "Air Pollution Emissions from Jet Engines," Journal of Air Pollution Control Association, June 1968, Vol. 18, No. 6.

46. Marteney, P. J., "Analytical Study of the Kinetics of Formation of Nitrogen Oxide in Hydrocarbon-Air Combustion," Combustion Science and Technology, 1970, Vol. 1, pp. 461-469.

47. McConnel, G., "Oxides of Nitrogen in Diesel Engine Exhaust Gases; Their Formation and Control," Proc. of Institution of Mechanical Engineers, London, 1963-64, p. 1001.

48. Myers, P. S. "Automobile Emission--A Study in Environmental Benefits versus Technological Costs," SAE paper 700182 (1970).

49. Newhall, H. K., "Theoretical and Experimental Investigation of Chemical Kinetics During Rapid Expansion of High Temperature Combustion Products," Ph. D. Dissertation, University of California, Berkeley, 1966.

50. Newhall, H. K., "Kinetics of Engine Generated Nitrogen Oxides and Carbon Monoxide," Twelfth Symposium (International) on Combustion, The Combustion Institute, 1969.

51. Newhall, H. K. and Shahed, S. M., "Kinetics of Nitric Oxide Formation in High Pressure Flames," Thirteenth Symposium (International) on Combustion, The Combustion Institute, 1971.

52. Newhall, H. K., and Starkman, E. S., "Direct Spectroscopic Determination of Nitric Oxide in Reciprocating Engine Cylinders," SAE Transactions, Vol. 76 (1968).

53. Nicksic, S. W., and Harkins, J., "Spectrophotometric Determination of Nitrogen Oxides in Auto Exhaust," Analytical Chemistry, Vol. 34, pp. 985-988.

54. Obert, E. F., "Internal Combustion Engines," International Textbook Co., Scranton, Pa., 1969.

55. Perez, J. M., and Landen, E. W., "Exhaust Emission Characteristics of Precombustion Chamber Engines," SAE Transactions, Vol. 77 (1968), paper 680421.

56. Pandya, T. P. and Weinberg, F. J., "The Study of Structure of Laminar Diffusion Flames by Optical Methods," Ninth Symposium (International) on Combustion, Academic Press, Inc., New York (1963), p. 587.

57. Pandya, T. P. and Weinberg, F. J., "The Structure of Flat Counterflow Diffusion Flames," Proc. of Royal Society (London), A279, 544 (1964).

58. Patankar, S. V. and Spalding, D. B., "Heat and Mass Transfer in Boundary Layers," 2nd ed., London, Intertext Books, 1970.

59. Reid, R. C. and Sherwood, T. K., "The Properties of Gases and Liquids, Their Estimation and Correlation," 2nd. ed., McGraw-Hill, 1966.

60. Saltzman, B. E., "Colorimetric Microdetermination of Nitrogen Dioxide in the Atmosphere," Anal. Chem., 26, 1949-55 (1954).

61. Sawyer, R. F. and Starkman, E. S., "Gas Turbine Exhaust Emissions," SAE paper 680462.

62. Shahed, S. M., "The Kinetics of Nitric Oxide Formation in High Pressure Combustion Processes," Ph.D. Dissertation, University of Wisconsin, Madison, 1970.

63. Shahed, S. M. and Newhall, H. K., "Kinetics of Nitric Oxide Formation in Propane-Air and Hydrogen-Air-Diluent Flames," Combustion and Flame, 17, 131 (1971).

64. Smith, S. R., and Gordon, A. S., "Studies of Diffusion Flames. I. The Methane Diffusion Flame," Journal of Physical Chemistry, Vol. 60, 759 (1956).

65. Smith, D. S., Sawyer, R. F. and Starkman, E. S., "Oxides of Nitrogen from Gas Turbines," Journal of the air Pollution Control Association, Vol. 18, No. 1 (1968), pp. 30-35.

66. D'Souza, M. V. and Karim, G. A., "An Analytical Study of Methane Oxidation in a Steady-Flow Reactor," Combustion Science and Technology, 1971, Vol. 3, pp. 83-89.

67. Spalding, D. B., "A Theory of the Extinction of Diffusion Flames," Fuel, March 1954, pp. 255-73.

68. Spalding, D. B., "The Theory of Mixing and Chemical Reaction in the Opposed Jet Diffusion Flame," ARS Journal, Vol. 31, June 1961, pp. 763-71.

69. Spalding, D. B. and Jain, V. K., "A Theoretical Study of the Effects of Chemical Kinetics on a One-Dimensional Diffusion Flame," Combustion and Flame, Vol. 6, No. 4, Dec. 1962, pp. 265-73.

70. Surugu, J., editor, "Experimental Methods in Combustion Research--A Manual," published for AGARD by Pergamon Press, 1961.

71. Tsuji, H. and Yamaoka, I., "The Counterflow Diffusion Flame in the Forward Stagnation Region of a Porous Cylinder," Eleventh Symposium (International) on Combustion, p. 979, The Combustion Institute, 1967.

72. Tsuji, H. and Yamaoka, I., "The Structure of Counterflow Diffusion Flames in the Forward Stagnation Region of a Porous Cylinder," Twelfth Symposium (International) on Combustion, p. 997, The Combustion Institute, 1969.

73. Tsuji, H. and Yamaoka, I., "Structure Analysis of Counterflow Diffusion Flames in the Forward Stagnation Region of a Porous Cylinder," Thirteenth Symposium (International) on Combustion, p. 723, The Combustion Institute, 1971.

74. Weinberg, F. J., "Optics of Flames," Butterworth, London, 1963.

75. Westenberg, A. A. and Fristrom, R. M., "Methane-Oxygen Flame Structure. II. Conservation of Matter and Energy in the One-Tenth Atmosphere Flame," Journal of Physical Chemistry, 64, 1393 (1960).

76. Westenberg, A. A. and Fristrom, R. M., "Methane-Oxygen Flame Structure IV, Chemical Kinetic Considerations," Journal of Physical Chemistry, 65, 591 (1961).

77. William, A. "The Mechanism of Combustion of Droplets and Sprays of Liquid Fuels," Oxidation and Combustion Review, 3 (1968), pp. 1-45.

78. Williem, F. A., "Combustion Theory," Addison-Wesley, Reading, Mass., 1965.

79. Wimmer, D. B. and McReynolds, L. A., "Nitrogen Oxides and Engine Combustion," SAE Transactions, Vol. 70, 733 (1962).

80. Wohl, K., Gazley, C., and Kapp, N. M., "Diffusion Flames," Third Symposium on Combustion, Flame and Explosion Phenomena, pp. 288-301, Williams and Wilkins, Baltimore, 1949.

81. Wolfhard, H. G. and Parker, W. G., "A New Technique for the Spectroscopic Examination of Flames at Normal Pressure," Proc. of Physical Society (London), 62A, 722 (1949).

82. Wolfhard, H. G. and Parker, W. G., "A Spectroscopic Investigation into the Structure of Diffusion Flames," Proc. of Physical Society (London), 65A, 2 (1952).

83. Wray, K. L. and Teare, J. D., "Shock Tube Study of the Kinetics of Nitric Oxide at High Temperatures," Journal of Chemical Physics, 36, 2582 (1962).

84. Yagi, S. and Saji, K., "Problems of Turbulent Diffusion and Flame Jets," Fourth Symposium (International) on Combustion, pp. 771-81, Williams and Wilkins, Baltimore, 1953.

85. Yumulu, V. S. and Carey, A. W., "Exhaust Emission Characteristics of Four-Stroke Direct-Injection Compression Ignition Engines," SAE paper 680042.

86. Zeldovich, Y. B., "On the Theory of Combustion of Initially Unmixed Gases," NACA Technical Memorandum 1296.

87. Zeldovich, Y. B., Sadonikov, P. Y., and Frank-Kamenetskii, D. A., "Oxidation of Nitrogen in Combustion," Academy of Sciences of USSR, Institute of Chemical Physics, Moscow-Leningrad, 1947 (Translated by M. Shelef, Ford Motor Company.)

APPENDIX A

EXPERIMENTAL DATA

FLAME CONDITION A

Fuel Mass Flow Rate = 2.67×10^{-3} lbm/min
Air Mass Flow Rate = 7.95×10^{-2} lbm/min

Av. Fuel Velocity = 0.721 ft/sec
Av. Air Velocity = 1.33 ft/sec

Overall F/A Eq. Ratio = 0.575
Air/Fuel Velocity Ratio = 1.841

TABLE A-A-1

Axial Location Z = 0.5 mm

Temperature Profile

Radial Distance From Wall in mm	Temp °F	Radial Distance From Wall in mm	Temp °F
0.0	81.0	13.9	958.0
0.2	81.0	14.0	977.5
1.2	81.0	14.1	976.0
2.2	81.0	14.2	978.0
3.2	81.0	14.3	979.0
4.2	81.0	14.4	950.0
5.2	81.0	14.7	865.0
6.2	81.0	14.9	765.0
7.8	81.0	15.2	705.0
8.2	81.0	15.4	527.0
9.2	88.0	15.6	480.0
9.7	98.0	15.9	422.0
10.2	98.0	16.2	401.0
10.7	106.0	16.4	361.0
11.2	112.0	16.9	279.0
11.9	140.0	17.4	242.0
12.2	154.0	17.9	216.0
12.4	180.0	18.4	180.0
12.6	244.0	19.0	166.0
12.9	333.0	19.4	164.0
13.1	381.0	19.9	162.0
13.3	611.0	20.4	155.0
13.5	708.0	20.9	147.0
13.6	785.0	21.4	147.0
13.7	867.0	21.5	147.0
13.8	920.0		

TABLE A-A-2

Axial Location Z = 1 mm

Tempriature Profile

Radial Distance From Wall in mm	Temp °F	Radial Distance From Wall in mm	Temp °F
0.0	81.0	14.0	1064.0
0.9	81.0	14.2	1094.0
1.9	81.0	14.5	1103.0
2.9	81.0	14.7	1096.0
3.9	81.0	15.0	1055.0
4.9	81.0	15.2	1034.0
5.9	81.0	15.5	967.0
7.0	81.0	15.7	911.0
8.0	84.0	16.0	559.0
8.5	85.0	16.3	506.0
9.0	92.0	16.5	444.0
9.5	94.0	16.7	375.0
10.0	104.0	17.0	317.0
10.5	121.0	17.5	236.0
11.0	155.0	18.0	184.0
11.5	180.0	18.5	164.0
12.0	261.0	19.0	160.0
12.2	336.0	19.5	158.0
12.5	455.0	20.0	150.0
12.7	692.0	20.5	147.0
13.0	992.0	21.0	147.0
13.2	1085.0	21.5	147.0
13.5	1097.0		
13.7	1064.0		

TABLE A-A-3-1

Axial Location Z = 2.0 mm

Temperature Profile

Radial Distance From Wall in mm	Temp °F	Radial Distance From Wall in mm	Temp °F
0.0	85.0	13.9	2414.0
1.0	85.0	14.0	2492.0
2.0	85.0	14.1	2559.0
3.0	85.0	14.2	2559.0
4.0	85.0	14.3	2466.0
5.0	85.0	14.4	2451.0
6.0	85.0	14.5	2343.0
7.0	85.0	14.6	2286.0
8.0	85.0	14.7	2259.0
8.5	90.0	15.0	2101.0
9.0	95.0	15.2	1805.0
9.5	101.0	15.5	1710.0
10.0	117.0	15.7	1629.0
10.5	165.0	16.0	1436.0
11.0	221.0	16.2	1308.0
11.5	340.0	16.5	1181.0
11.7	425.0	16.7	596.0
12.0	755.0	17.0	446.0
12.2	1029.0	17.2	416.0
12.5	1368.0	17.5	321.0
12.7	1723.0	17.7	276.0
12.9	2055.0	18.0	236.0
13.1	2325.0	18.2	207.0
13.3	2400.0	18.5	194.0
13.4	2371.0	19.0	164.0
13.5	2376.0	19.5	158.0
13.6	2436.0	20.0	158.0
13.7	2403.0	20.5	147.0
13.8	2411.3	21.0	147.0
		21.5	147.0

TABLE A-A-3-2

Axial Location Z = 3.0 mm

Species Concentration [illegible]

Radial Distance From Wall in mm	Species Concentration (Dry) in Mole Percent				
	CO_2	O_2	N_2	CH_4	CO
0.0	-	21.0	79.0	-	-
1.0	-	21.0	79.0	-	-
2.0	-	21.0	79.0	-	-
3.0	-	21.0	79.0	-	-
4.0	-	21.0	79.0	-	-
5.0	-	21.0	79.0	-	-
6.0	-	21.0	79.0	-	-
7.0	-	21.0	79.0	-	-
8.0	-	21.0	79.0	-	-
9.0	-	21.0	79.0	-	-
10.0	-	21.0	79.0	-	-
11.0	0.05	20.8	78.8	-	-
11.5	0.15	20.6	78.7	-	-
12.0	0.55	19.5	78.5	-	0.02
12.5	1.35	17.95	78.1	-	0.145
12.7	1.7	16.6	77.5	-	0.25
13.0	1.5	17.2	77.5	0.4	0.51
13.3	1.05	17.7	75.5	2.0	0.64
13.5	0.66	17.7	75.0	3.51	0.64
13.7	0.92	17.8	74.5	4.0	0.69
14.0	0.67	16.6	71.5	6.2	0.69
14.3	0.9	17.3	70.5	9.0	0.73
14.5	1.0	15.0	68	13.0	0.83
14.7	1.1	13.6	63.1	18.0	0.89
15.0	1.12	12.0	59.0	27.0	0.95
15.3	1.15	10.7	59.0	31.0	0.91
15.5	1.21	9.5	51.5	37.0	0.93
16.0	1.53	4.8	39.6	53.0	1.12
16.5	1.46	3.9	30.0	64.0	1.05
17.0	1.06	3.13	22.0	73.0	0.73

(To be Continued)

TABLE A-A-1-2 Continued

Radial Distance From Wall in mm	Species Concentration (Dry) in Mole Percent				
	CO_2	O_2	N_2	CH_4	CO
17,5	0,72	2,6	17,0	80,0	0,48
18,5	0,25	2,0	10,0	87,0	0,16
19,5	0,05	2,0	6,0	90,0	-
20,5	-	0,75	1,8	96	-
21,5	-	0,6	1,4	98	-

TABLE A-A-4-1

Axial Location Z = 17.0 mm

Temperature Profile

Radial Distance From Wall in mm	Temp °F	Radial Distance From Wall in mm	Temp °F
0.4	81.0	13.5	3040.0
1.4	81.0	13.7	3004.0
2.4	81.0	13.9	2917.0
3.4	81.0	14.1	2875.0
4.4	81.0	14.3	2732.0
5.4	81.0	14.5	2684.0
6.4	81.0	14.7	2552.0
7.4	90.0	14.9	2444.0
8.4	121.0	15.2	2269.0
8.9	186.0	15.4	2230.0
9.4	317.0	15.7	2160.0
9.7	412.0	15.9	2137.0
9.9	496.0	16.2	2040.0
10.2	721.0	16.4	2005.0
10.4	871.0	16.7	1959.0
10.6	988.0	16.9	1881.0
10.8	1148.0	17.2	1796.0
11.0	1398.0	17.5	1722.0
11.2	1546.0	17.8	1615.0
11.4	1810.0	18.1	1524.0
11.5	1886.0	18.4	1410.0
11.7	2033.0	18.7	1309.0
11.9	2155.0	19.0	1198.0
12.1	2301.0	19.3	1050.0
12.3	2587.0	19.6	971.0
12.5	2757.0	19.9	873.0
12.7	2861.0	20.2	754.0
12.8	2942.0	20.5	636.0
13.0	3003.0	20.8	569.0
13.1	3063.0	21.1	465.0
13.2	3096.0	21.4	385.0
13.3	3078.0	21.5	373.0
13.4	3055.0		

TABLE A-A-4-2

Axial Location Z = 17.0 mm

Species Concentration (Dry) in Mole Percent

Radial Distance from Wall in mm	Species Concentration (Dry) Mole Percent				
	CO_2	O_2	N_2	CH_4	CO
0.0	-	21.0	79.0	-	-
1.0	-	21.0	79.0	-	-
2.0	-	21.0	79.0	-	-
3.0	-	21.0	79.0	-	-
4.0	-	21.0	79.0	-	-
5.0	-	21.0	79.0	-	-
6.0	-	21.0	79.0	-	-
7.0	-	21.0	79.0	-	-
8.0	0.02	21.0	79.0	-	-
8.5	0.06	20.82	79.1	-	-
9.0	0.195	20.5	79.2	-	-
9.5	0.4	20.12	79.4	-	-
10.0	0.704	19.81	79.5	-	-
10.5	1.575	17.95	80.46	-	-
10.8	2.29	16.56	81.12	-	0.01
11.1	2.60	15.63	81.74	-	0.0197
11.4	3.24	14.29	82.4	-	0.0595
11.7	4.23	12.2	83.37	-	0.178
12.0	4.94	10.48	84.2	-	0.336
12.3	5.82	8.96	84.33	-	0.577
12.6	6.85	6.16	85.8	-	1.15
12.8	7.39	4.60	86.07	-	1.92
12.9	7.46	4.47	86.1	-	1.95
13.1	7.81	3.564	85.9	-	2.72
13.3	7.7	2.52	86.5	-	3.48
13.4	7.67	2.93	85.2	.101	4.06
13.5	7.52	2.47	85.2	0.406	4.32
13.6	7.62	2.42	84.8	0.505	4.57
13.7	7.5	2.32	84.7	0.832	4.94
13.8	7.37	2.26	84.0	1.25	5.13

(To be Continued)

TABLE A-A-4-2 Continued

Radial Distance From Wall in mm	Species Concentration (Dry) in Mole Percent				
	CO_2	O_2	N_2	CH_4	CO
13.9	7.25	2.61	83.5	1.67	5.07
14.1	7.093	2.64	82.4	2.6	5.22
14.3	6.98	2.5	81.5	3.84	5.25
14.4	6.92	2.32	81.3	4.02	5.39
14.6	6.77	2.42	79.5	5.88	5.46
14.8	6.27	2.72	77.2	8.35	5.35
15.3	6.28	1.77	73.5	13.0	5.3
15.8	5.29	2.05	65.4	22.7	4.65
16.3	4.7	2.065	61.5	27.8	3.98
16.8	4.17	2.18	57.0	33.2	3.53
17.3	3.24	1.97	47.7	44.2	2.87
17.8	2.48	2.09	38.4	55.0	2.09
18.3	1.79	2.1	32.18	61.7	1.56
18.8	1.35	1.71	25.4	70.3	1.17
19.3	0.67	1.59	18.7	78.5	0.69
19.8	0.365	1.58	13.7	83.8	0.345
20.3	0.1485	1.83	10.5	87.2	0.1485
20.8	0.065	1.53	9.4	89.25	0.0675
21.3	0.04	1.52	7.5	90.5	-

TABLE A-A-4-3

Axial Location Z = 17,0 mm

NO Concentration (Dry) Profile

Radial Distance From Wall in mm	NO Concentration in P.P.M.	Radial Distance From Wall in mm	NO Concentration in mm
0,0	8,7	13,4	84,0
1,0	10,0	13,5	84,0
2,0	6,0	13,6	79,0
3,0	14,0	13,7	80,0
4,0	6,5	13,8	70,0
5,0	7,0	13,9	66,0
6,0	5,5	14,1	54,0
7,0	16,5	14,3	60,0
8,0	15,5	14,4	57,0
8,5	7,0	14,6	46,0
9,0	10,0	14,8	49,0
9,5	10,0	15,3	44,0
10,0	15,5	15,8	39,0
10,5	12,5	16,3	37,5
10,8	15,8	16,8	32,0
11,1	23,0	17,3	26,0
11,4	25,0	17,8	20,5
11,7	37,5	18,3	17,5
12,0	40,0	18,8	19,0
12,3	42,0	19,3	10,0
12,6	51,0	19,8	18,0
12,8	60,0	20,3	11,0
12,9	62,0	20,8	12,0
13,1	68,0	21,3	7,0
13,3	70,0		

TABLE A-A-5-1

Axial Location Z = 47,5 mm

Tempterature Profile

Radial Distance From Wall in mm	Temp °F	Radial Distance From Wall in mm	Temp °F
0,0	108,5	14,1	2763,0
0,9	108,0	14,4	2622,0
1,5	103,0	14,7	2502,0
2,9	101,5	14,9	2367,0
3,9	97,5	15,4	2238,5
5,1	93,0	15,9	2127,5
5,9	121,0	16,4	2075,0
6,5	136,5	16,9	2014,0
7,0	298,0	17,4	1958,0
8,0	527,0	17,9	1836,0
8,5	712,0	18,4	1746,0
9,0	907,0	18,9	1615,0
9,5	1135,0	19,4	1500,0
9,7	1186,0	19,9	1398,0
10,0	1406,0	20,4	1245,0
10,2	1500,0	20,9	1170,0
10,4	1660,0	21,4	1094,0
10,8	1877,0		
11,0	2000,0		
11,2	2074,0		
11,5	2255,0		
11,8	2450,0		
12,0	2562,0		
12,2	2708,0		
12,5	2890,0		
12,8	2968,0		
13,0	3046,0		
13,2	3025,0		
13,4	2985,0		
13,6	2921,0		
13,9	2810,0		

TABLE A-A-5-2

Axial Location Z = 47.5 mm

Species Concentration (Dry) Profiles

Radial Distance From Wall in mm	Species Concentration (Dry) in Mole Percent				
	CO_2	O_2	N_2	CH_4	CO
0.0	-	21.0	79.0	-	-
1.0	-	21.0	79.0	-	-
2.0	-	21.0	79.0	-	-
3.0	-	21.0	79.0	-	-
4.0	-	21.0	79.0	-	-
5.0	-	21.0	79.0	-	-
6.0	-	20.9	79.1	-	-
7.0	-	20.2	79.8	-	-
8.0	-	18.8	81.2	-	-
9.0	0.15	17.7	82.1	-	-
9.5	0.34	16.6	83.0	-	-
10.0	0.70	14.2	85.2	-	-
10.5	1.15	12.4	86.5	-	0.02
11.0	2.162	10.12	87.5	-	0.11
11.5	4.0	8.1	87.2	-	0.42
12.0	6.18	6.4	87.0	-	0.98
12.2	6.76	6.0	86.9	-	1.15
12.6	7.7	4.2	86.6	-	1.68
12.8	8.05	3.5	86.5	-	2.05
13.0	8.37	3.05	86.3	-	2.36
13.2	8.25	2.5	86.1	-	3.05
13.5	8.14	2.0	85.7	0.005	4.8
*					
17.5	4.44	1.26	63.8	28.3	2.18
18.0	3.92	1.0	57.5	33.0	4.28
19.0	2.72	1.39	46.2	46.5	3.39
19.9	1.85	1.26	41.5	52.3	2.67
20.0	1.685	0.61	37.0	58.2	2.54
21.0	1.16	1.19	32.55	63.1	1.9
21.5	0.95	1.23	30.00	67.0	1.65

* At some radial locations samples could not be withdrawn due to excessive soot.

TABLE A-A-5-3

Axial Location Z = 47.5 mm

NO Concentration (Dry) Profile

Radial Distance From Wall in mm	NO Concentration in P.P.M.	Radial Distance From Wall in mm	NO Concentration in P.P.M.
0.0	10.5	11.2	46.3
1	11.0	11.5	53.0
2.0	10.0	11.8	61.0
3.0	11.5	12.0	51.0
4.0	13.0	12.2	68.0
5.0	13.0	12.5	82.0
5.5	12.0	12.8	91.0
6.0	16.0	13.0	96.0
6.5	15.0	13.2	89.0
7.0	16.0	13.5	84.0
7.5	15.0	*------------	------------
8.0	16.0	18.0	42.0
8.5	17.0	18.5	39.0
9.0	20.0	19.0	35.0
9.5	24.5	19.5	30.0
10.0	28.0	20.0	28.0
10.5	33.0	20.5	27.0
11.0	43.0	21.0	27.0
		21.5	27.0

---

* At some radial locations samples could not be drawn due to excessive soot.

TABLE A-A-6-1

Axial Location Z = 117,5

Temperature Profile

Radial Distance From Wall in mm	Temp °F
0,0	209.0
1,0	220.0
2,0	220.0
3,0	277,5
4,0	353.0
5,0	469.0
5,5	535.0
6,0	640.0
6,5	731.0
7,0	893.0
7,5	1045.0
8,0	1172.0
8,5	1360.0
9,0	1522.0
9,5	1728,0
10,0	1910.0
10,2	1975.0
10,5	2075.0
10,8	2130,0
11,0	2275.0
11,2	2350,0
11,5	2475.0
11,8	2582.0
12,0	2645.0
12,2	2722.0
12,5	2823,0
12,8	2905.0
13,0	2950,0
13,2	2982,0
13,5	3012,0
13,8	2985,0
14,0	2960,0
14,2	2925,0
14,5	2837,0
14,8	2746,0
15,0	2773,0
15,2	2723,0
15,5	2504,0
16,0	2284,0
16,5	2227,0
17,0	2175,0
17,5	2122,0
18,0	2072,0
19,0	2030,0
19,5	2009,0
20,0	1971,0
20,5	1955,0
21,0	1970,0
21,5	1965,0

TABLE A-A-6-2

Axial Location Z = 117.5 mm

Species Concentration (Dry) Profiles

Radial Distance From Wall in mm	Species Concentration (Dry) in Mole Percent				
	CO_2	O_2	N_2	CH_4	CO
0.0	-	21.0	79.0	-	-
1.0	-	21.0	79.0	-	-
2.0	-	20.7	79.3	-	-
3.0	-	20.2	79.8	-	-
4.0	0.15	19.6	80.2	-	-
5.0	0.4	19.0	80.5	-	-
5.3	0.5	18.62	80.7	-	-
6.3	0.815	18.1	81.0	-	-
7.3	1.365	16.84	81.8	-	-
8.3	2.1	15.2	82.7	-	-
9.3	3.45	13.1	83.4	-	-
10.3	4.73	11.0	84.6	-	0.02
10.6	5.44	9.64	85.5	-	0.04
11.3	6.175	8.3	85.5	-	0.13
11.8	7.05	6.62	86.6	-	0.32
12.3	7.5	5.72	87.5	-	0.535
12.8	8.075	4.35	86.1	-	1.24
13.1	8.0	4.18	85.8	-	1.33
13.5	8.26	3.31	86.2	-	2.1
13.6	8.2	3.24	86.1	-	2.34
13.8	8.15	2.9	86.0	-	2.7
14.1	8.03	2.9	85.5	-	3.62
14.3	7.92	2.7	85.0	0.17	4.2
*--------	--------	--------	--------	--------	--------
19.5	5.88	2.52	70.0	10.6	4.6
20.0	5.8	2.27	69.5	12.1	4.6
20.5	5.73	2.234	67.5	13.4	4.49
21.0	5.46	2.23	66.4	15.0	4.5
21.5	5.5	2.23	66.0	10.0	4.5

* At some radial locations, samples could not be withdrawn due to excessive soot.

TABLE A-A-6-3

Axial Location Z = 117,5 mm

NO Concentration (Dry) Profile

Radial Distance From Wall in mm	NO Concentration in P.P.M.	Radial Distance From Wall in mm	NO Concentration in P.P.M.
0,0	5	13,0	96
0,2	12	13,1	100
1,2	12	13,3	99,5
2,2	12	13,6	102
3,2	15	13,8	93
4,2	14	14,1	92
5,2	14	14,3	88
5,7	13	19,5	46
6,2	11	20,0	42
6,7	16	20,5	40
7,2	16	20,8	42
7,7	17	21,0	39
8,2	18	21,5	39
8,7	20		
9,3	25,5		
9,8	32		
10,3	36		
10,8	48		
11,0	56		
11,3	59		
11,5	70		
11,8	72		
12,0	80		
12,3	83		
12,8	94		

* At some radial locations samples could not be drawn due to excessive soot.

TABLE A-A-7-1

Axial Location Z = 324.0 mm

Temperature Profile

Radial Distance From Wall in mm	Temperature °F
0.0	315.0
2.2	730.0
2.4	820.0
3.1	990.0
4.2	1167.0
4.7	1295.0
6.7	1507.0
7.6	1568.0
9.2	1728.0
10.1	1829.0
11.0	1878.0
13.5	2076.0
14.1	2112.0
15.5	2216.0
16.2	2274.0
17.5	2304.0
18.2	2306.0
19.7	2307.0
20.4	2296.0
20.8	2289.0
21.2	2278.0
21.5	2275.0

TABLE A-A-7-2

Axial Locations Z = 324.0 mm

Species Concentrations (Dry) Profiles

Radial Distance From Wall in mm	Species Concentration (Dry) Mole Percent				
	CO_2	O_2	N_2	CH_4	CO
0.0	2.9	15.2	80.0	-	-
1.0	2.95	15.1	80.0	-	-
2.0	2.9	14.8	81.0	-	-
3.0	2.98	14.8	80.5	-	-
4.0	3.25	14.5	80.5	-	-
5.0	3.55	13.9	81.0	-	-
6.0	3.8	13.3	80.5	-	-
7.0	4.15	12.8	81.0	-	-
8.0	4.75	12.0	81.0	-	-
9.0	5.18	11.2	82.0	-	-
10.0	5.8	10.4	82.0	-	-
11.0	6.27	9.5	82.0	-	-
12.0	6.8	8.7	81.5	-	-
13.0	7.6	7.8	81.0	-	-
14.0	7.91	7.4	83.5	-	-
15.0	8.6	6.28	82.5	-	0.025
16.0	9.6	4.85	83.2	-	0.125
17.0	9.9	4.05	83.5	-	0.25
18.0	10.5	3.17	83.5	-	0.5
18.5	10.9	2.5	86.0	-	0.54
19.0	11.0	2.15	86.0	-	0.74
19.5	11.0	2.1	86.5	-	0.72
20.0	11.15	1.85	86.0	-	0.81
20.5	10.9	1.75	86.0	-	0.86
21.0	11.2	1.7	86.5	-	0.83
21.5	11.1	1.87	86.0	-	0.72

TABLE A-A-7-3

Axial Location Z = 324.0 mm

NO Concentration (Dry) Profile

Radial Distance From Wall in mm	NO Concentration (Dry) in P.P.M.
0,0	27,5
1,0	28,5
2,0	28,0
3,0	35,5
4,0	32,5
5,0	33,0
6,0	37,0
7,0	41,0
8,0	46,0
9,0	47,5
10,0	51,5
11,0	56,0
12,0	61,0
13,0	62,0
14,0	67,0
15,0	71,0
16,0	75,0
17,0	82,0
18,0	82,0
18,5	83,0
19,0	83,0
19,5	83,5
20,0	82,0
20,5	81,0
21,0	81,3
21,5	82,0

FLAME CONDITION B

Fuel Mass Flow Rate	= 2.67×10^{-3}	lbm/min
Air Mass Flow Rate	= 1.062×10^{-1}	lbm/min
Av. Fuel Velocity	= 0.721	ft/sec
Av. Air Velocity	= 1.779	ft/sec
Overall F/A Eq. Ratio	= 0.433	
Air/Fuel Velocity Ratio	= 2.47	

TABLE A-8-1-1

Axial Location Z = 0,5 mm

Temperature Profile

Radial Distance From Wall in mm	Temp °F	Radial Distance From Wall in mm	Temp °F
0,0	80,0	15,9	422,0
1,0	80,0	16,4	338,0
2,0	80,0	16,9	270,0
3,0	80,0	17,4	218,0
4,0	80,0	17,9	186,0
5,0	80,0	18,4	161,0
6,0	80,0	18,9	149,0
7,0	80,0	19,4	146,0
8,0	81,0	19,9	140,0
9,0	81,0	20,4	139,0
10,0	88,0	20,9	136,0
10,5	91,0	21,1	135,0
11,0	94,0	21,3	135,0
11,5	102,0	21,4	135,0
12,0	108,0	21,5	135,0
12,5	141,0		
12,9	204,0		
13,1	258,0		
13,3	338,0		
13,5	395,0		
13,7	410,0		
14,0	678,0		
14,2	739,0		
14,4	788,5		
14,6	799,0		
14,8	781,0		
15,0	715,0		
15,4	547,0		

TABLE A-8-2-1

Axial Location Z = 2.0 mm

Temperature Profile

Radial Distance From Wall in mm	Temp °F	Radial Distance From Wall in mm	Temp °F
0.0	81.0	15.3	1859.0
1.0	81.0	15.7	1715.0
2.0	81.0	16.0	1514.0
3.0	81.0	16.2	1360.0
4.0	81.0	16.5	660.0
5.0	81.0	17.0	473.0
6.0	81.0	17.5	299.0
7.0	81.0	18.0	207.0
8.0	81.0	18.5	164.0
9.0	81.0	19.0	137.0
10.0	94.0	19.5	137.0
10.5	108.0	20.0	137.0
11.0	134.0	20.5	130.0
11.5	183.0	21.0	125.0
12.0	374.0	21.5	125.0
12.2	653.0		
12.5	770.0		
12.7	1076.0		
13.0	1544.0		
13.2	1871.0		
13.5	2049.0		
13.7	2123.0		
14.0	2151.0		
14.2	2147.0		
14.5	2180.0		
14.7	2273.0		
15.0	2182.0		
15.2	2103.0		

TABLE A-B-3-1

Axial Location Z = 17,0 mm

Temperature Profile

Radial Distance From Wall in mm	Temp °F	Radial Distance From Wall in mm	Temp °F
0,0	81,0	14,0	3038,0
0,8	81,0	14,2	2945,0
1,8	81,0	14,4	2858,0
2,8	81,0	14,6	2823,0
3,8	81,0	14,8	2724,0
4,8	81,0	15,1	2486,0
5,8	81,0	15,3	2388,0
6,8	81,0	15,6	2311,0
7,8	84,0	15,8	2249,0
8,8	99,0	16,1	2162,0
9,8	211,0	16,3	2126,0
10,3	473,0	16,6	2083,0
10,8	789,0	16,8	2013,0
11,1	960,0	17,1	1900,0
11,3	1121,0	17,6	1837,0
11,7	1312,0	17,7	1746,0
11,8	1630,0	18,0	1663,9
12,1	1953,0	18,3	1558,0
12,3	2122,0	18,6	1431,0
12,5	2351,0	18,9	1330,0
12,8	2532,0	19,2	1183,0
13,0	2690,0	19,6	1058,0
13,2	2922,0	19,9	955,0
13,3	2991,0	20,2	760,0
13,4	3010,0	20,6	705,0
13,5	3041,0	21,0	556,0
13,6	3067,0	21,4	422,0
13,7	3075,0	21,5	380,0
13,8	3070,0		

TABLE A-8-3-2

Axial Location Z = 17.0 mm

Species Concentration (Dry) Profiles

Radial Distance From Walls in mm	Species Concentration (Dry) in Mole Percent				
	CO_2	O_2	N_2	CH_4	CO
0.0	-	21.0	79.0	-	-
1.0	-	21.0	79.0	-	-
2.0	-	21.0	79.0	-	-
3.0	-	21.0	79.0	-	-
4.0	-	21.0	79.0	-	-
5.0	-	21.0	79.0	-	-
6.0	-	21.0	79.0	-	-
7.0	-	21.0	79.0	-	-
8.0	-	21.0	79.0	-	-
9.0	0.025	20.8	79.0	-	-
9.5	0.131	20.6	79.3	-	-
10.0	0.305	20	79.7	-	-
10.5	0.715	19.25	80.2	-	-
10.8	1.12	18.3	80.6	-	-
11.1	1.51	17.3	81.0	-	-
11.4	2.04	16.25	81.7	-	0.015
11.7	2.98	13.01	82.2	-	0.056
12.0	3.76	12.9	83.3	-	0.09
12.3	4.38	11.4	84.1	-	0.183
12.5	5.04	9.97	84.6	-	0.312
12.8	6.19	7.47	85.6	-	0.657
13.0	6.6	6.6	86	-	0.87
13.2	7.08	5.57	86	-	1.355
13.4	7.48	4.31	86.3	-	1.96
13.6	7.7	3.17	86	-	3.21
13.8	7.5	2.58	84.5	0.27	4.07
14.0	7.47	2.53	85.2	0.41	4.38
14.3	7.27	2.34	83.9	1.35	5.11
14.5	7.08	2.05	82.3	3.07	5.5
14.9	6.90	2.1	80.54	4.82	5.63

(To be Continued)

TABLE A-8-3-2 Continued

Radial Distance From Wall in mm	Species Concentration (Dry) in Mole Percent				
	CO_2	O_2	N_2	CH_4	CO
15.2	6.57	1.94	78.2	7.61	5.64
15.5	6.20	2.04	74.7	11.79	5.275
15.8	5.98	2.00	72.1	14.64	5.188
16.3	5.48	2.25	68.2	19.44	4.625
16.8	4.665	2.307	60.76	28.22	4.03
17.3	4.1	2.236	51.6	38.3	3.67
17.8	3.2	2.13	42.85	48.91	2.9
18.3	2.44	1.925	35.03	58.42	2.2
18.8	1.81	1.84	28.22	66.4	1.722
19.3	1.08	2.02	22.8	72.94	1.15
19.8	0.59	1.94	17.0	79.82	0.654
20.3	.306	1.755	13.01	84.5	0.388
20.5	.124	1.855	11.7	86.06	.263
20.7	0.07	1.66	10.05	88.02	.184
20.9	0.02	1.69	9.53	88.62	0.143
21.1	-	1.77	9.06	89.08	0.08
21.3	-	1.52	7.9	90.5	-

TABLE A-B-4-1

Axial Location Z = 47.5 mm

Temperature Profile

Radial Distance From Wall in mm	Temp °F	Radial Distance From Wall in mm	Temp °F
0.0	116.0	13.2	3025.0
0.7	115.0	13.3	3012.0
1.7	99.0	13.5	2980.0
2.7	95.0	13.7	2912.0
3.7	90.0	13.9	2812.0
4.7	90.0	14.2	2718.0
5.2	93.0	14.5	2594.0
5.7	100.0	14.7	2552.0
6.2	135.0	15.2	2308.0
7.2	191.0	15.7	2188.0
7.7	276.0	16.2	2114.0
8.2	451.0	16.7	2065.0
8.7	668.0	17.2	1981.0
9.2	912.5	17.7	1900.0
9.7	1155.0	18.2	1742.0
9.9	1226.0	18.7	1640.0
10.2	1362.0	19.2	1485.0
10.5	1555.0	19.7	1409.0
10.7	1714.0	19.9	1333.0
10.9	1868.0	20.2	1271.0
11.2	2024.0	20.5	1225.0
11.5	2174.3	20.7	1179.0
11.7	2323.0	20.9	1141.0
11.9	2511.0	21.1	1132.0
12.2	2672.0	21.2	1090.0
12.5	2775.0	21.3	1082.0
12.7	2925.0	21.4	1066.0
12.9	2985.0	21.5	1060.0
13.1	3010.0		

TABLE A-8-4-2

Axial Location Z = 47.5 mm

Species Concentration (Dry) Profiles

Radial Distance From Wall in mm	Species Concentration (Dry) in Mole Percent				
	CO_2	O_2	N_2	CH_4	CO
0.0	-	21.0	79.0	-	-
1.0	-	21.0	79.0	-	-
2.0	-	21.0	79.0	-	-
3.0	-	21.0	79.0	-	-
4.0	-	21.0	79.0	-	-
5.0	-	21.0	79.0	-	-
6.0	-	21.0	79.0	-	-
6.5	-	20.8	79.2	-	-
7.0	-	20.5	79.5	-	-
7.5	0.15	20.0	79.8	-	-
8.0	0.4	19.4	80.1	-	-
8.5	0.8	18.5	80.5	-	-
9.0	1.2	17.4	81.3	-	-
9.5	1.7	16.0	82.9	-	-
10.0	2.3	14.25	83.5	-	-
10.5	3.1	12.4	84.5	-	-
10.7	3.9	11.18	85.0	-	0.078
11.0	4.08	9.95	85.9	-	0.157
11.3	4.57	8.87	86.35	-	0.235
11.5	5.2	7.78	86.7	-	0.364
11.7	5.96	6.3	88.2.0	-	0.64
12.0	5.62	5.95	87.6	-	0.861
12.3	6.6	5.1	87.0	-	1.3
12.5	6.94	4.34	86.85	-	1.67
12.7	8.05	3.39	85.0	-	2.35
13.0	8.17	2.96	85.7	0.1	3.12
13.2	8.35	2.70	85.5	0.117	3.35
13.5	8.22	2.65	84.0	0.2	3.85
17.7	4.02	1.605	55.9	34.8	3.68

(To be Continued)

TABLE A-8-4-2 Continued

Radial Distance From Wall in mm	Species Concentration (Dry) in Mole Percent				
	CO_2	O_2	N_2	CH_4	CO
18.2	3.845	1.7	51.4	39.6	3.36
18.7	3.24	1.56	47.7	45.5	2.985
19.0	2.25	1.605	43.6	49.7	2.88
19.5	1.95	1.63	40.5	53.6	2.5
20.0	1.64	1.525	35.05	59.6	2.16
20.5	1.595	1.5	33.6	61.4	2.06
21.0	1.34	1.38	30.1	65.5	1.765
21.5	1.3	1.41	29.4	66.2	1.75

TABLE A-8-4-3

Axial Location Z = 47,5 mm

NO Concentration (Dry) Profile

Radial Distance From Wall in mm	NO Concentration (Dry) Profile in P.P.M.
0,0	9,0
1,5	9,0
3,0	9,0
4,0	7,0
5,0	15,0
6,0	10,0
7,0	12,0
8,0	12,0
8,5	16,0
9,0	19,0
9,5	23,0
10,0	25,0
10,5	41,0
10,7	37,0
11,2	43,0
11,5	49,0
12,0	60,0
12,2	61,0
12,5	71,0
12,7	78,0
13,0	85,0
13,2	92,0
13,5	87,0
13,8	85,0
========================	========================
17,7	48,0
18,0	40,0
18,3	83,0
18,8	37,0
19,0	39,0
19,5	35,0
20	33,0
20,5	30,0
21,0	28,0
21,5	27,0

TABLE A-8-5-1

Axial Location Z = 117,5 mm

Temperature Profile

Radial Distance From Wall in mm	Temp °F	Radial Distance From Wall in mm	Temp °F
0,0	197,0	13,8	2996,0
0,9	192,0	13,9	2990,0
1,9	172,0	14,1	2975,0
2,9	162,0	14,4	2952,0
3,9	180,0	14,7	2912,0
4,9	254,0	14,9	2880,0
5,4	314,0	15,1	2837,0
5,9	385,0	15,4	2780,0
6,4	470,0	15,7	2712,0
6,9	597,0	15,9	2675,0
7,4	730,0	16,1	2565,0
7,9	913,0	16,3	2652,0
8,4	1077,0	16,3	2328,0
8,9	1256,0	16,7	2250,0
9,4	1474,0	16,9	2193,0
9,9	1646,0	17,2	2160,0
10,1	1716,0	17,5	2104,0
10,4	1864,0	17,7	2116,0
10,7	1994,0	17,9	2092,0
10,9	2070,0	18,2	2056,0
11,1	2202,0	18,5	2015,0
11,4	2322,0	18,7	2047,0
11,7	2400,0	18,9	2056,0
11,9	2514,0	19,2	2068,0
12,1	2571,0	19,5	2068,0
12,4	2708,0	19,7	2068,0
12,7	2824,0	19,9	2026,0
12,9	2875,0	20,2	2033,0
13,1	2923,0	20,5	2025,0
13,4	2966,0	20,7	2041,0
13,5	2975,0	20,9	2006,0
13,6	2988,0	21,2	1973,0
13,7	2989,0	21,5	1986,0

TABLE A-B-5-2

Axial Location Z = 117,5 mm

Species Concentration (Dry) Profiles

Radial Distance From Walls in mm	CO_2	O_2	N_2	CH_4	CO
	Species Concentration (Dry) in Mole Percent				
0,0	-	20,0	80,0	-	-
1,0	-	19,95	80,0	-	-
2,0	-	19,8	80,2	-	-
3,0	-	19,7	80,3	-	-
4,0	-	19,5	80,4	-	-
5,0	0,1	19,2	80,7	-	-
6,0	0,392	18,9	80,7	-	-
7,0	0,77	18,1	81,2	-	-
8,0	1,43	16,75	81,8	-	-
9,0	2,23	15,9	82,0	-	-
10,0	3,62	12,53	84,1	-	-
11,0	4,87	10,51	84,6	-	0,05
11,5	5,85	8,67	85,3	-	0,125
12,0	6,62	7,36	85,7	-	0,253
12,5	7,52	5,8	86,1	-	0,6
13,0	7,97	4,64	86,3	-	1,01
13,3	8,375	3,75	86,5	-	1,47
13,5	8,43	3,41	86,3	-	1,855
13,8	8,45	2,93	86,4	-	2,4
14,0	8,47	2,84	86,0	-	2,84
14,3	8,33	2,54	85,7	0,066	3,56
14,5	8,25	2,49	85,1	0,1525	4,02
14,8	8,3	2,18	84,7	0,337	4,47
- - - - - -	- - - - - -	- - - - - -	- - - - - -	- - - - - -	- - - - - -
20,0	5,07	1,74	65,3	15,0	4,6
20,5	4,93	2,07	65,3	15,3	4,55
21,0	5,0	1,82	65,2	15,3	4,6
21,5	4,95	2,86	67,2	15,8	4,5

TABLE A-8-5-3

Axial Location Z = 117.5 mm

NO Concentration (Dry) Profile

Radial Distance From Wall in mm	NO Concentration (Dry) in P.P.M.
0.0	8.5
2.0	9.0
4.0	11.0
6.0	16.5
7.0	9.5
8.0	18.0
9.0	17.5
10.0	26.0
11.0	36.0
11.5	61.0
12.0	68.5
12.5	81.5
13.0	87.0
13.3	95.0
13.5	96.0
13.8	100.0
14.0	97.0
14.5	94.5
14.8	92.5
20.0	37.5
20.5	39.0
21.0	36.0
21.5	28.5

TABLE A-B-6-1

Axial Location Z = 324.0 mm

Temperature Profile

Radial Distance From Wall in mm	Temperature °F
0.0	322.0
0.8	460.0
1.4	594.0
2.9	843.0
4.2	1049.0
5.6	1205.0
6.2	1255.0
7.0	1306.0
8.2	1395.0
9.2	1440.0
9.9	1498.0
10.9	1568.0
12.7	1707.0
13.5	1777.0
14.6	1908.0
15.9	2052.0
17.5	2164.0
18.3	2211.0
19.0	2267.0
19.4	2269.0
20.2	2301.0
21.0	2332.0
21.4	2332.0

TABLE A-B-6-2

Axial Location Z = 324.0 mm

Species Concentration (Dry) Profiles

Radial Distance From Wall in mm	Species Concentration in Mole Percent				
	CO_2	O_2	N_2	CH_4	CO
0.0	2.16	16.3	81.5	-	-
2.0	1.82	16.58	81.6	-	-
4.0	2.1	15.8	82.1	-	-
6.0	2.58	15.1	82.3	-	-
8.0	3.15	14.52	82.33	-	-
10.0	4.085	12.76	83.15	-	-
11.0	4.332	12.31	83.35	-	-
12.0	5.29	11.47	83.22	-	-
13.0	5.57	10.9	83.5	-	-
14.0	6.33	9.39	84.25	-	-
15.0	7.15	8.44	84.4	-	-
16.0	7.71	7.51	84.75	0	0.026
17.0	8.29	6.7	85.0	0	0.055
18.0	8.94	6.13	84.8	0	0.112
19.0	9.53	5.23	85.03	0	0.203
20.0	9.93	4.77	85.0	0	0.286
21.0	10.34	4.27	85.02	0	0.358
21.5	10.34	4.05	85.17	0	0.425

TABLE A-8-6-3

Axial Location Z = 324.0 mm

NO Concentration (Dry) Profile

Radial Distance From Wall in mm	NO Concentration (Dry) in P.P.M.
0.0	20.0
2.0	17.0
4.5	21.5
6.0	25.0
8.0	30.5
10.0	43.0
11.0	41.0
12.0	47.5
13.0	48.2
14.0	58.0
15.0	64.5
16.0	67.0
17.0	73.5
18.0	76.0
19.0	79.5
20.0	81.0
21.0	80.0
21.5	80.0

FLAME CONDITION C

Fuel Mass Flow Rate = 2.67×10^{-3} lbm/min
Air Mass Flow Rate = 1.312×10^{-1} lbm/min

Av. Fuel Velocity = 0.721 ft/sec
Av. Air Velocity = 2.2 ft/sec

Overall F/A Eq. Ratio = 0.351
Air/Fuel Velocity Ratio = 3.05

TABLE A-C-1-1

Axial Location Z = 0.5 mm

Temperature Profile

Radial Distance From Wall in mm	Temp °F	Radial Distance From Wall in mm	Temp °F
0.0	79.0	15.9	336.0
1.0	79.0	16.4	283.0
2.0	79.0	16.9	217.0
3.0	79.0	17.4	179.0
4.0	79.0	17.9	160.0
5.0	79.0	18.4	148.0
6.0	79.0	18.9	138.0
7.0	79.0	19.4	135.0
8.0	79.0	19.9	125.0
9.2	79.0	20.4	123.0
10.0	82.0	20.9	120.0
11.0	89.0	21.1	120.0
12.0	98.0	21.3	120.0
12.4	107.0	21.5	120.0
12.9	159.0		
13.4	295.0		
13.6	318.0		
13.8	377.0		
14.0	439.0		
14.2	474.0		
14.4	565.0		
14.5	566.0		
14.6	598.0		
14.7	600.0		
14.9	497.0		
15.1	491.0		
15.4	433.0		

TABLE A-C-2-1

Axial Location Z = 2.0 mm

Temperature Profile

Radial Distance From Wall in mm	Temp °F	Radial Distance From Wall in mm	Temp °F
0.0	80.0	15.2	1808.0
1.0	80.0	15.5	1649.0
2.0	80.0	15.7	1456.0
3.0	80.0	16.0	750.0
4.0	80.0	16.5	435.0
5.0	80.0	17.0	365.0
6.0	80.0	17.5	230.0
7.0	80.0	18.0	159.0
8.0	80.0	18.5	139.0
9.0	80.0	19.0	124.0
10.0	86.0	19.5	124.0
11.0	107.0	20.0	124.0
11.5	135.0	20.5	120.0
12.0	267.0	21.0	120.0
12.5	440.0	21.5	120.0
13.0	996.0		
13.2	1420.0		
13.5	1577.0		
13.7	1712.0		
14.0	1708.0		
14.2	1640.0		
14.5	1799.0		
14.7	2079.0		
15.0	1976.0		

TABLE A-C-3-1

Axial Location Z = 17.0 mm

Temperature Profile

Radial Distance From Wall in mm	Temp °F	Radial Distance From Wall in mm	Temp °F
0.0	83.0	14.5	3049.0
1.0	80.0	14.7	3003.0
1.8	80.0	14.9	2930.0
2.8	80.0	15.1	2805.0
3.8	80.0	15.3	2759.0
4.8	80.0	15.5	2627.0
5.8	80.0	15.8	2490.0
6.8	80.0	16.1	2337.0
7.8	90.0	16.3	2259.0
8.8	93.0	16.6	2215.0
9.8	123.0	16.8	2149.0
10.8	306.0	17.1	2084.0
11.3	562.0	17.3	2004.0
11.8	1006.0	17.6	1961.0
12.1	1265.0	17.8	1869.0
12.3	1451.0	18.1	1761.0
12.5	1616.0	18.4	1693.0
12.7	1820.0	18.8	1520.0
12.9	1982.0	19.1	1407.0
13.1	2151.0	19.4	1295.0
13.3	2411.0	19.7	1190.0
13.5	2547.0	20.0	1049.0
13.7	2712.0	20.3	930.0
13.9	2849.0	20.6	826.0
14.1	3018.0	20.9	725.0
14.3	3064.0	21.2	582.0
		21.5	489.0

TABLE A-C-4-1

Axial Location Z = 47.5 mm

Temperature Profile

Radial Distance From Wall in mm	Temp °F	Radial Distance From Wall in mm	Temp °F
0,0	146,5	13,1	2836,0
0,9	126,0	13,4	2934,0
1,9	113,0	13,6	2985,0
2,9	99,0	13,7	3011,0
3,9	93,0	13,9	2975,0
4,4	93,0	14,1	2931,0
4,9	89,5	14,4	2862,0
5,4	93,0	14,7	2731,5
5,9	97,0	14,9	2725,0
6,4	105,0	15,1	2617,0
6,9	120,5	15,4	2510,0
7,4	161,0	15,7	2354,0
7,9	204,0	15,9	2278,0
8,4	309,0	16,4	2170,0
8,9	488,0	16,9	2112,0
9,4	646,0	17,4	2035,0
9,9	876,0	17,9	1948,0
10,1	1026,0	18,4	1835,0
10,4	1119,5	18,9	1733,0
10,7	1257,0	19,4	1471,0
10,9	1392,0	19,9	1464,0
11,1	1562,0	20,1	1396,0
11,4	1723,0	20,4	1316,0
11,7	1869,0	20,7	1249,0
11,9	2024,0	20,9	1246,0
12,1	2175,0	21,1	1209,3
12,4	2339,0	21,3	1167,0
12,7	2491,0	21,4	1145,0
12,9	2600,0	21,5	1141,0

TABLE A-C-4-2

Axial Location Z = 47.5 mm

Species Concentration (Dry) Profiles

Radial Distance From Wall in mm	Species Concentration (Dry) in Mole Percent				
	CO_2	O_2	N_2	CH_4	CO
0.0	-	21.0	79.0	-	-
2.0	-	21.0	79.0	-	-
4.0	-	21.0	79.0	-	-
6.0	-	21.0	79.0	-	-
7.0	-	20.65	79.35	-	-
7.5	0.01	20.25	79.6	-	-
8.0	0.15	19.7	80.2	-	-
8.5	0.4	18.9	80.7	-	-
9.0	0.95	17.8	81.2	-	-
9.5	1.7	16.5	81.8	-	-
10.0	2.6	14.8	82.6	-	-
10.5	3.49	13.2	83.3	-	0.026
11.0	4.79	10.55	84.5	-	0.185
11.5	6.05	8.4	85.2	-	0.413
12.0	6.16	6.48	86.5	-	0.95
12.5	7.59	5.24	85.6	-	1.56
13.0	7.5	4.4	86.7	0.053	1.28
13.5	7.66	2.89	85.5	0.305	3.71
13.7	7.63	2.7	85.2	0.483	4.12
14.0	7.71	1.71	84.1	1.49	5.05
14.2	7.15	3.1	83.4	1.6	4.82
14.5	7.7	1.815	84.3	1.295	5.09
17.5	5.05	1.85	57.8	31.2	4.12
18.0	4.23	3.08	55.4	33.9	3.45
18.5	3.86	1.645	50.0	41.4	3.09
19.0	3.54	1.43	45.8	46.3	2.99
19.5	2.98	1.51	39.8	53.2	2.68
20.0	2.81	1.61	37.7	55.5	2.4
20.5	2.52	1.575	35.9	58.0	2.15
21.0	2.21	1.67	34.5	59.7	2.03
21.2	2.07	2.075	34.1	60.0	1.91
21.5	2.0	1.85	33.3	61.0	2.0

TABLE A-C-4-3

Axial Location Z = 47.5 mm

NO Concentration (Dry) Project

Radial Distance From Wall in mm	NO Concentration (Dry) in P.P.M.
0.0	9.0
1.0	10.0
2.0	13.0
3.0	10.0
5.0	10.0
7.0	13.0
8.0	12.0
9.0	20.5
10.0	32.0
10.5	35.0
11.0	45.0
11.5	49.0
12.0	45.0
12.5	60.0
13.0	69.0
13.2	74.0
13.5	79.0
13.7	81.0
14.0	78.0
14.2	73.0
*------------------	------------------
17.5	43.0
18.0	45.0
18.5	36.0
19.0	36.0
19.5	32.0
20.0	26.0
20.5	28.0
21.0	25.0
21.5	21.0

*At some radial locations, samples could not be withdrawn from the flame due to excessive soot.

TABLE A-C-5-1

Axial Location Z = 117.5 mm

Temperature Profile

Radial Distance From Wall in mm	Temp °F	Radial Distance From Wall in mm	Temp °F
0,0	152,0	13,5	2743,0
1,0	152,0	13,8	2799,0
2,0	145,0	14,0	2872,0
3,0	134,0	14,2	2906,0
4,0	145,0	14,4	2960,0
5,0	159,0	14,5	2960,0
5,5	243,0	14,6	2955,0
6,0	302,0	14,8	2945,0
6,5	387,0	15,0	2937,0
7,0	481,0	15,2	2925,0
7,5	585,0	15,5	2907,0
8,0	707,0	15,8	2860,0
8,5	850,0	16,0	2825,0
9,0	990,5	16,2	2779,0
9,5	1175,0	16,5	2691,0
10,0	1367,0	16,8	2636,0
10,5	1548,5	17,0	2342,0
11,0	1700,0	17,5	2212,0
11,2	1816,0	18,0	2113,0
11,5	1970,0	18,5	2072,0
11,8	2045,0	19,0	2065,0
12,0	2192,0	19,5	2045,0
12,2	2216,0	20,5	2023,0
12,5	2377,5	21,0	20241,0
12,8	2417,0	21,5	1981,0
13	2510,0		
13,2	2644,0		

TABLE A-C-5-2

Axial Location Z = 117.5 mm

Species Concentration (Dry) Profiles

Radial Distance From Wall in mm	Species Concentration (Dry) in Mole Percent				
	CO_2	O_2	N_2	CH_4	CO
0.0	-	20.0	80.0	-	-
1.0	-	19.95	80.1	-	-
3.0	-	19.75	80.2	-	-
5.0	0.0925	19.55	80.3	-	-
6.0	0.227	19.22	80.5	-	-
7.0	0.465	18.75	80.9	-	-
8.0	0.875	17.9	81.3	-	-
9.0	1.365	17.1	81.5	-	-
10.0	2.29	15.12	82.7	-	-
11.0	3.33	13.16	83.5	-	-
11.5	3.95	11.68	84.5	-	-
12.0	4.86	10.3	85.5	-	0.092
12.5	5.68	8.6	85.5	-	0.334
13.0	6.36	7.37	85.8	-	0.511
13.5	7.09	5.79	86.3	-	0.87
14.0	7.6	4.92	86.1	-	1.435
14.5	8.01	3.75	86.2	-	1.99
14.7	7.96	3.39	86.0	0.062	2.71
15.0	8.05	2.81	85.7	0.153	3.31
15.2	7.76	3.18	85.6	0.163	3.35
15.5	7.85	2.58	85.0	0.412	4.08
======	======	======	======	======	======
20.5	5.6	2.5	72	14	5.2
21.0	5.5	2.4	70	16.5	5.0
21.5	5.45	2.5	70	17	4.9

TABLE A-C-5-3

Axial Location Z = 117,5 mm

NO Concentration (Dry) Profile

Radial Distance From Wall in mm	NO Concentration (Dry) in P.P.M.
0,0	9,0
1,0	5,0
3,0	8,5
5,0	8,5
6,0	8,5
7,0	11,0
8,0	7,0
9,0	10,0
10,0	18,0
11,0	29,0
11,5	36,0
12,0	45,0
12,5	59,5
13,0	71,0
13,5	81,0
14,0	88,5
14,5	95,0
14,7	94,0
15,0	92,0
15,2	89,0
15,5	84,0
= = = = = = = =	= = = = = = = =
20,5	39,0
21,0	36,0
21,5	34,0

TABLE A-C-6-1

Axial Location Z = 324.0 mm

Temperature Profile

Radial Distance From Wall in mm	Temperature °F
0.0	268.0
1.7	559.0
3.1	768.0
3.9	908.0
4.7	971.0
5.5	1057.0
6.3	1078.0
7.5	1191.0
8.3	1210.0
9.1	1287.0
9.7	1362.0
10.6	1393.0
11.7	1489.0
12.5	1577.0
13.5	1664.0
14.7	1730.0
15.6	1834.0
17.2	1932.0
18.2	2060.0
18.9	2087.0
20.0	2170.0
20.5	2172.0
21.4	2192.0

TABLE A-C-6-2

Axial Location Z = 324.0 mm

Species Concentration (Dry) Profiles

Radial Distance From Wall in mm	Species Concentration (Dry) in Mole Percent CO_2	O_2	N_2	CH_4	CO
0.0	0.94	17.28	81.8	-	-
2.0	1.15	17.73	81.1	-	-
4.0	1.411	17.23	81.35	-	-
6.0	1.86	16.43	81.7	-	-
8.0	2.39	15.82	81.77	-	-
10.0	3.08	14.55	82.3	-	-
12.0	4.07	12.66	83.26	-	-
14.0	5.54	10.60	83.85	-	-
15.0	6.13	10.19	83.66	-	-
16.0	6.83	8.92	84.2	-	.026
17.0	7.57	8.03	84.35	-	0.06
18.0	8.02	7.18	84.7	-	0.08
19.0	8.83	6.18	84.8	-	0.123
20.0	9.38	5.55	84.9	-	0.2
21.0	9.7	5.12	84.9	-	0.2
21.5	10.0	4.81	84.8	-	0.3

TABLE A-C-6-3

Axial Location Z = 324.0 mm

NO Concentration (Dry) Profile

Radial Distance From Wall in mm	NO Concentration (Dry) in P.P.M.
0.0	13.5
2.0	13.5
4.0	17.0
6.0	16.5
8.0	19.0
10.0	27.0
12.0	40.5
14.0	47.5
15.0	51.0
16.0	55.0
17.0	62.0
18.0	64.0
19.0	68.0
20.0	74.0
21.0	74.0
21.5	76.0

APPENDIX B
IGNITION SYSTEM

In order to ignite the diffusion flame, an automotive ignition system (54) was modified by replacing the breaker point by a vibrator to give a continuous spark. The circuit is presented in Fig. B.1.

In this ignition system, a modified spark plug was used. The modification consisted of removing the ground electrode and extending the central electrode as shown in Figure B.2. The spark plug was introduced into the burner through the lowermost flange with extended electrode protruding into the air stream. The fuel tube served as the ground electrode. The gap used was .25".

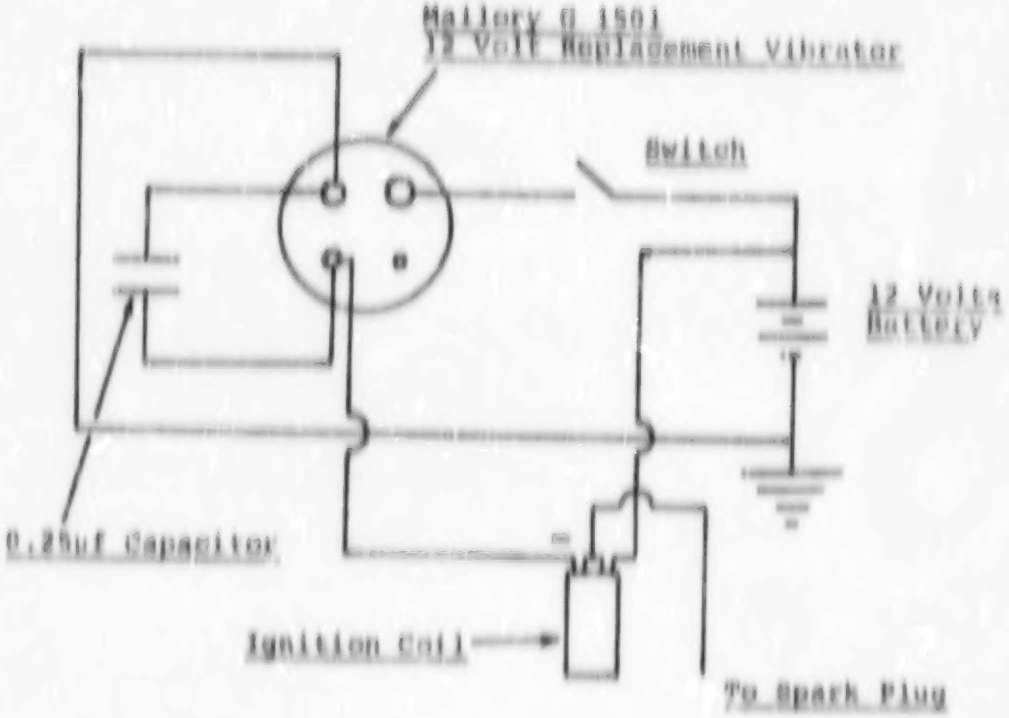
Mallory G 1501
12 Volt Replacement Vibrator
Switch
12 Volts Battery
0.25uf Capacitor
Ignition Coil
To Spark Plug

Figure B.1: Circuit diagram of modified automotive ignition system

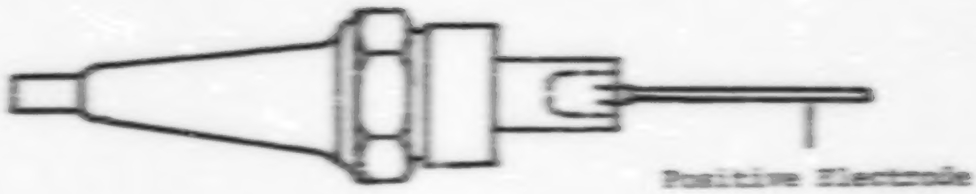
Positive Electrode

Standard 14 mm. Spark Plug

Figure B.2: Modified Spark Plug

APPENDIX C

OUTLINE FOR MISCELLANEOUS CALCULATIONS

In Chapter VI, the mass or mole of nitric oxide flowing through a plane downstream of the fuel tube mouth is reported. These values were obtained by spatial integration of calculated or experimental concentration profiles of NO, using the same flow field computed in the program indicated in Article 5.4. The average residence time of gases at axial location was also calculated and is reported in Table 6.2.

In the following, the relations used to calculate the above values are briefly outlined.

The Program Under Consideration

It will be recalled from Articles 5.3 and 5.6 that in the program under consideration, the independent variables are ω, the nondimensional stream function as the cross stream variable, and z instead of the usual r and z in the cylindrical geometry.

The relation between r, Ψ and ω is as follows:

$$z = \text{fixed} \qquad d\Psi = \rho u r dr \tag{C.1}$$

$$\omega = \frac{\Psi - \Psi_I}{\Psi_E - \Psi_I} \tag{C.2}$$

where Ψ is the stream function

u is the fluid velocity in z direction

ρ is the density of fluid

Ψ_I is the value of stream function at the axis of symmetry

Ψ_E is the value of stream function at the wall.

At $z = 0$, initial condition and the distribution of ω are specified and corresponding values of r are determined. The calculation at successive planes Dz apart are made by solving finite difference equation by successive substitution formulas developed by Patankar & Spalding (58). The calculations are carried out along the initially specified values of ω and corresponding value of r at each axial location is calculated within the program.

Average Residence Time

The average residence time RT at the Nth step corresponding to z_N is determined by the following relation:

$$RT_N = RT_{N-1} + \frac{z_N - z_{N-1}}{\bar{u}} = RT_{N-1} + \frac{Dz}{\bar{u}} \qquad (C.\ 3)$$

where $\bar{u}$ is the average fluid velocity at Nth step and axial location z_N, and is determined by the following relation:

$$\bar{u} = \frac{\int u d\omega}{\int d\omega} = \sum_j \frac{1}{2}(u_j + u_{j+1})(\omega_{j+1} - \omega_j) \qquad (C.\ 4)$$

$$\int d\omega = 1$$

where j represents the cross stream node.

Spatial Integration of Concentration Profiles

In order to calculate the mass or number of moles flowing through a particular axial plane, the concentration profiles are integrated taking into account the density, velocity and effect of geometry.

It can be easily seen that in cylindrical geometry the total mass flow rate through an axial plane will be given by:

$$\begin{aligned} \dot{m} &= 2\pi \int \rho u r dr \\ &= 2\pi \int d\Psi \\ &= 2\pi \int (\Psi_E - \Psi_I)\, d\omega \qquad (C.5) \\ &= 2\pi (\Psi_E - \Psi_I) \end{aligned}$$

The mass flow rate of any species i at any axial location would be given by

$$\begin{aligned} \dot{m}_i &= 2\pi \int y_i \rho u r dr = 2\pi \int y_i d\Psi \\ &= 2\pi (\Psi_E - \Psi_I) \int y_i\, d\omega \qquad (C.6) \\ &= \dot{m} \Sigma \quad \frac{1}{2} (y_i)_j + y_i)_{j+1}) (\omega_{j+1} - \omega_j) \end{aligned}$$

Similarly, the total number of moles r moles of a particular species flowing through a particular axial location are calculated by the following relations:

Total number of moles flowing through a plane

$$\begin{aligned} &= 2\pi \int \frac{d\Psi}{\bar{M}} dr \\ &= 2\pi (\Psi_E - \Psi_I) \int \frac{d\omega}{\bar{M}} \\ &= \dot{m} \Sigma \frac{1}{2} \left(\frac{1}{\bar{M}_j} + \frac{1}{\bar{M}_{j+1}} \right) (\omega_{j+1} - \omega_j) \end{aligned}$$

and

Total number of moles of species i flowing through a plane

$$\begin{aligned} &= 2\pi \int \frac{x_i}{\bar{M}} \rho u r dr \\ &= 2\pi (\Psi_E - \Psi_I) \int \frac{x_i}{\bar{M}} d\omega \\ &= \dot{m} \Sigma \frac{1}{2} (\omega_{j+1} - \omega_j) \left(\frac{x_i}{\bar{M}} \right)_j + \frac{x_i}{\bar{M}})_{j+1}) \end{aligned}$$

where $\overline{M}$ is the average molecular weight at any point.

In the above calculations, while integrating calculated profiles value of mass fraction of species i, y_i, was obtained from the program, y_i being a dependent variable.

While integrating experimental profile values of mole fraction of species i was obtained from experimental profile corresponding to value of r calculated in the program for ω distribution.

The interconversion of x_i, y_i and $\overline{M}$ was achieved by the following relation:

$$\overline{M} = \Sigma\, x_i M_i \qquad\qquad \frac{1}{\overline{M}} = \Sigma\, \frac{y_i}{M_i}$$

$$x_i = \frac{y_i}{M_i} \times \overline{M} \qquad\qquad y_i = \frac{x_i M_i}{\overline{M}}$$

APPENDIX D

OUTLINE OF ADIABATIC FLAME TEMPERATURE PROGRAM

For adiabatic combustion process at constant pressure, the following relation is satisfied:

$$H\Big]_{\substack{\text{reactants}\\ T_i,\, p}} = H\Big]_{\substack{\text{products}\\ T_{eq},\, p}} \qquad \text{(D. 1)}$$

where

H is the absolute enthalpy

T_i is the initial temperature

T_{eq} is the equilibrium flame temperature

p is the system pressure

A trial value of T_{eq} is selected and used to calculate equilibrium species concentrations using previously developed subroutines (49). These subroutines calculate equilibrium specie concentration for any fuel-oxidant combination, $C_w H_x O_y N_z$, and require as input besides composition (w, x, y and z) and equivalence ratio, the temperature and pressure of the system. All the required input including T_{eq} is supplied through the main program.

Thus product composition for this trial value of equilibrium flame temperature is obtained. Using thermochemical data from the literature (JANAF Tables), the absolute enthalpies on the right and left hand sides of equation D. 1 are calculated. The trial value of T_{eq} is adjusted until the two enthalpy values match.